Aalto University
School of Electrical
Engineering

Zeeshan Ahmed

ANALYSIS AND DE-NOISING OF PARTIAL DISCHARGE SIGNALS IN MEDIUM VOLTAGE XLPE CABLES

School of Electrical Engineering

Master's Thesis submitted in partial fulfilment of the requirement for the degree of Master of Science in Technology.

Espoo

Thesis supervisor:

Prof. Matti Lehtonen

Thesis instructor:

Mr. Ghulam Amjad Hussain

Aalto University

School of Electrical Engineering **ABSTRACT OF THE MASTER'S THESIS**

Master's Programme in Electrical Engineering

Author: Zeeshan Ahmed

Title: ANALYSIS AND DE-NOISING OF PARTIAL DISCHARGE SIGNALS IN MEDIUM VOLTAGE XLPE CABLES

Number of pages: 11+94 **Date**: 14-12-2015
Language: English

Department: Electrical Engineering
Professorship: Power Systems and High Voltage Engineering
Code: S-18

Supervisor: Professor Matti Lehtonen

Instructor : Mr. Ghulam Amjad Hussain

Abstract

The partial discharge (PD) measurements have been widely used in the field of insulation diagnostics. The presence of partial discharges inside the cable indicates the degradation of insulation material. This thesis deals with the development of insulation diagnostic method based on the partial discharge measurements. The useful information about the partial discharge activity and insulation defects is extracted by the experimental results.

A measuring test setup was established in the high voltage laboratory. Artificial cavity was introduced inside the MV XLPE cable by using the traditional needle-plane configuration. The aim of study was to interpret the variations in the partial discharge characteristics over the insulation ageing period in terms of physical phenomenon's taking place in PD sources. The statistical characteristics formulated with the help of PRPDA technique and ultra-wideband discharge characteristics by using HFCT sensor were studied and analyzed. The variations in these characteristics allow to diagnose the insulation conditions as well as detect the type of discharge mechanisms.

In the second part of thesis, detailed analytical study about the de-noising techniques has been conducted. In order to design an efficient de-noising filter for onsite and online PD monitoring system, various factors such as optimal wavelet selection, number of decomposition levels and threshold setting has been studied. An automated self-adaptive de-noising algorithm based on the frequency characteristics of partial discharge signals has been presented in this study.

Keywords: Partial Discharge characteristics, XLPE insulated cables, insulation degradation, monitoring, diagnostics, PRPDA, De-noising, wavelet transformation, Adaptive De-noising, Thresholding

Acknowledgment

I would like to express my gratitude to my supervisor Prof. Matti Lehtonen for allowing me to work in this wonderful research project. He has always supported me to explore the new ideas and concepts and ensure me with all the available tools required to execute my research work.

My sincere appreciation goes to High Voltage Laboratory, Technology Manager Mr. Petri Hyvönen who spent a lot of his precious time helping me in everything related to this thesis. His knowledge on establishing partial discharge measurement setup has been extremely beneficial for me. I will always remember his calm and relaxed nature whenever I ask him something. At the same time, I want to thank Dr. Joni Klüss and Dr. Lauri Kütt for initially guiding me in establishing the partial discharge measurement setup. Also, special thanks to Mr. Jouni Mäkinen for his laboratory instrumentation support and Finnish talks during the long experimental works.

Also, my deepest gratitude to few dearest friends Dr. Amjad Hussain, Toni Tukia, Ammar Arshad and Ingrid Nobre for their continuous support and making my stay pleasant in Finland

Last but not least I would like to remember and thank my parents and dear sisters for striving hard to provide a good education for me and always encouraging me to continue my studies.

Zeeshan Ahmed
Espoo, Dec 2015

Table of Contents

List of Figures

List of Tables

List of Symbols

$C_a, C_a^{'}$ & $C_a^{''}$	Capacitance of bulk insulation between cavity and electrodes
$C_b, C_b^{'}$ & $C_b^{''}$	Stray capacitance of healthy insulation
C_c	Capacitance of cavity
cc	cross-correlation factor for statistical analysis
coif'x'	Coieflets family wavelet functions
db'x'	Daubechies family wavelet functions
d_c	Cavity diameter
E_i	Inception field strength
$H_n(\emptyset)$	Pulse count phase distribution
$H_{qm}(\emptyset)$	Maximum pulse height phase distribution
$H_{qn}(\emptyset)$	Mean pulse height phase distribution
$H_{qs}(\emptyset)$	Discharge sum phase distribution
I_a	Apparent Current/cycle (Stress Indicator)
ku	kurtosis
mcc	Modified cross correlation factor
N(t)	Number of discharge pulses over half cycle period
P_i	probability distribution function of the distribution
P_m	Dipole moment
q_a	Cavity internal charge
q_i	discharge magnitude
Q	Discharge Asymmetry
R^2	Determination coefficient
Sk	Skewness
sym'x'	Symlets family wavelet functions
thr	Threshold
U_{cav}	Voltage over the cavity center
U_{crit}	Critical Voltage for discharge process
U_{ext}	Critical Voltage for discharge extinguishing
U_i	ignition voltage

α	Weighting factor
γ	correlation coefficient
σ	noise estimating rescaling factor
λ_i	estimated threshold value of the detail coefficient at level i.
μ	mean value of distribution
σ^2	variance of distribution
ϑ	phase asymmetry
τ_{stat}	Statistical time lag

List of Abbreviations

CBWS	Correlation Based Wavelet Selection
CDPV	Contaminants, Defects, Protrusions, Voids
DFT	Discrete Fourier Transform
DSP	Digital Signal Processing
DWT	Discrete Wavelet Transform
EBWS	Energy Based Wavelet Selection
FFT	Fast Fourier Transform
HFCT	High Frequency Current Transformer
HFRC	High Frequency Rogowski Coil
IDWT	Inverse Discrete Wavelet Transform
IIR	Infinite Impulse Response
LDPE	Low Density Polyethylene
LMS	Least Mean Square Method
MSD	Multi-resolution Signal Decomposition
MSE	Mean Square Error
MV	Medium Voltage
NWDLS	Number of Wavelet Decomposition Levels
PD	Partial Discharge
PRPDA	Phase Resolved Partial Discharge Analyzer
QMF	Quadrature Mirror Filters
RMSE	Root Mean Square Error
SNR	Signal to Noise Ratio
SNRBWS	Signal to Noise Ratio Based Wavelet Selection
SSE	Sum of square errors
TBD	Time to Breakdown
WT	Wavelet Transform
XLPE	Cross-linked Polyethylene

Chapter 1 INTRODUCTION

1.1 Background

Nowadays, Medium Voltage (MV) distribution networks include a large infrastructure of expensive underground power cable systems. These cable systems are constructed with either oil-paper or Cross-linked Polyethylene (XLPE) insulation materials. The use of XLPE insulated cables has been expanding in the MV networks over the last few decades. All the new installations and repairing of the old cables are performed by using the XLPE insulated cables [1].

During normal operation, power cables are subject to various kind of stresses which results in insulation deterioration and degradation. The breakdown of the insulation may lead to complete failure of high voltage equipment which results in large outages and disturbances across the distribution networks. Hence, preventive measures must be performed in order to keep the system reliable and avoid costly damages. Insulation diagnostics has been used to examine the cable insulation system. Traditionally, the diagnostics are performed periodically after a certain defined period of operation. This requires the complete shutdown of the equipment and may result in unnecessary maintenance activity. Therefore, predictive maintenance techniques such as condition based maintenance is becoming more common. Condition monitoring also designated as on-line monitoring system constantly monitors the operating characteristics which can project the equipment's health and predicts the expected failure [2].

The partial discharge (PD) measurements have been widely used in the field of insulation diagnostics. Partial discharges are localized electrical discharges which partly bridges the insulation between the electrodes. The detection and continuous monitoring of PD data can provide useful information regarding the insulation condition. As PD occurs before the complete breakdown, PD monitoring can alarm for necessary emergent actions in order to remove the system component before the occurrence of catastrophic failure [3]. Further, it has been observed that polymeric insulation materials, like XLPE, may have a complete breakdown within a few days after the inception of partial discharge. Therefore, many researchers still aim to relate partial discharge to the lifetime of insulation materials. However, defining such a quantitative relationship is difficult to confirm.

Partial discharge measurements are performed with the help of Phase Resolved Partial Discharge Analyzer (PRPDA). This technique is used to analyze the PDs with respect to the phase angle of applied voltage [4]. The PD pattern recorded with the help of PRPDA can be used to recognize the insulation defects which are the root cause of partial discharges. The aim of many researches regarding the PD measurements is to automate the

PD pattern recognition process which allows predicted behavior of partial discharge activity. It is believed that each type of PD mechanism has a unique set of statistical parameters like skewness, kurtosis [2-4]. The variations in PD pattern with respect to phase angle can be reflected by change in these statistical quantities. Different techniques of automated learning such as neural networks, fuzzy logic and clustering are used to compare the PD patterns which allows to predict insulation degradation. Furthermore, the ultra-wideband characteristics of the individual discharge pulses observe by means of non-conventional PD detection methods allows to detect various type of ageing mechanisms taking place inside the insulation [5]. Thus, it is quite possible to devise an intelligent and automated insulation diagnostic system based on the quantification of the partial discharge signals.

1.2 Objective of Thesis

This thesis work is divided into two parts. The first part is related to study about the partial discharge phenomenon in detail. The aim is to interpret the variations in the partial discharge characteristics over the insulation ageing period in terms of physical phenomenon's taking place in PD sources. The results of this work are based on the partial discharge measurements for lifetime tests conducted over the MV XLPE cable samples at High Voltage Laboratory.

Second part of the thesis work is related to analyzing the de-noising methods with the aim to create an automated and self-adaptive de-noising algorithm. The devised algorithm de-noises the partial discharge signals coupled with different kind of noises without the human participation which is the key requirement in establishing an online partial discharge monitoring system.

1.3 Organization of Thesis

The thesis is organized into the following chapters:

Chapter 2 gives general background about the XLPE insulation. The process of XLPE manufacturing is studied and different type of partial discharge mechanisms are investigated that affect the cable insulation.

Chapter 3 deals with the in depth study about the partial discharge theory. The discharge mechanisms and an approach to model the partial discharge process has been studied. Furthermore, the partial discharge characteristics both statistically and time & frequency domain analysis has been examined.

Chapter 4 describes the experimental setup established for measuring the partial discharge. The results from the laboratory measurements and analysis has been provided.

Chapter 5 gives introduction about the de-noising of partial discharge signals. Different existing DSP techniques for de-noising have been examined.

Chapter 6 introduces the Wavelet transformation (WT). Different stages of WT has been studied and investigated. Conclusions have been made for each step of WT.

Chapter 7 deals with algorithms of different de-noising methods presented in the literature with their analysis on the basis of various performance indices.

Chapter 8 presents the novel self-adaptive technique. The basis of this algorithm and methodology has been presented. Performance comparison with the other existing de-noising methods has been also provided at end.

Chapter 9 summarizes the results and present the conclusions observed by the experimental work. Few ideas about the future research in this field has been discussed as well.

Chapter 2 CROSS-LINKED POLYETHYLENE (XLPE) INSULATION

2.1 XLPE Manufacturing

XLPE is formed by mixing low density polyethylene (LDPE) with the activation chemical agent i.e. dicumyl peroxide. During the cable manufacturing, the mixture is pressed on to the conductor for forming the inner conductor screen, main insulation and outer semi-conducting layer. This method is known as triple extrusion as all the layers are extruded at the same time. XLPE is finally formed when the insulated core is passed through pressurized and heated nitrogen gas. High heat and pressure effects the polyethylene molecular crosslinking structure which results in improved physical and electrical properties [1].

During XLPE manufacturing process, several crosslinking byproducts are formed. These include water bubbles forming inside the crosslinked polyethylene. Other harmful and reactive chemical agents such as acetophenone and cumyl alcohol are also formed during crosslinking polyethylene [6]. In addition, while cooling down the cable, residual mechanical stresses are formed inside the insulation due to difference in the temperature gradients. These stresses may not be uniformly distributed across the cable insulation resulting in large number of stress points. It is reported that these residual mechanical stresses or stress points are the weakest points in insulation where electrical trees can be originated which eventually leads to cable breakdown [7].

2.2 Degradation of XLPE

The mechanisms involved in XLPE ageing are not fully understood. The XLPE insulated transmission cables are aged under different kind of stresses such as thermal, mechanical and electrical over long periods of their operation. Ageing of XLPE insulation also depends on the environmental conditions. It has been observed that the insulation dielectric strength reduces much faster in wet conditions as compare to dry conditions [8].

Ageing factors are classified as either extrinsic or intrinsic. Extrinsic aging is due to presence of voids, small imperfections, contaminants etc. in the insulation core. They can either grow during the manufacturing process or during the normal operation. On the other hand, intrinsic ageing is due to changes in physical and chemical properties or due to the presence of trapped charges inside the insulation. Intrinsic ageing affects the properties of insulation material, e.g. the loss of tensile strength in polyethylene degradation. However, these changes may not necessarily lead to electrical breakdown [8]. The extrinsic ageing affects the insulation only at the localized channels whereas the intrinsic ageing is considered to have larger impact on greater part of insulation. For example, thermal degradation of the insulation material.

The polymers do not achieve their crystalline structure right after the manufacturing process. The process of curing can take several years. During this time, micro cavities and locally dense areas may form inside the polymeric insulation. These areas may accelerate the electrical degradation process and eventually lead to electrical breakdown [1].

2.2.1 Electrical Degradation

Electrical, mechanical and chemical stresses are the major mechanisms for polymeric insulation degradation. However, electrical degradation is considered most dangerous for creating severe defects in the polymeric insulation. Electrical degradation is a local phenomenon as compare to other degradation methods which affects the whole cable length [1]. Electrical degradation of insulation takes place in the form of partial discharges, electrical treeing and water treeing phenomenon's. The presence of contaminants, defects, protrusions and voids (CDPV) inside the insulation are the major stress points for these degradation phenomenon's. It is impossible to remove the presence of CPDVs completely from the polymeric insulated cables. Cable terminations and joints are most likely sites for the formation of CPDV's and considered as most vulnerable to insulation ageing. However, CDPV's influence on the insulation ageing is relatively small if their intensity is controlled to very low levels during XLPE manufacturing process [9].

2.2.2 Water Treeing

The major part of medium voltage cable network is installed underground. Therefore, the power cables are exposed to moisture contents available in the environment. This makes the underground cable susceptible to water treeing degradation. The water trees can be initiated by penetration of water inside the insulation from the outside environment through faulty joints or terminations [1]. The polyolefin's are capable of absorbing 2000 to 5000 ppm of water depending on the crystalline structure which in the case of polyethylene is directly related to the material specific density [6]. Also, the presence of impurities inside the insulation will increase the risk of water tree initiation. Small water bubbles are formed while crosslinking polyethylene during XLPE manufacturing [8]. Water tree retardant's like polyphenol compounds are used to cease the initiation of water trees.

Two types of water trees exist in extruded type cable insulation, bow tie and vented or streamer trees. Bow tie trees grow due to the presence of the soluble contaminants or water filled voids inside the insulation. The bow tie trees tend to grow only for some tens of μm and do not cause a significant effect on insulation degradation at the stress levels used in the medium voltage cable networks i.e. 2kV/mm [9]. On the other hand, the vented trees grow at the interfaces such as between semi-conducting screens and insulation. The vented trees propagate continuously in the direction of electric field and may cover the whole insulation thickness. The vented trees may take a longer time to initiate, however, they cause more severe degradation as compared to bow tie trees [1].

The presence of water inside the insulation accelerates the degradation process by providing free ions and forming electrolytes. The resulting water trees cause local stress enhancement which may initiate the electrical tree sites. In addition, at high temperature significant amount of oxidation may occur inside the water trees. This can lead to increase absorption, higher conductivity and eventually thermal runaway [9]. However, at lower temperatures the oxidation phase is slow which results in longer time for converting them into electrical trees. It has been observed that the partial discharges do not occur in the water trees. Only when the electrical trees are originated from the water trees then the PD's may occur. Water trees are formed at lower electrical field strength $E < 10^7\ Vm^{-1}$ as compare to electrical trees $E < 10^8\ Vm^{-1}$. Hence, it is necessary to protect the cable from the water contaminations particularly if installed at the moist environments.

2.2.3 Electrical Treeing

The presence of CPDV's within insulation and formation of gas bubbles during the manufacturing and installation of cables results in a partial breakdown of insulation under high electric fields. Consequently, positive ions and electrons are formed which degrades the insulation due to their collisions with the insulation surface. The partial breakdown phenomenon can lead to formation of a locally concentrated region of degradation inside the insulation. A tree or bush-like conducting canal starts to develop. This conducting canal is known as an electrical tree [1]. Figure 2-1, shows few examples of discharge channels developing in the insulation material [10].

Electrical trees are small conductive channels formed inside the insulation that propagates relatively quicker within insulation to cause complete failure. They can be initiated from the eroded surfaces in the void, water trees or due to increased stress enhancements at microcavities within the polymer insulation. For the latter cause, there are two phases of formation of electrical trees [9]:

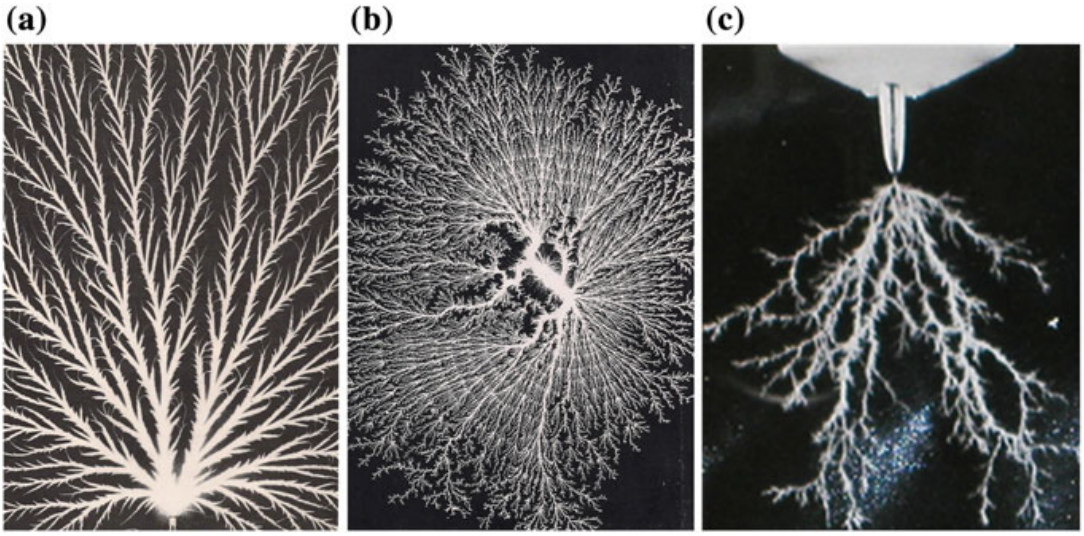

Figure 2-1 Different types of electrical treeing structures [10]

1. The first phase is the formation of a small void. The charge motion (0,1 – 0,2 pC) during each half cycle of applied voltage degrades the strength of insulation resulting in the formation of a small void.
2. The growth phase is the formation of tree-shaped electrical network from the initial void due to the occurrence of PD within the conductive branches.

The presence of impurities, contaminants or defects which are produced accidently during the manufacturing and synthesis of XLPE play a central role in the initiation phase of electrical trees. Due to electric field enhancement at these sites, phenomenon's such as charge injection and electroluminescence occurs inside the insulation. Above a certain threshold voltage, polymeric insulation emits light in the visible and ultraviolet spectra due to injection of the electrons and holes and their recombination at luminescent centers. It is recognized that the UV light photo-degrades the insulation due to photochemical reactions which create free radicals and break bonds, ultimately leads to the formation of a micro cavity and subsequently an electrical tree. The presence of oxygen in the free volume of the insulation also plays a significant role in the photo degradation of the material. The absence of oxygen inside the insulation will result in higher tree inception voltage as compared to that of the normal polymer [11].

During the growing phase of an electrical tree, cracks and voids produce partial discharges and counter discharges which can provide more than 10eV of kinetic energies to the electrons. These micro-cavity discharges can lead to increase in the cavity size and higher discharge energies but the formation of the free radicals limits the massive failure expansion [6]. However, discharges of 5 pC energy are sufficient to create thermal runaway and extensive thermal degradation of the polymer [8].

The growth rate of electrical tree depends on the applied electrical stress, temperature and environmental conditions. Total breakdown of the insulation can happen when the branch of electrical tree bridges the electrodes. However, it is also possible that the electric breakdown may occur before the electrical tree bridges the electrodes [1].

Chapter 3 PARTIAL DISCHARGE THEORY

3.1 Partial Discharge in Cavities

As previously mentioned in chapter 2, due to the presence of impurities and formation of gas bubbles during the manufacturing and installation of the cable, micro-cavity and stress enhancement sites are formed within the solid insulation. Formally, a cavity is defined as gas-filled void in a solid insulation material. A cavity is a weak point of insulation as it has relatively lower electrical permittivity and breakdown strength as compared to rest of solid insulation. This leads to local electric field enhancement which may exceed the intrinsic field strength resulting in the ignition of self-sustaining electron avalanches [10]. Partial discharge occurs within the cavity at higher voltage stresses. Partial discharges inside the cavity degrade the insulation material through the combination of chemical, mechanical, thermal and radiative processes [12]. All these mechanisms lead to local electric field enhancement which eventually results in the concentration of PDs at the cavity site.

3.1.1 Partial Discharge (PD)

Partial discharge is defined as localized small electric discharge either on the surface or inside the insulation which does not completely bridge the electrodes. These discharges appear as pulses having a duration of much less than 1 μs. Partial discharges deteriorate the insulation but it does not cause immediate failure or breakdown. If the partial discharges continue to occur for a long time, it might take up to several years for the complete failure of the insulating properties [13]. There are two necessary conditions for initiation of partial discharges within a cavity:

1. The electrical field strength must be larger than certain critical value
2. Free electrons must be available to start the electron avalanche

If the electric field is below the critical field, the amount of electron generation is not sufficient to keep the discharge self-sustained [12]. The phenomenon of partial discharges is associated with the ionization of gas molecules as shown in Figure 3-1 [12]. PD's ionize the gas in the cavity and the resulting charges move towards cavity surfaces in the direction of electric field. These charges get trapped at the cavity surface resulting in net accumulation of the cavity charge which opposes the applied electric field. Thus, leading to the extinction of the discharge within a cavity.

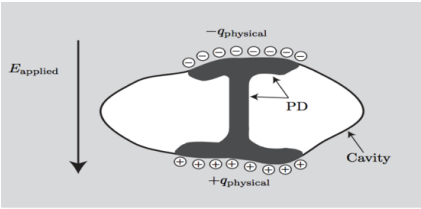

Figure 3-1 Schematic representation of PD inside a cavity [12]

3.1.2 Statistical Time Lag

During the PD activity, it is quite possible that the electrical field in the cavity exceeds the critical value for PD ignition without the start of any discharge. This might happen due to lack of free electrons. The average waiting time for a free electron to appear given that the electrical field condition for PD is fulfilled is known as statistical time lag (τ_{stat}) [12].

The effect of statistical time lag is to shift the PDs forward in phase at larger values of the applied electric field. This results in larger PD magnitudes. The statistical time lag decreases with the increase in the rate of electron emission inside the cavity [14].

The initial free electrons are generated through the surface emissions at the cavity walls during an ongoing PD event. In addition, the electrons are also released due to ion and photon impact. These events can be best described by Richardson –Schottky law for thermionic emissions. On the other hand, in the virgin cavity where no PD event has occurred the free electrons are released due to radiative gas ionization. The rate of electron emission during this initial phase is relatively constant [15].

3.1.3 Surface Charge Decay

Due to surface conduction and recombination, the trapped charges at the cavity surface decreases with time. The trapped charges diffuse into deeper traps in the surface which further reduces the availability of free electrons. Subsequently, the electron emission as well as the electric field in the cavity reduces [15,16]. In the case of charge diffusion, the electron emission decreases as electrons in deeper traps are difficult to be emitted as compared to the electrons in surface traps. However, the charge diffusion process has a less significant effect on the reduction of electrical field [14].

3.1.4 Ageing Mechanisms

As discussed earlier, the partial discharges inside a cavity cause degradation of the cavity surface. Partial discharge activity is accompanied by several other aging mechanisms which accelerate the degradation process. It is observed that during the aging of polymeric insulation, the gas pressure inside the cavity reduces and a layer of discharge by-products are formed on the cavity surface which changes the cavity surface properties [16]. The experimental results presented in [17] concludes that the surface conductivity of cavity increases during initial few hours of PD exposure and then tends towards saturation point. Also, this increase in surface conductivity is not necessarily be accompanied by the increase of discharge amplitude. However, the change in cavity surface properties affects the PD activity. Different type of discharge mechanisms such as streamer-like, Townsend-like and pitting discharges are observed inside the cavity during the time of PD exposure [16].

3.2 Partial Discharge Modeling

It is a matter of great interest for researchers to somehow correlate the actual PD activity with different modeling methods. It is a quite challenging task to suggest a single model for PD activity due to the involvement of many physical parameters which are hard to determine. In order to analyze PD activity, simple geometrical shape cavity surfaces such as cylindrical, spherical and elliptical cavities are investigated instead of more realistic imperfections are taken into account. The main aim of these models is to describe the sequence of PDs in cavity against a time scale which is comparable with the time period of applied voltage [12].

An approach based on sub-dividing a PD model was suggested by [15]. His method is based on dividing the PD event into five parts: classification and characterization of a defect, local electric field enhancement, generation of initial electrons, discharge process and finally charge. A brief introduction to these modeling steps is presented in the following sections.

3.2.1 Defect Classification and Characterization

The defects are classified on the basis of parameters which are dependent on the geometry and size of the defect. The first parameter is normalized voltage U at the defect site compared to the applied voltage U_0 i.e. $\mu_o = \frac{U}{U_0}$. It defines how the insulation system controls the electric field at the defect location. The second parameter λ_0 characterizes the location of the defect to the electrode at which the PD signal is measured. A detailed theoretical background of these parameters is presented in reference [15]. Furthermore, the nature of defect boundary also affects the partial discharge activity. For example, the insulating surface (insulated cavity) has the discharge characteristics different from the conducting surface (electrode bounded cavity) [12].

3.2.2 Local Electric Field Enhancement

The electric field inside the cavity is composed of two parts: the local field due to the surface charges left by the previous PD event and the background field due to the applied voltage. Depending on the choice of method used to calculate the local electric field inside the cavity, PD models are divided into different groups. Among them, an electric circuit model known as Capacitive (abc) PD model has been widely used by researchers. Due to various limitations of capacitive PD model, an alternative PD model based on dipole moment was introduced by Pedersen.

A. Capacitive PD Model

Figure 3-2 (a) [12] shows the schematic diagram of the Capacitive PD model introduced by Whitehead and Kruger in 1950s. This model has been extensively used in research for calculating the relationships between the detectable external PD charge and the internal PD charge at the cavity site. C_c represents the cavity capacitance; C_b' and C_b'' represents the stray capacitance of healthy insulator between cavity and electrodes whereas C_a' and C_a'' are the capacitance of the bulk insulator between cavity and electrodes. The equivalent circuit is reduced to the form shown in Figure 3-2 (b) [12] by putting $C_b = \frac{C_b' C_b''}{C_b' + C_b''}$ and $C_a = C_a' + C_a''$. Due to these characteristic capacitances, this equivalent model is traditionally referred as abc-model.

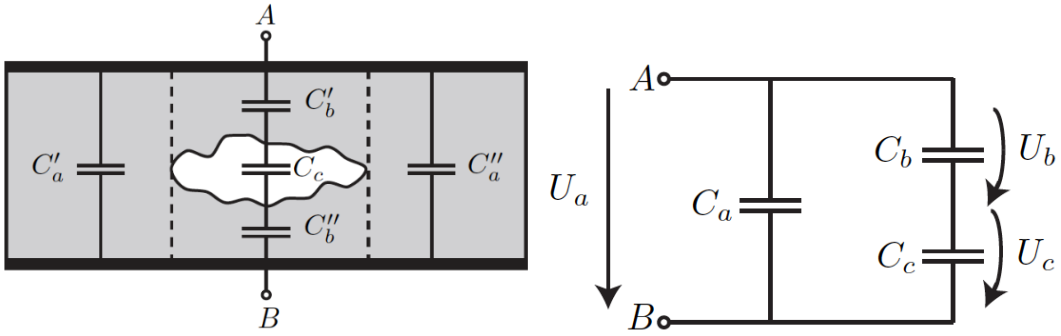

Figure 3-2 Capacitive (abc) model [12]

The critics of abc-model are of the viewpoint that PD activity cannot be modeled by the equivalent capacitance which does not reflect the physics of the gas discharges insides the cavity [10,18]. Ionization of gas molecules inside the cavity creates space and surface charges due to which the cavity surface can not be represented as an equipotential surface. Therefore, the concept of capacitance is not well suited for describing the PD activity.

B. Dipole Model

A concept based on dipole moment was established in order to describe the method for estimating the charge inside the cavity [10,15,18,19]. Due to the presence of space charges of both polarities on the cavity boundary as a consequence of the ionization process, a dipole moment is established. Figure 3-3 [10] illustrates the formation of the dipole model inside the cavity discharge. Field due to the space charges is referred as Poisson field which opposes the electrostatic field (background field) due to the applied voltage. Therefore, during ionization process of PD discharge, the discharges are quenched immediately within nanoseconds range.

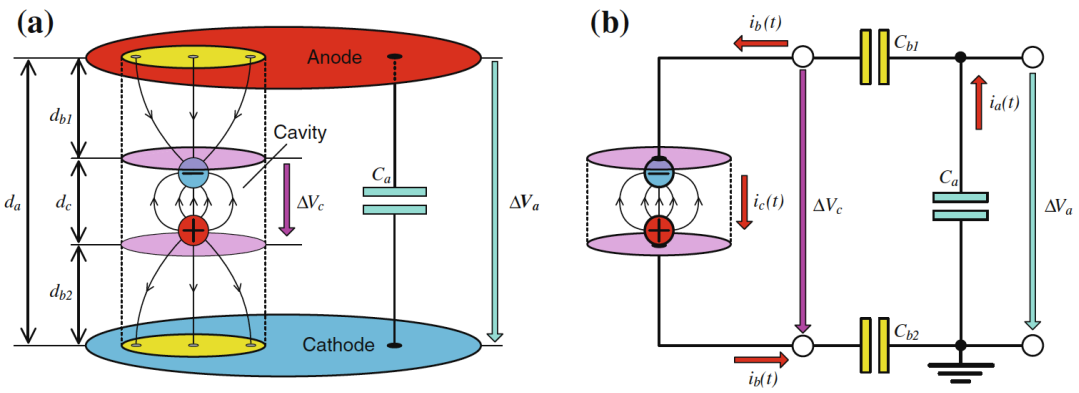

Figure 3-3 Dipole Model of Cavity Discharge [10]

The dipole moment is given by the term $P_m = e.n_i.d_c$ for the PD model described in figure above. The charge delivered from the electrodes of the test object i.e. cavity boundary can be written in terms of dipole moment by the following equation [10]:

$$q_a = e.n_i.d_c.\frac{E_i}{V_i} = P_m.\frac{E_i}{V_i} \qquad (1)$$

where E_i represents the inception field strength.
A comparison between the abc-model and dipole model based on the computer simulations is given in the section 4.8.1. Also, in order to ascertain the models validity, the experimental PD results are compared with simulation values.

3.2.3 Initial Free electrons generation

Initiation of the first electron in order to start the avalanche of the ionization process is considered as the most necessary condition for starting partial discharge activity. The initiation of free electron also controls several statistical parameters such as charge delay, frequency of occurrence and distribution of discharge with respect to the phase of applied voltage. In order to model the electron generation mechanism, an approach based on estimating the electron generation rate is usually used. Two major factors distinguish the electron generation rate, first the generation of free electrons due to the background radiation and second due to field emission from the cavity surface [15]. While modeling the electron generation rate, it is assumed that the electron generation due to field emission is much more dominant than due to background radiation.

The electron generation rate can be modeled with the help of using Richardson-Schottky law. The modified form of this law is given by equation (2) where N_e (number of electrons generated per unit time) is electron generation rate, N_{eo} is constant, U_{cav} is voltage over the cavity center and U_{crit} is the critical voltage for discharge process to takes place [20].

$$N_e(t) = N_{eo} \exp\left(\frac{U_{cav}(t)}{U_{crit}}\right) \qquad (2)$$

Provided that the electric field condition is satisfied ($U_{cav} > U_{crit}$), the probability of free electron generation inside the cavity during the time interval $[t, t + \Delta t]$ is assumed as $N_e(t)\Delta t$. The corresponding probability distribution function is given by equation (3). Using the Monte Carlo procedure, the partial discharge event can be simulated in the following way:

1. Random number (R) uniformly distributed in range [0,1] is generated for each time step.
2. The future values of N_e are calculated to estimate the value of F from equation (3).
3. If F > R, PD event occur at the time step, otherwise it is not.

$$F(t) = 1 - \exp\left(-\int_0^t N_e(t')dt'\right) \quad (3)$$

3.2.4 Discharge Process

The most common approach to model the actual discharge process in a cavity is estimating the instantaneous voltage drop across the cavity. The voltage drop instantaneously effects the charge across the cavity surface. The voltage drop can be determined from the critical voltage, statistical time lag and critical extinction voltage of PD [15,21]. In the most common PD models based on capacitive (abc) model, the discharge process is modeled with a streamer resistance.

An alternative approach based on the increase in conductivity inside the cavity can be used to model the discharge process [20]. The increase in surface conductivity results in a current flow through cavity which subsequently decrease the cavity voltage U_{cav}. As U_{cav} decreases below a critical voltage U_{ext} , the surface conductivity decreases which quenches the discharge. It is common to assume that a PD in a cavity affects the whole cavity. Hence, the surface conductivity discharging radius can be considered constant for the whole process.

3.2.5 Charge

Most common PD models describing the physical phenomenon of PD calculates the physical charge on the basis of voltage drop across the cavity. In case of abc-model the physical charge is given by the following equation:

$$q_{phy} = C_c \Delta U_c \quad (4)$$

Similar approach is used in the model proposed by Niemeyar [15] in which the capacitance is expressed by a constant 'g'. However, in these capacitive PD model, the apparent charge is related to physical charge by the λ function which is defined earlier in defect classification section.

In the case of dipole model, the charge is calculated on the basis of current caused by the charge carriers which are moving inside the cavity like the displacement current [10]. Using this approach, the detectable external PD charge must be equal to the internal PD charge flowing inside the cavity. The detectable charge calculated on the basis of dipole model is given by the equation (1)

3.3 Partial Discharge Characteristics

During PD measurements, it is impossible to measure the true shape of PD current pulses owing to the fact that exact PD defect location is not accessible. Therefore, the PD signals are measured at the test object terminals. Under this condition, the useful frequency content of the measured PD signal is reduced due to attenuation and dispersion while propagating from the PD source to test object terminals. Nevertheless, it is common to describe the characteristics of partial discharge on the basis of two methods; statistical parameters and time & frequency domain discharge pulse characteristics. The statistical analysis includes the phase resolved partial discharge pattern classifications. The statistical analysis is performed to calculate different fundamental quantities related to PD over definite acquisition period which can be further used to deduce various statistical operators. The second method is to analyze the shape parameters of the discharge pulse which includes both time and frequency domain waveforms of individual PD pulses.

3.3.1 Statistical Analysis

A large number of discharge quantities can be determined in order to study the behavior of several statistical parameters over the insulation lifetime. These quantities can be subdivided into three categories with respect to the observation time as shown in Figure 3-4 [22]:

1. The fundamental quantities, which are observed during one voltage cycle.
2. The derived quantities, which are integrated values of fundamental quantities over several voltage cycles depending on the set acquisition period.
3. Statistical operators, which are statistically deduced parameters from the derived quantities.

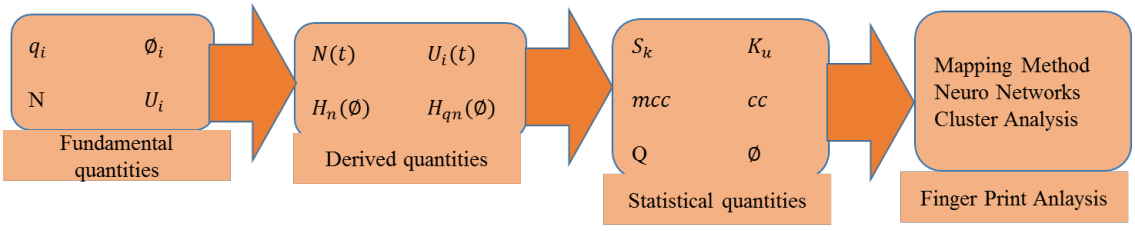

Figure 3-4 Block diagram for statistical analysis of PD related quantities

A. Fundamental Quantities

Three fundamental quantities: discharge magnitude q_i, ignition voltage U_i and discharge position with respect to phase angle $\emptyset_i$ of test voltage can be used to represent the partial discharge activity. In addition, the number of discharges N for each half period of voltage cycle can also be processed to describe the whole discharge process.

B. Derived Quantities

The derived quantities are used to analyze the behavior of partial discharge activity as a function of phase angle and as a function of time. In order to derive these quantities from the fundamental quantities, the observation period must be longer than the duration of the voltage cycle.

It is known that during the course of aging period the PD activity goes through statistical variations both in magnitude as well as the temporal behavior of discharges. These variations may take place partly due to the changes in the discharge sites e.g. creation of several conductive discharge channels. Therefore, the derived quantities such as a number of discharge pulses over half cycle period $N(t)$ and time variation of the inception voltage $U_i(t)$ are processed to describe the condition of insulation at discharge sites.

The derived quantities as the function of phase angle are usually observed in order to describe the recurrence behavior of the PD activity. The commercially available phase resolved partial discharge analyzers (PRPDA) records the partial discharge activity by dividing the whole voltage cycle into phase windows (0 to 360°) for some certain acquisition period. Therefore, it is possible to determine the several discharge quantities for each phase window over several voltage cycles. These discharge quantities include: sum of discharge magnitudes, number of discharges, average value of discharges and maximum value of discharges. The observation of these discharge quantities over the whole phase angle axis can provide the distribution of discharge recurrence as a function of the phase angle. These pulse distributions as function of phase angle provide useful information on the phenomenon causing these distributions [22]. Following phase-position quantities are usually observed during the experimental PD studies:

- **Pulse count phase distribution** $\boldsymbol{H_n}(\emptyset)$ which is used to represent the number of discharges in each phase window as a function of phase angle.
- **Mean pulse height phase distribution** $\boldsymbol{H_{qn}}(\emptyset)$ which is used to represent the average amplitude of discharges in each phase window as a function of phase angle. It can be derived from the total discharge amount in each phase window $\boldsymbol{H_{qs}}(\emptyset)$ divided by pulse number of discharges $\boldsymbol{H_n}(\emptyset)$ for the same phase window.

- **Maximum pulse height phase distribution** $\boldsymbol{H_{qm}(\emptyset)}$ which is used to represent the maximum amplitude of discharges in each phase window as a function of phase angle.

Figure 3-5, gives an example of the type of phase-position distributions for one particular acquisition period for both the positive and negative half of voltage cycle. Similar discharge patterns and distributions can be expected for each half of the voltage cycle if the internal discharge inception conditions remain same. According to many researchers, the time dependence of $\boldsymbol{H_{qn}(\emptyset)}$ and $\boldsymbol{H_n(\emptyset)}$ provides information about the changes in the discharge patterns. For example, $\boldsymbol{H_n(\emptyset)}$ quantity allows the recognition of discharge sources and their behavior in time.

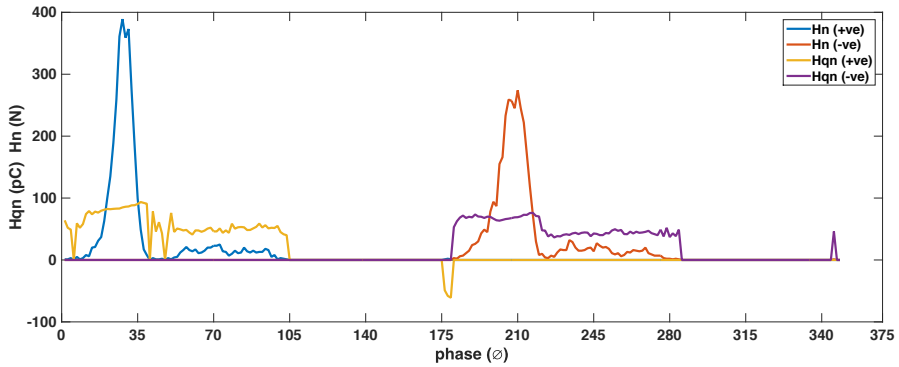

Figure 3-5 Typical distribution of phase-position quantities, $H_n(\emptyset)$ pulse count distribution and $H_{qn}(\emptyset)$mean pulse height phase distribution

C. Statistical Operators

Several statistical operators such as skewness Sk and kurtosis ku provides significant information about the shape of distribution. They can be used to characterize the distribution functions $\boldsymbol{H_{qn}(\emptyset)}$ and $\boldsymbol{H_n(\emptyset)}$ more precisely [22]. In addition, many other derived statistical operators are also defined in order to study the difference between the distributions in both halves of the voltage cycle. Brief introduction about these statistical operators is given below:

a. Skewness *Sk* & Kurtosis Ku

Skewness indicates the asymmetry of the distribution as compared to the normal distribution. It is calculated by the following equation:

$$Sk = \frac{\sum(x_i - \mu)^3 . P_i}{\sigma^3} \qquad (5)$$

where μ is the mean value of distribution, σ^2 is the variance of distribution, x_i Is the magnitude of discharge quantity in phase window 'i' and P_i is the probability value for phase window 'i' calculated from the probability distribution function of the distribution.

Skewness is zero for totally symmetric distribution, it is positive for the left skewed asymmetric distribution and negative for the right skewed asymmetric distribution. In contrast to skewness, kurtosis indicates the sharpness of the distribution with respect to the normal distribution. Kurtosis is positive for sharper distribution and negative if distribution is flatter than normal distribution. It is calculated according to following equation:

$$Ku = \frac{\sum(x_i - \mu)^4 . P_i}{\sigma^4} - 3 \tag{6}$$

For normal distribution kurtosis is 3. Therefore, the kurtosis value is subtracted by 3 as illustrated in the equation 6.

b. Discharge Asymmetry

The discharge asymmetry defined as Q is given by the following equation:

$$Q = \frac{Q_s^- \ / \ N^-}{Q_s^+ \ / \ N^+} \tag{7}$$

where Q_s^- and Q_s^+ are the sum of discharges of the $\boldsymbol{H_{qn}}(\emptyset)$ for the positive and negative half of voltage cycle; N^- and N^+ are the number of discharges of the $\boldsymbol{H_n}(\emptyset)$ for the positive and negative half of voltage cycle.

c. Phase Asymmetry

The phase asymmetry ϑ is used to study the difference in inception voltage for the positive and negative half of the voltage cycle. It is given by the following equation:

$$\vartheta = \frac{\vartheta_{in}^-}{\vartheta_{in}^+} \tag{8}$$

where ϑ_{in}^- and ϑ_{in}^+ are the inception phase of the $\boldsymbol{H_{qn}}(\emptyset)$ for the positive and negative half of voltage cycle.

Both discharge and phase asymmetry are defined in such a way that they are equal to one in case of totally symmetric distributions and less than one in case of asymmetric.

d. Cross-correlation factor

The cross-correlation factor cc is used to describe the difference in the shape of distributions $\boldsymbol{H_{qn}^+}(\emptyset)$ and $\boldsymbol{H_{qn}^-}(\emptyset)$**.** It is defined by the following formula:

$$cc = \frac{\sum xy - \sum x \sum y/n}{\sqrt{[\sum x^2 - (\sum x)^2/n][[\sum y^2 - (y)^2/n]]}} \quad (9)$$

where x and y are the mean discharge magnitudes of the positive and negative half of voltage cycle for corresponding phase windows and n is the total number of phase windows in one half voltage cycle.

Cross-correlation value of 1 indicates complete symmetry whereas cc value of zero means totally asymmetry. The cc value does not indicate the height of the distribution. However, using phase and charge asymmetry the distribution height can be defined. Therefore, an operator mcc is defined by multiplying the three asymmetry factors [20].

e. Modified cross-correlation factor

This factor mcc as defined above is used to describe the discharge patterns in the positive and the negative voltage cycle. It is evaluated as the product of phase asymmetry ϑ, charge asymmetry Q and cross-correlation factor cc.

$$mcc = \vartheta . Q . cc \quad (10)$$

3.3.2 Ultra-wideband (UWB) Partial Discharge Characteristics

Recently, the time-resolved measurements gained significant importance in the field of studying discharge mechanisms on different kinds of insulations. The availability of highly sensitive and large bandwidth RC type detectors for measuring partial discharge signals has made it possible to observe and analyze shape characteristics of discharge pulses both in time and frequency domain.

Formerly, due to the phase shaping circuitry and low bandwidths of the detection system, it was not possible to preserve the shape of electrical discharge pulse. Furthermore, if the time constant of the detector is longer than the width of discharge pulse, integration of discharge pulse is performed which is not a well-suited method to study the discharge mechanisms. The ultra-wideband or time resolved system can be used to study the temporal behavior of the discharge process in the nanoseconds range [5]. With the development of ultra-wideband digital oscilloscopes having bandwidth up to several GHz, the true pulse shape can be preserved and can be further related to physics of discharge process.

A. Time Resolved Discharge Parameters

When the partial discharge signal is recorded with the help of UWB detection circuit, several discharge parameters can be measured to describe the true shape of PD pulse. Figure 3-6 illustrates the discharge pulse shape parameters which are described below:

- **Rise Time:** the time interval between 10% and 90% of PD pulse amplitude.
- **50% pulse width:** it's the time interval between 50% PD pulse amplitude during rise and fall of pulse.
- **20% pulse width:** it's the time interval between 20% PD pulse amplitude during rise and fall of pulse.
- **Pulse height:** The maximum PD pulse amplitude.

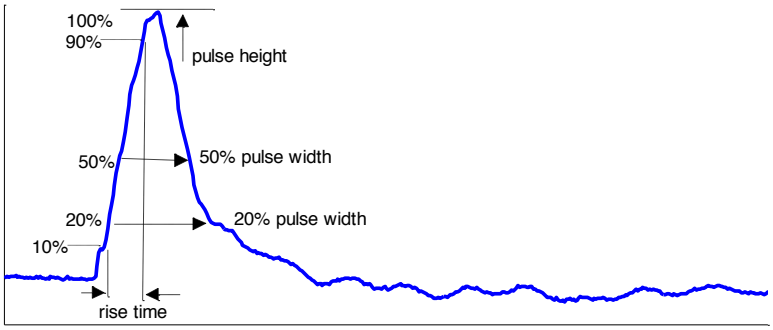

Figure 3-6 Time resolved partial discharge parameters

B. Characteristic Discharge Pulses

The recognition of partial discharge characteristics based on the time-resolved parameters provide significant information regarding the physics of discharge process. It has been observed that the shape of PD pulse changes significantly over the prolonged insulation aging [5]. Discharge pulses with extremely short rise time and pulse width are observed during the initial phase of an electrical tree inside the insulation. These discharge pulses have characteristics similar to streamer like discharge pulses.

After the severe degradation of the insulation over a long period, the discharge pulses show characteristics of very high-intensity discharge activity. The pulses have characteristics quite similar to pitting type discharge pulses indicating the formation of small pits across the discharge cavity. These discharge pulses have very small rising time and relatively smaller discharge pulse widths. The very fast rising front of discharge pulse also indicates the presence of high-frequency energy contents in the frequency spectrum. These discharge theories have been observed during the lifetime tests of insulation aging and verified by the experimental results provided later in this study.

3.4 PD Diagnostics

Depending on the nature of the insulation material, different diagnostic methods are used in order to detect the actual condition of the insulation or to monitor the changes in the insulation condition. For example, in paper and oil insulation systems, primarily diagnostics are performed in order to analyze the moisture content or detect the formation of gasses inside the insulation. However, in polymeric insulation's dielectric response and lately the partial discharge measurements are used as diagnostic methods. Further, the

diagnostic methods are divided into two categories: destructive and non-destructive methods. In recent years, the concept of online condition monitoring of electrical equipment has gained significant importance which requires the diagnostic methods to be non-destructive in nature [23].

PD diagnostic method is extensively used for early detection and localization of the failure inside the electrical insulation of the underground cable. The accuracy of diagnostics depends on the technique used for measurement, continuous or periodic monitoring method and performance of the PD detecting sensor. The continuous monitoring of the system involves obtaining the data from the equipment under observation with the help of implemented sensors. After that, the data is analyzed using calculations, historical trends or by signatures which provide enough information to evaluate the state of equipment.

Due to PDs low amplitude and high-speed transient nature they cannot be detected with the help of conventional protection system or by the smart fault location devices and algorithms. Therefore, high-frequency sensing technologies are needed to monitor the PD activity. However, during the PD activity energy is released in the form of heat, acoustics, sound, electromagnetic radiations or ultraviolet light. Considering the high frequency and bandwidth requirements for PD detection, induction sensors like HFCT and HFRC are usually preferred for the underground cable network [23].

3.4.1 PD Pattern Recognition

The PD patterns as described earlier are helpful in predicting the insulation degradation behavior. Theses patterns can also be used to distinguish between the different PD mechanisms. This allows the experts to analyze the PD pattern after regular time intervals and diagnose the condition of electrical insulation. However, in order to reduce the human involvement, the continuous PD monitoring requires the techniques to automate the pattern recognition process. Different methods based on neural networks, fuzzy logic and cluster analysis have been proposed in research. All these methods require distinctive learning techniques for the discharge patterns [2].

The use of neural networks for automated PD recognition requires pre-processing of the PD data in terms of statistical parameters. The learning process can be online and continuous or it can be based on previously processed statistical data. Once the learning process completes, the undetermined PD pattern can be compared and processed in order to evaluate the cause of PD defect.

Another PD pattern recognition tool which characterizes the PD parameters with the physical phenomenon is based on the fuzzy logic [2,24]. This method defines the number of vague and non-specific set of rules on the variables deduced from the actual PD characteristics. For example, the PD pulse magnitudes are set as one variable and set of rules then define the cause and size of the PD defect. However, in order to define the PD mechanism, numerous variables are required. There are many possible variations in these

variables making the whole pattern recognition process random and complex. In addition, a large number of rules have to be devised which complicates the application of fuzzy logic.

The fuzzy logic is usually performed on the clusters of the 3D PD patterns created by the PRPDA [25]. Figure 3-7 [13] illustrates the process of discriminating different failure mechanisms on the basis of identifiable clusters. This technique is also known as fractal analysis.

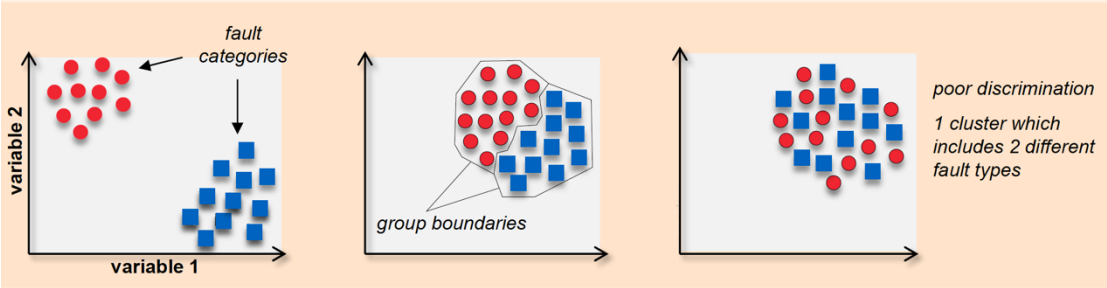

Figure 3-7 Cluster mapping of variables [13]

3.4.2 Limitations of Applying PD Diagnostics in Cables

In distribution network systems, a large number of parallel MV feeders originate from the primary substation to distribute the electrical power. The distribution network follows the interconnected network by using the ring main units (RMUs) which require a large number of cable branches and sections for better system reliability. Each RMU has multiple incoming and outgoing cables, all of them contains numerous cable joints and terminations. Therefore, it is difficult to judge the exact location of the PD faults as they can be located anywhere in the network [23].

Chapter 4 TEST SETUP & EXPERIMENTAL RESULTS

It was known that degradation of the XLPE insulated cables can be detected by means of electrical measurements and the cable age must have a correlation with the experimental electrical measurements which in this study are partial discharge measurements. Hence, an experimental setup was established to perform the lifetime tests in the High Voltage laboratory of Aalto University. The tests were carried out on XLPE insulated medium voltage cables.

4.1 Preparation of Specimen

Specimen preparation setup was established with the aim of producing similar and small size cable samples with minimum mechanical stresses applied during their preparation. Careful considerations regarding the preparation of cable sample were taken into account. The major problem expected was the inception of corona at the cable terminals at low voltages which hinder the establishment of discharge free experimental setup.

4.1.1 Cable Sample

As mentioned earlier, cable samples of 24kV rated light power MV cables with XLPE insulation thickness of 4.3mm were used. Due to limitations of mechanical tools used in sample preparation, 50 cm small cables samples were prepared. The outer jacket and insulation screen were removed which leaves the cable with XLPE insulation and conductor screen with center conductor as shown in the Figure 4-1. The mechanical tools which are used in order to prepare the test specimens are also shown in same figure. To produce a more realistic test specimen, the insulation screen was not removed from the center of cable where the voltage stress was applied.

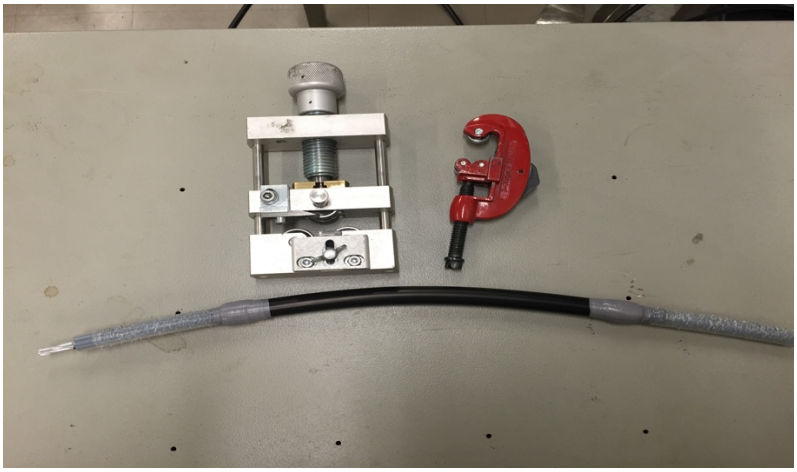

Figure 4-1 Cable Specimen and mechanical tools used in sample preparation

4.1.2 Creation of Artificial Cavity

In order to produce an artificial cavity inside the insulation, a steel needle-plane geometry was opted. This approach is widely used in research for simulating the electrical stress enhancements and initiating the electrical treeing inside the polymeric insulation. The insertion of the sharp needle inside the polymer creates a micro-void at the tip of the needle resulting in the inception of partial discharge activity at relatively low voltages [11].

Suitable steel needle of 1.5 mm diameter with a tip radius of 10 μm was inserted inside the insulation to 2.5 mm depth in order to realize the internal discharge phenomenon. This gives around 1.8 mm of remaining insulation for the treeing propagation. The needle was carefully inserted to the specified depth with the help of dial indicator as shown in Figure 4-2. The needle was moved back by 0.5 mm in order to create an air-filled cavity in addition to the micro-cavity at the tip of the needle. This approach was used so that different type of discharge mechanisms could be observed. High voltage terminal was connected to the steel needle electrode whereas one end of the cable was connected to the ground.

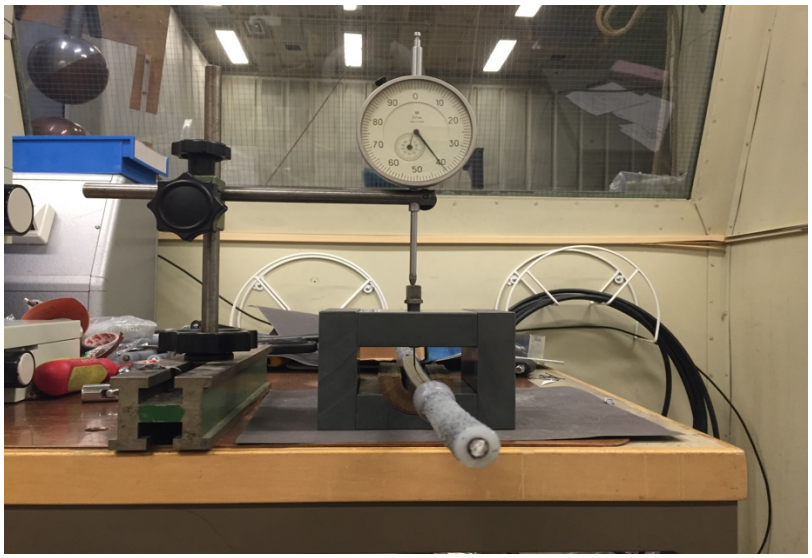

Figure 4-2 Needle-plane electrode configuration for creation of artificial cavity and the use of dial indicator

4.2 Corona Free Test Setup

The main difficulty in establishing the PD measurements test setup is to create an environment around the test specimen which is free from discharges other than the specimen own internal discharges. The inception of corona at low voltages is observed at cable terminations at relatively low voltages. In order to avoid this situation, a proper test setup must be built. Placing the specimen inside silicone oil bath is one of the possible ways to resolve this problem [26]. However, in order to develop a cable test arrangements similar to the field applications, proper cable terminations were arranged in this study. These terminations were installed at the cable terminals to ensure that only internal discharges will be recorded by the measuring instruments.

4.2.1 Measurement Procedure

1. Voltage magnitude was kept constant through out the lifetime test at the rated voltage of MV cable i.e. 12 kV RMS phase voltage.
2. The end criterion for the test was selected as the final breakdown of the insulation.
3. The partial discharge intensity was monitored with Phase Resolved Partial Discharge Analyzer (PRPDA). The PD data was recorded for one minute after every three minutes. The data obtained was post processed to obtain the parameters such as average charge, accumulated charge etc. for analyzing the insulation degradation by means of partial discharges. Furthermore, variations in the statistical parameters such as skewness, kurtosis of different phase distributions for each acquired data were also calculated.
4. In order to identify the shape parameters of individual PD pulses and their variation with time, 12bit, 2GHz oscilloscope was used. PD pulses after every five hours of stress were recorded with the help of High Frequency Current Transformer (HFCT) sensor.
5. The progression of electrical treeing inside the insulation was observed by means of special arrangement of optical microscope.

4.3 Phase Resolved Partial Discharge Analyzer (PRPDA)

The PRPDA technique has been widely used by the commercially available PD diagnostic systems. This technique records the apparent charge with respect to the phase of the voltage cycle for each PD detected. In this study, PD-ICM (Insulation Condition Monitoring) system software was used to monitor and record the PD values. The system records the PD data for each acquisition period in the form of image pixels. The image file represents the mapping of charge values for each pixel. The whole image is divided into 256x256 pixels. Each horizontal pixels represent the phase value along the phase axis dividing the positive and negative half cycles into 128 pixel windows. The corresponding vertical pixels represents the discharge magnitude and intensity. Similarly, positive and negative charge values are divided into 128 pixel windows. Figure 4-3 describes the decrypted mapping image used by the ICM system. The decryption of the image file saved by the ICM system is one of the most difficult tasks in this study. The data saved in the image file is in the binary form to utilize less memory. It was the requirement of this study to analyze the data over long periods and manually analyze the recorded data was not a feasible procedure. Hence, a post processing program was developed in Matlab which allowed detail analysis of data recorded in these encrypted data files.

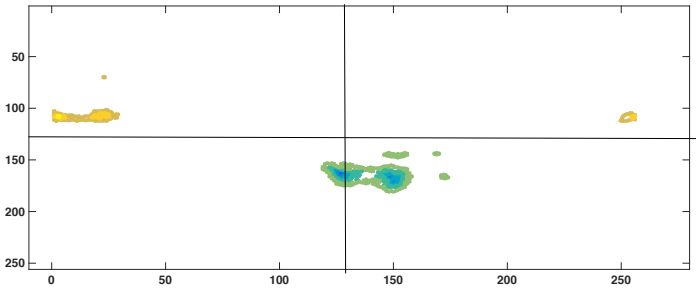

Figure 4-3 Decrypted mapping image of ICM system.

4.4 Non-Conventional PD Detection

In order to observe the ultra-wideband discharge characteristics, PD measurements were being observed by means of non-conventional PD detection system. This requires the installation of highly sensitive and large bandwidth sensor across the ground connection of test object. For this purpose, HFCT sensor was being used. Fixed contact HFCT sensor has a large bandwidth and reliable frequency response up to 100 MHz. The PD discharge pulses have frequency contacts concentrated largely in the frequency range of 10 to 30 MHz.

The PD pulses were observed by 12bit, 2GHz LeCroy digital oscilloscope. The observed data size was selected as 400K samples for one discharge pulse. This limits the file size as well as requires less computational time for analysis. Figure 4-4 shows the whole PD measurement setup.

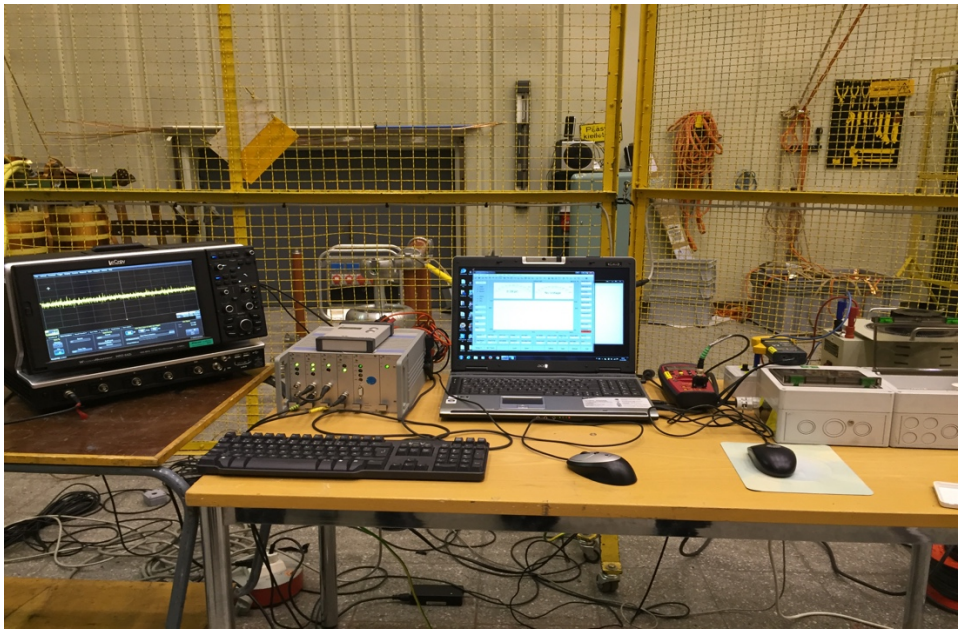

Figure 4-4 Measurement Setup

4.5 Results

After establishing a satisfactory partial discharge measurement setup, tests were carried out with the aim to study the time behavior of partial discharge characteristics and estimate the time to breakdown for one particular PD test setup. Tests were carried out at constant rated voltage of cable i.e. 12 kV (phase voltage).

4.5.1 Lifetime Tests

Primarily tests were carried out on specimens for estimating the average time to breakdown (TBD) while keeping the test conditions same. Phase-resolved analysis of partial discharge activity were recorded with the help of partial discharge diagnostic box (PDIX). Initially, ten (10) cable samples were prepared. The average TBD values of 5 cable samples are provided in Table 4-1. Two cable samples namely cable 2 and cable 3 were observed to breakdown in very early stages of electrical stress. The peculiar behavior shown by these two samples can be due to inconsistent cable sample manufacturing process. The tools used in sample preparation mechanically stress the cable, hence, introducing additional stress concentrated points which are considered to be the cause of these cable samples breakdown. Subsequently, careful measures were being taken to avoid the formation of additional stress points. However, these samples results are not considered further in the analysis. Rest of the cable samples were used to study the behavior of electrical tree growth.

Table 4-1 Time to breakdown (TBD) values

Sample No.	Time to Breakdown (TBD) [hrs]	Sample No.	Time to Breakdown (TBD) [hrs]
Cable 1	72	Cable 2	6.9
Cable 4	82.1	Cable 3	7.3
Cable 5	94		
Cable 6	95.4		
Cable 7	78.6		

A. PD Monitoring

The conventional method of PD detection allows to correlate the recorded PD signal amplitude with the apparent charge. Hence, the observed PD data can be processed to obtain different parameters such as average charge, accumulated charge, charge frequency and charge per second during each acquisition period. Figure 4-5 illustrates the PD intensity pattern in terms of the average charge for each acquisition period over the lifetime of the cable samples used in the experiment. It can be observed that the PD intensity pattern shows almost similar behavior for all the cable samples. The discharge pattern can be divided into four stages; initiation of the PD, concentration of charge, insulation disruption (initiation of electrical treeing) and breakdown.

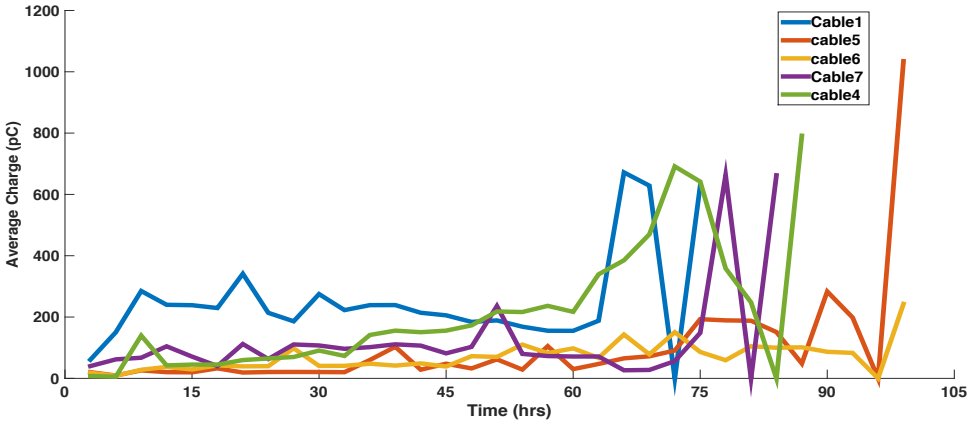

Figure 4-5 Behavior of Partial Discharge intensity over the insulation aging period

As it can be seen, the PD intensity tends to increase initially in the range of 50 to 400 pC. This indicates the increase in surface conductivity of the cavity wall due to the erosion and chemical reactions creating dissociation products of air. This results in roughness of the surface and formation of more localized solid by-products, for example, the formation of hydrated oxalic acid crystals [16,27,29]. In the case of cable 1, 4 and 7 the increase in surface conductivity can be observed within first 10 hours of aging. However, cable 5 and cable 6 shows relatively constant PD behavior indicating very slow insulation deterioration. Consequently, these two cable samples had the largest breakdown time as given in Table 4-1. For a larger period of the insulation aging, PD intensity tends to stabilize with very small variations. For example, in cable 1 the period between 15 to 60 hrs. of insulation aging the PD intensity remains around 200 pC. It is believed that during this phase the PD process tends to localize in a certain areas forming field enhancement at the tips of the crystal structures which can eventually result in the initiation of the electrical treeing [16]. This phase can be described as charge concentration phase. Also, as described earlier in the partial discharge theory section, the surface conductivity of cavity increases during initial few hours of PD exposure and then tends to saturation point. This increase in surface conductivity is not necessarily be accompanied by the increase of discharge amplitude PD intensity. However, the PD intensity increases sharply once the electrical treeing starts, resulting in severe degradation of the insulation.

PD intensity drops to almost zero for very short period of time before the cable breakdown. According to research [28], this may take place as a result of carbonization of the partial discharges inside the void. This phenomenon prevents the voltage build up across the void and creating a very low resistive path for very high currents flow. These high current pulses are known as ‘tiny arcs’. It results in increased heating and severe insulation deterioration. The intense heat can cause molecular and chemical breakdown of the insulation which further accelerates the deterioration process.

One of the main goals of this study was to evaluate the detection threshold which allows the Distribution companies to take emergent action in order to keep the system reliable and avoid the devastating effects of the insulation breakdown. The partial discharge pattern for

the insulation aging allows detection of the progressive phases of insulation deterioration. The time before the breakdown when the partial discharge activity limits to very small value were calculated for the cable samples and are expressed in Table 4-2. For the particular PD setup, the detection threshold time is not consistent and have no clear correlation with the time to breakdown values. However, the minimum detection threshold time observed is 32 minutes for cable 7 and overall average detection threshold time for five cable samples is 83 minutes.

Table 4-2 Detection threshold values

Sample No.	**Time before breakdown (Detection threshold) [min]**
Cable 1	124
Cable 4	64
Cable 5	56
Cable 6	140
Cable 7	32

As mentioned earlier, during the detection threshold period the resistive component of the insulation has reduced to such an extent where the partial discharge activity vanishes and allows the direct path for current flow. The reduction in insulation resistance can be detected by means of traditional methods of measuring insulation resistance or Megger testing. Thus, partial discharge trend identification together with traditional insulation resistance testing can provide an effective solution for insulation diagnostics.

B. Stress Indicator

Many researchers have tried to formulate stress indicators for partial discharge activity. Models based on the maximum applied voltage, V_{max} or recently the apparent current/cycle, I_a has been proposed. These stress indicators can be used to establish life models for insulation aging [26]. The models based on I_a depicts the actual degradation behavior and is considered more efficient as compared to models based on V_{max}. Therefore, only the I_a as stress indicator is calculated for this study.

C. Apparent Current/cycle I_a

The data recorded by the PRPDA was analyzed for each acquisition period to compute several partial discharge quantities. These quantities include Q_a defined as charge per cycle and is computed by the following equation:

$$Q_a = \frac{\sum_{i=1}^{256} N_i \ * q_i}{\mathrm{t_{acq}} \ * \mathrm{f}} \tag{11}$$

where ‘i’ indicates the phase window, t_{acq} is acquisition time and f is fundamental frequency. The quantity in the numerator is defined as accumulated charge and is a useful indicator for the intensity of PD phenomenon.

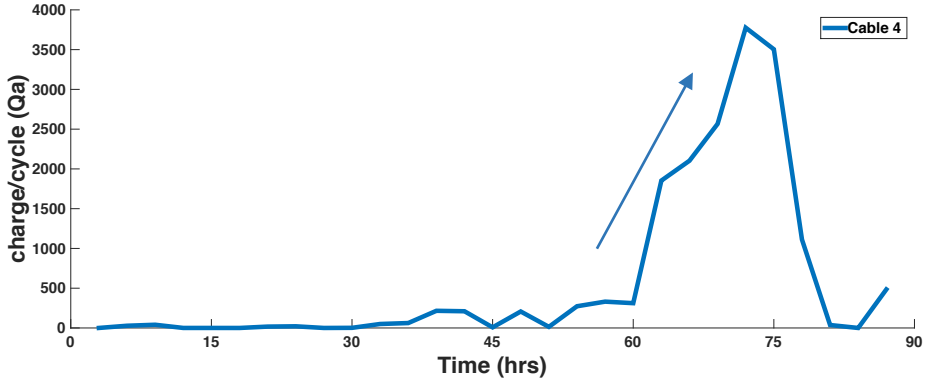

Figure 4-6 Behavior of charge/cycle quantity over the insulation aging

The behavior of Q_a as shown in Figure 4-6 is an important indicator for the inception of the electrical treeing inside the cable insulation. The value of Q_a increases rapidly after the onset of electrical treeing. Similar kind of behavior was observed for the other cable samples as shown in Figure 4-7. The slope of this rise in Q_a value is called ‘apparent current per cycle’, I_a. This calculated I_a value can be used as a stress indicator [26].

Table 4-3 Stress Indicator values

Sample No.	**Stress Indicator (I_a) (pC/sec)**	**Time to Breakdown (TBD) [hrs]**
Cable 1	2.12e3	72
Cable 4	2.25e3	82.1
Cable 5	396	94
Cable 6	561	95.4
Cable 7	1.62e3	78.6

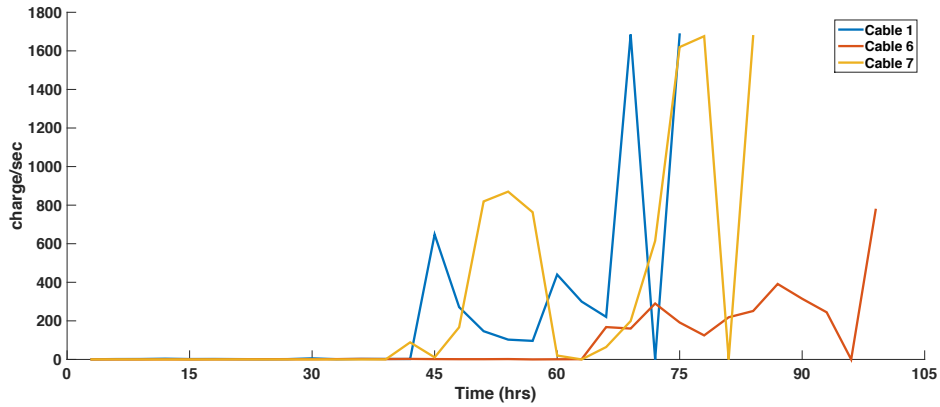

Figure 4-7 Charge/second Qa behavior

The Q_a pattern observed during the experiments can be best fitted and described with the help of high degree polynomials. Taking the maximum value for the derivative of these high degree polynomials gives the desired I_a value for each cable sample which are provided in Table 4-3.

D. Life Predicting Model

It can be seen from Table 4-3 that with few exceptions the stress indicator I_a indicates correlation with the time to breakdown values. Cable samples (1,4 and 7) having larger values of I_a has shorter breakdown time whereas, cable 5 and cable 6 having larger breakdown period have very small values of I_a. Hence, the stress indicator can be related to the time to breakdown value by using the inverse power law.

The generic inverse power law for the stress indicator I_a and time to breakdown TBD is given by the equation:

$$\boldsymbol{TBD = A * I_a^{-B}} \tag{12}$$

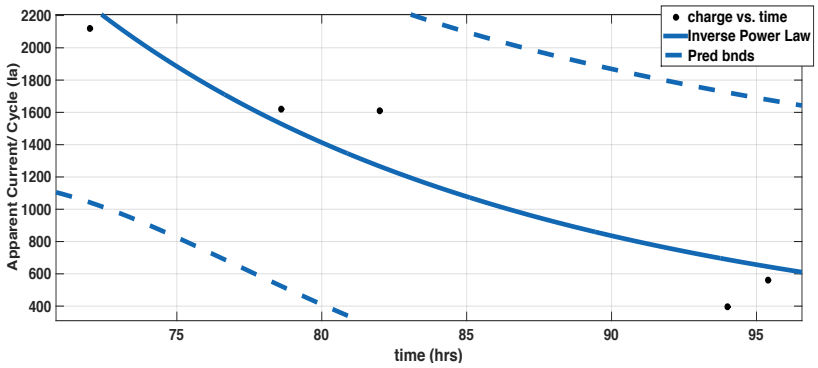

Figure 4-8 The inverse power law plot for stress indicator Ia vs time

Figure 4-8 shows the plot of stress indicator I_a vs the TBD values for five cable samples used in experimental work. The parameters of the inverse power law A and B can be estimated by using the linear regression techniques. The analysis provides the estimated numerical values with the determination coefficient values as given in Table 4-4.

Table 4-4 Estimated parameters values for life prediction model

A	B	R^2	SSE	RMSE
4.37e3	-4.46	0.89	2.391e05	282

The determination coefficient value of 0.89 and relatively moderate root mean square error value signifies the validity of the inverse power law model. Also, the stress indicator I_a takes into account the actual degradation process i.e. growth of electrical treeing by the

partial discharge phenomenon. Therefore, selecting I_a as stress indicator provides much more accurate life prediction model and also allows improved monitoring of electrical treeing aging phenomenon.

4.6 Statistical Parameters

As already discussed, the statistical parameters defining the $H_n(\emptyset)$,$H_{qn}(\emptyset)$ and $H_{qm}(\emptyset)$ distribution profiles are useful in providing the information regarding the partial discharge pattern and insulation condition. In particular, the electrical treeing phenomenon follows a specific discharge pattern which can be observed with different statistical parameters such as skewness and kurtosis.

Figure 4-9 illustrates the behavior of skewness and kurtosis parameters for $H_n(\emptyset)$,$H_{qn}(\emptyset)$ and $H_{qm}(\emptyset)$ distribution profiles. The parameters were calculated separately for positive half and negative half of voltage cycle in order to observe the asymmetrical behavior of the discharge patterns. It can be seen that the phase distribution profiles are characterized by strong fluctuating values of statistical parameters for a better period of aging time. However, after the electrical treeing inception i.e. after 60 hours of stress, the parameters tend to follow a specific pattern. The skewness as well as the kurtosis for $H_{qn}(\emptyset)$ and $H_{qm}(\emptyset)$ for both positive and negative half cycle phase distributions starts to decrease indicating the movement of charge symmetry from left to right along the phase axis. Skewness greater than 0 indicates that the distribution profile is right skewed with its right tail longer. The decreasing skewness value is the indication of the distribution profiles moving right along the phase axis. This behavior can be supported by the fact that the electrical tree propagates along the insulation creating more branches or bushes in the form of conducting channels or micro-cavities. Partial discharges in these conductive channels develop at relatively larger voltage magnitude as compare to the previous discharge sites which are deteriorated over a long period. An alternative explanation for the movement of charge symmetry is on the basis of an increase in statistical time lag. Due to degradation of the cavity surface, the free electrons get trapped inside the discharge sites due to surface conduction and recombination. This phenomenon as explained in chapter 3 is known as surface charge decay. The surface charge decay and increase in statistical time lag shift the PDs forward in phase at larger values of the applied electric field. Also, the PD magnitude increases with increase in statistical time lag which is evident from the mean pulse height phase distributions shown in Figure 4-10. As we can see in this figure, the mean pulse height phase distribution tends to increase in magnitude as well as shifting towards right along the phase angle axis with the insulation aging period. This behavior is quite accurate in the case of positive half cycle phase distribution as compared to negative half cycle phase distribution. It can also be noticed that the distribution becomes flatter as compared to normal distribution with insulation aging due to electrical tree propagation. This can also be verified by the corresponding variations in the kurtosis values indicated in Figure 4-9 (c&d). Similar kind of behavior is shown by the maximum pulse height phase distribution profile as evident by the Figure 4-11.

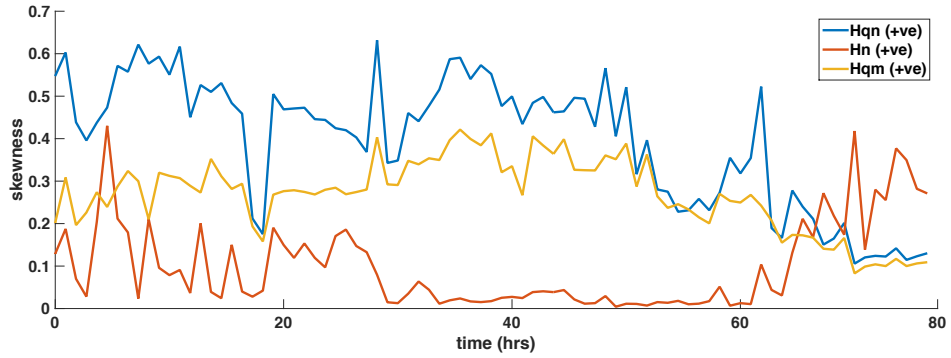

(a)

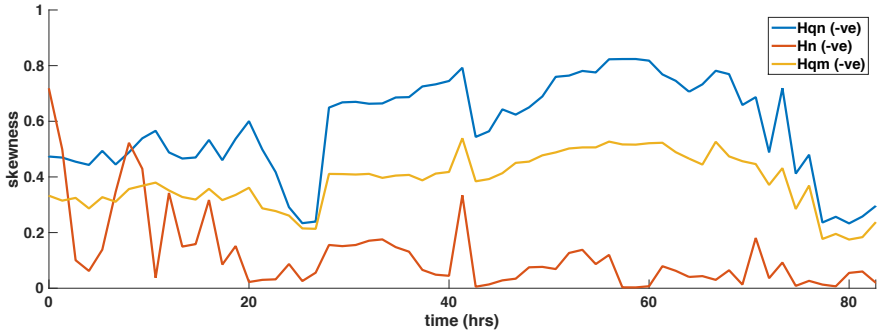

(b)

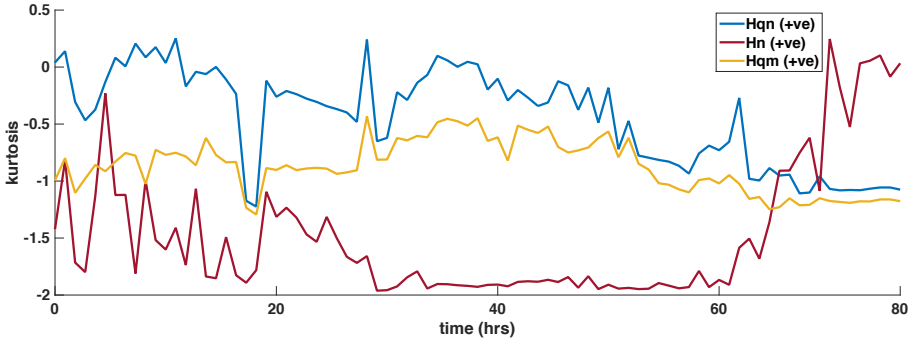

(c)

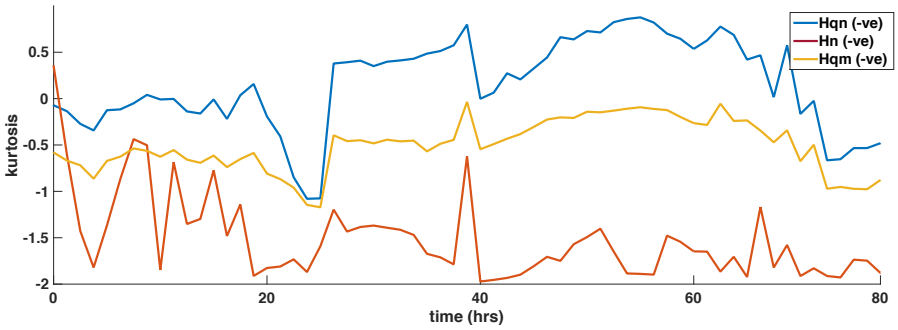

(d)

Figure 4-9 Behavior of Skewness and Kurtosis for different phase-position distributions over the insulation ageing

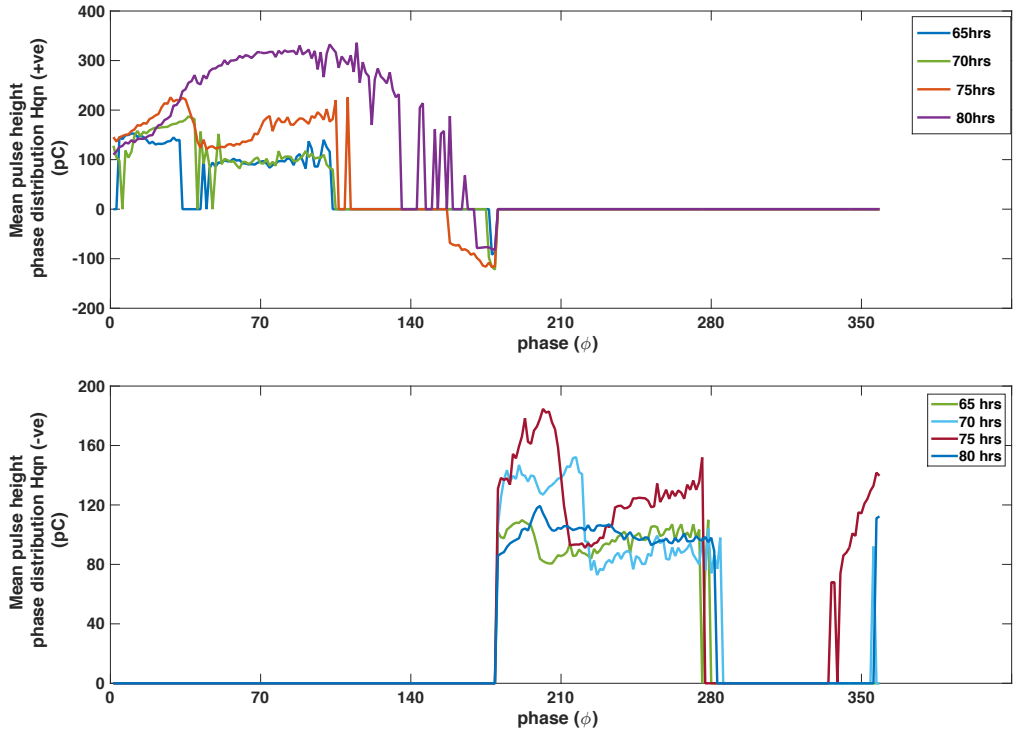

Figure 4-10 Mean pulse height phase distributions after the inception of electrical tree . (a) For positive half cycle (b) For negative half cycle

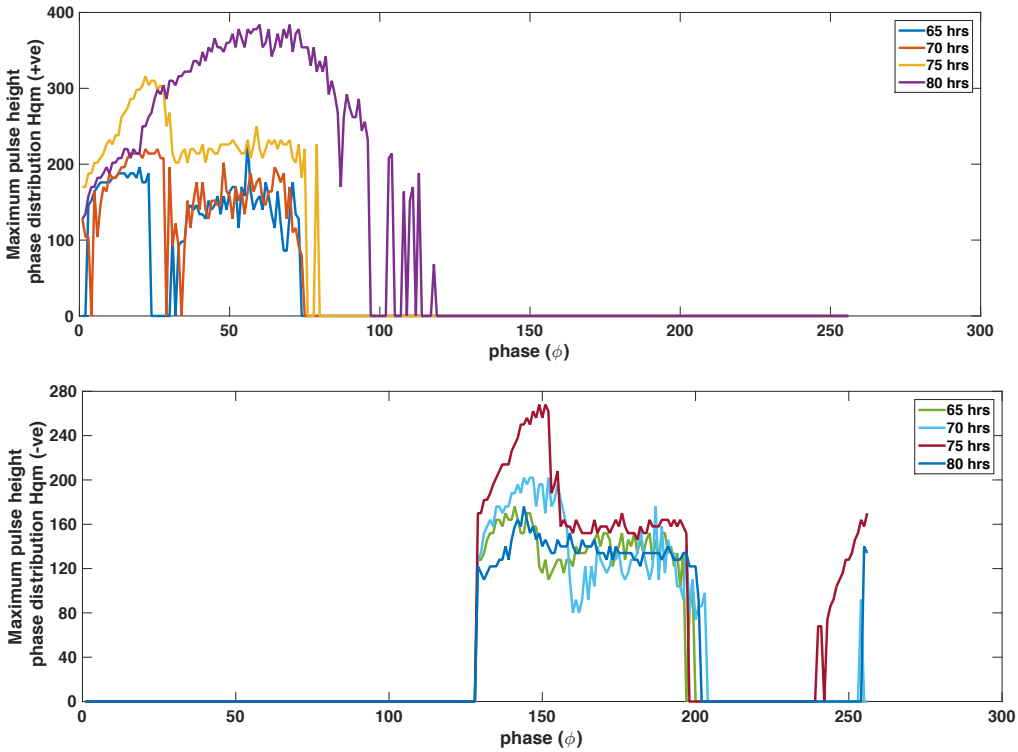

Figure 4-11 Maximum pulse height phase distributions after the inception of electrical tree . (a) For positive half cycle (b) For negative half cycle

On the other hand, skewness and kurtosis for $H_n(\emptyset)$ distribution profile have shown rising behavior after the onset of electrical tree particularly in the positive half of voltage cycle. One of the possible explanation for this behavior is the charge concentration in the multiple

sites or micro-cavities which have a higher frequency and repetition rate of PDs as compared to the new and virgin cavities which are formed as a result of the electrical tree.

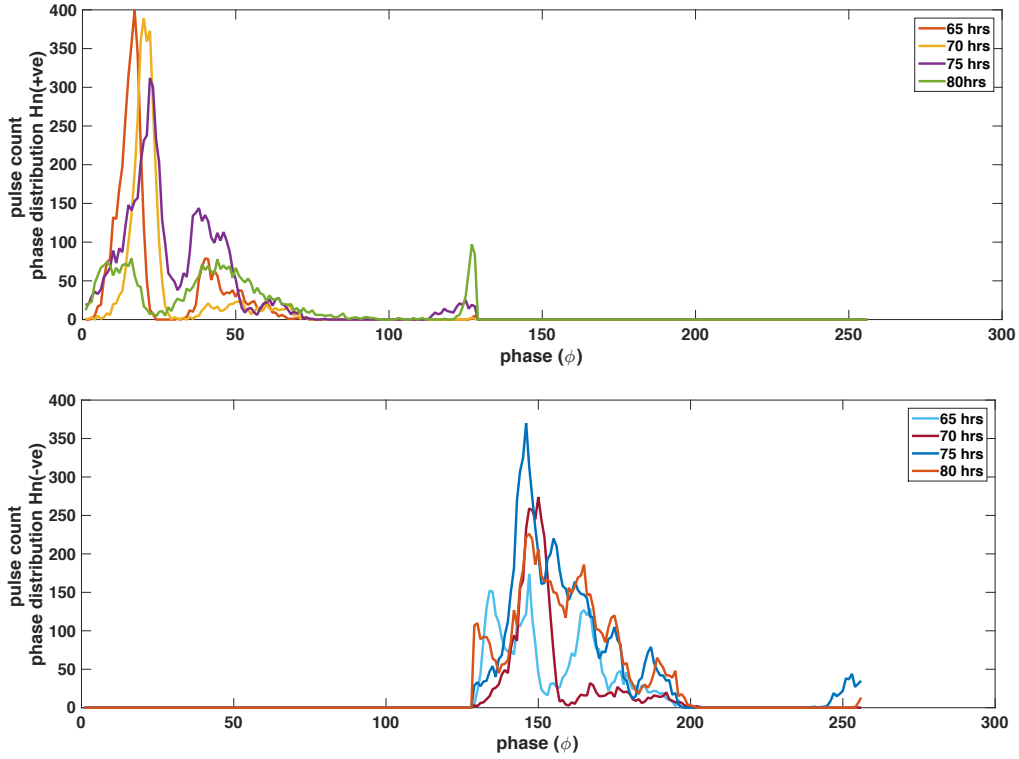

Figure 4-12 Pulse count phase distributions after the inception of electrical tree . (a) For positive half cycle (b) For negative half cycle

It has been observed that during the positive half of the voltage cycle, the phase position distributions show many clear and distinctive patterns as compared to the negative half. The asymmetry of distributions for positive and negative half cycles are represented with different statistical operators as explained earlier. The behavior of these parameters over the insulation ageing is shown in Figure 4-13. As we can see, the pattern of these operators is not consistent indicating the occurrence of several discharge mechanisms during the insulation aging. The mcc is a reliable operator for explaining the different type of discharge mechanisms. It is calculated by multiplication of the other three operators i.e. $cc, Q \; and \; \vartheta$. A higher value of mcc is the indication of the insulated bounded discharge activity which accounts for the charge accumulation whereas, lower mcc value indicates the occurrence of treeing phenomenon [22].

Large values of phase asymmetry during the initial stages of insulation ageing indicate that the PD activity during the positive cycle incepts at higher voltage magnitude as compared to the PD activity inception during negative cycle. During the greater part of aging period, the charge asymmetry Q remains constant at a value of 1 indicating the total symmetry in the occurrence of positive and negative PDs. However, as it can be seen, the amplitude asymmetry tends to increases after the inception of electrical tree. On the other hand, ϑ becomes constant to the value of around 0.4. The correlation coefficient cc remains almost constant around 0.7 with very small variations. However, its value starts to decrease significantly after the onset of treeing phenomenon.

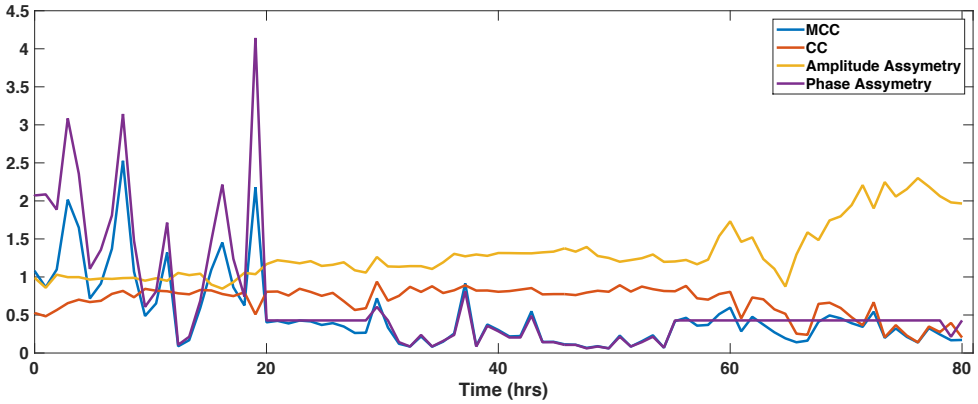

Figure 4-13 Behavior of statistical operators describing the partial discharge asymmetry between positive and negative half cycles

All the statistical operators which are calculated in this study and provided in the literature are useful in creating a PD distribution pattern which can provide important information regarding the condition of insulation. Particularly, the discharge mechanisms involved in the PD activity can be recognized by comparing the variations in the statistical operators. The theoretical knowledge and experimental results along with the physical inspection of the discharge sites can provide a detailed diagnostic analysis.

4.7 Time & Frequency domain characteristics

In addition to statistical calculations based on phase resolve analysis, ultra-wideband discharge characteristics were observed by means of time resolved discharge parameters and energy contents of discharge spectrum. Figure 4-14 and 4-12 shows the behavior of discharge parameters i.e. rise time and 50% pulse width of the individual partial discharge pulses respectively. It is evident from the figures that both the rise time and 50% discharge pulse width of discharge pulses over the insulation ageing period tends to decrease particularly before the final breakdown.

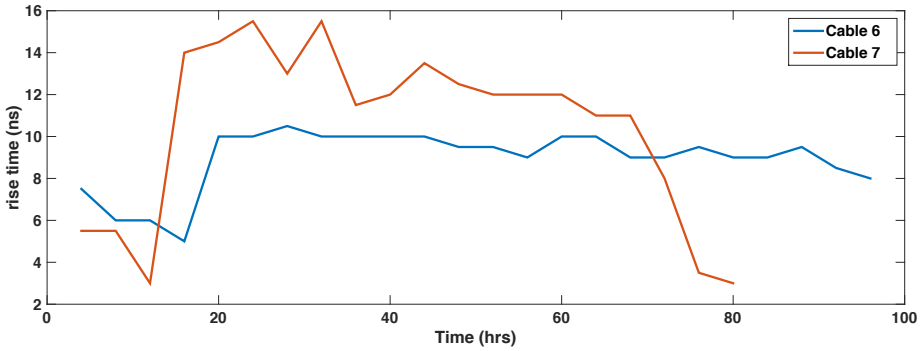

Figure 4-14 Behavior of time rise of individual discharge pulses

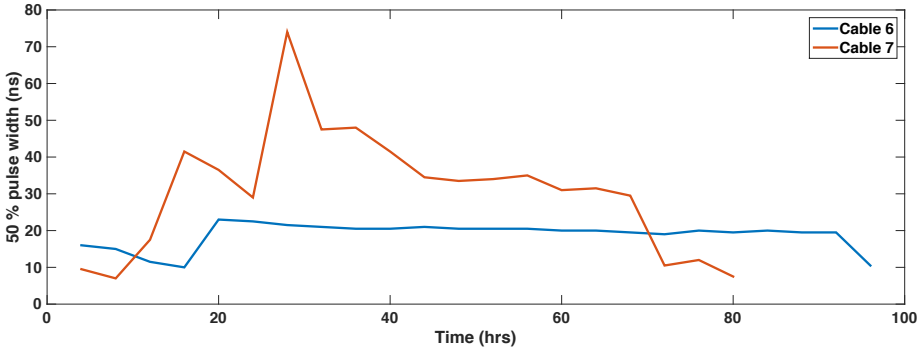

Figure 4-15 Behavior of 50% pulse width of individual discharge pulses

As explained earlier in the theory about ultra-wideband discharge characteristics, the discharge parameters provide very useful information regarding the physics of partial discharge mechanisms. The discharge pulses observed during the initial stages of insulation ageing are observed to have characteristics similar to pitting type discharges. These discharge pulses are characterized by smaller rise times and pulse widths. However, the discharge pulses during the charge concentration period have characteristics similar to streamer type discharge pulses. Streamer pulses are observed to have larger rise times and pulse width durations. However, before the breakdown of cable the discharge pulses again show the characteristics of pitting type discharge pulses. The type of streamer and pitting type discharges observed during the experiments are shown in the Figure 4-17.

In the frequency spectrum, the discharge pulses have energy density mostly concentrated in the range of 1 to 25 MHz frequency range. High frequency energy contents in the range of 50 to 100 MHz and very small energy contents in the range of 100 to 200 MHz are observed in the discharge pulses after long ageing times. These discharge pulses also have high energy contents as compared to discharge pulses observed during initial ageing periods. The energy density in the frequency spectrum for several discharge pulses observed during the insulation ageing is shown in Figure 4-17 . Table 4-5 summarizes the energy distribution in the frequency spectrum with respect to the insulation ageing time.

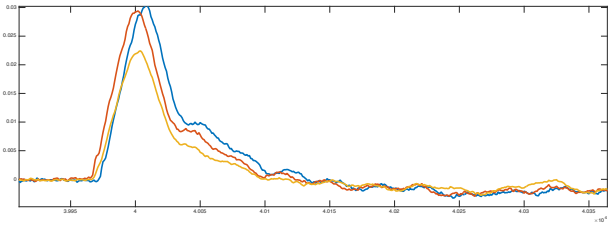

(a)

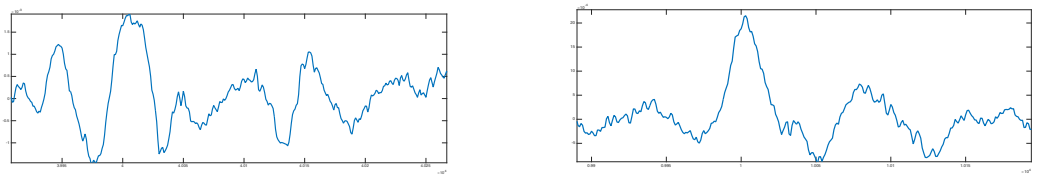

(b)

Figure 4-16 Characteristic discharge pulses. (a) Streamer like discharge pulses (b) Pitting type discharge pulses

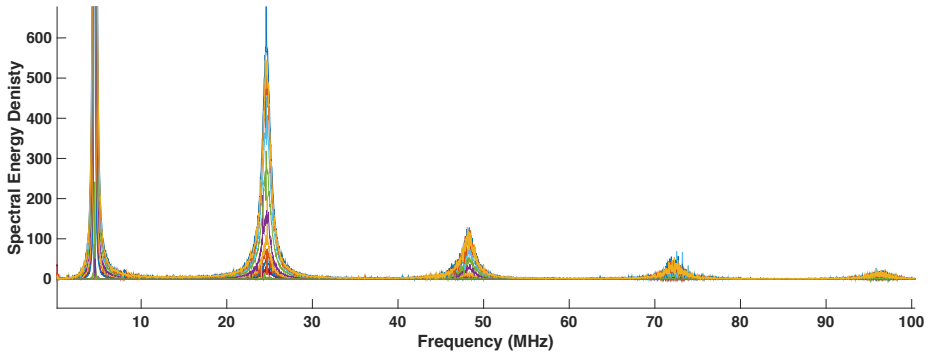

Figure 4-17 Frequency contents of discharge pulses

From the observations and experiment results, it can be concluded that the UWB characteristics are useful in evaluating the condition of insulation as well as can explain the discharge mechanisms taking place inside the cavity. However, this method of insulation diagnostics requires high bandwidth oscilloscopes for observing the true shape of discharge pulses. Continuous monitoring by means of these highly expensive oscilloscopes may not be a cost effective method.

Table 4-5 Frequency content of discharge pulse with respect to ageing time

Ageing time (hrs)	Discharge Energy frequency contents
0~10	850 KHz~7MHz
10~70	0~50MHz
70~90	0.9~50 , 100~200 MHz

4.8 Electrical Tree Growth

The propagation of electrical treeing inside the insulation was also observed. Due to the unavailability of CCD camera, it was not possible to monitor the tree growth continuously and without any means of non-destructive methods. After primary tests, an estimated average time to breakdown was calculated based on which the partial discharge behavior can be predicted over the insulation ageing. Therefore, it was decided that the cable samples will be removed from the test setup after stressing for a certain period of time and observe the electrical treeing growth with the help of special arrangement of the optical microscope as shown in Figure 4-19. The short-circuited cable samples were being observed under the microscope. Figure 4-20 shows the development of electrical tree inside the cable insulation at the needle tip. It can be seen that the electrical treeing has bush type morphology. Because of the carbon left over at the discharge site due to the short circuit after cable breakdown, the treeing pattern can be seen clearly. However, during the normal operation, the conductive channels or micro-cavities formed as a result of the electrical tree has very thin patterns inside the insulation which is very difficult to observe. To study these patterns, a very delicate slicing tool for insulation is required. The thin films obtain from slicing tool can then be analyzed under the microscope. Due to destructive nature of this method and also the random behavior of the partial discharge activity, the results obtained

may not have an accurate estimation of the tree propagation rate. A better and more research designated approach can be the installation of CCD (Charge Coupling Device) camera across the test sample. This scheme will allow to detect and continuously monitor the discharge movement across the XLPE insulation core by means of digital imaging. Due to the limited research period for this master's thesis study and also the limitations of cutting tools available in the laboratory it was not possible to measure the propagation rate of electrical tree. However, computer simulations based on the partial discharge models were performed in order to realize the behavior of partial discharge with the increase in depth of cavity and results are compared with the experimental observations.

4.8.1 Partial Discharge Simulation

As explained in chapter 3, the partial discharge can be modelled by several different approaches. The capacitive abc model and dipole model based on the Poisson's equation has been used in this study for modeling the partial discharge activity. Figure 4-18 provides the schematics of the partial discharge model built in the Matlab Simulink environment. The simulation was performed in order to observe the partial discharge intensity with respect to the varying the cavity depth. The parameters of MV cable used in the experimental laboratory work has been used in the simulations. The Matlab program has been designed accordingly. The program calculates the PD intensity for every 0.1mm increase in the depth of cavity. The charge value based on the dipole model and abc model has been studied.

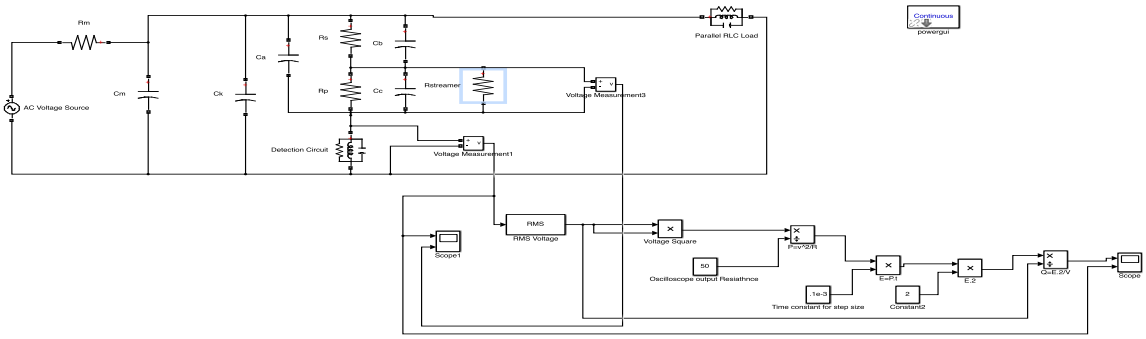

Figure 4-18 Simulink Model for partial discharge simulations

Figure 4-19 Microscope arrangement for observing the treeing propagation

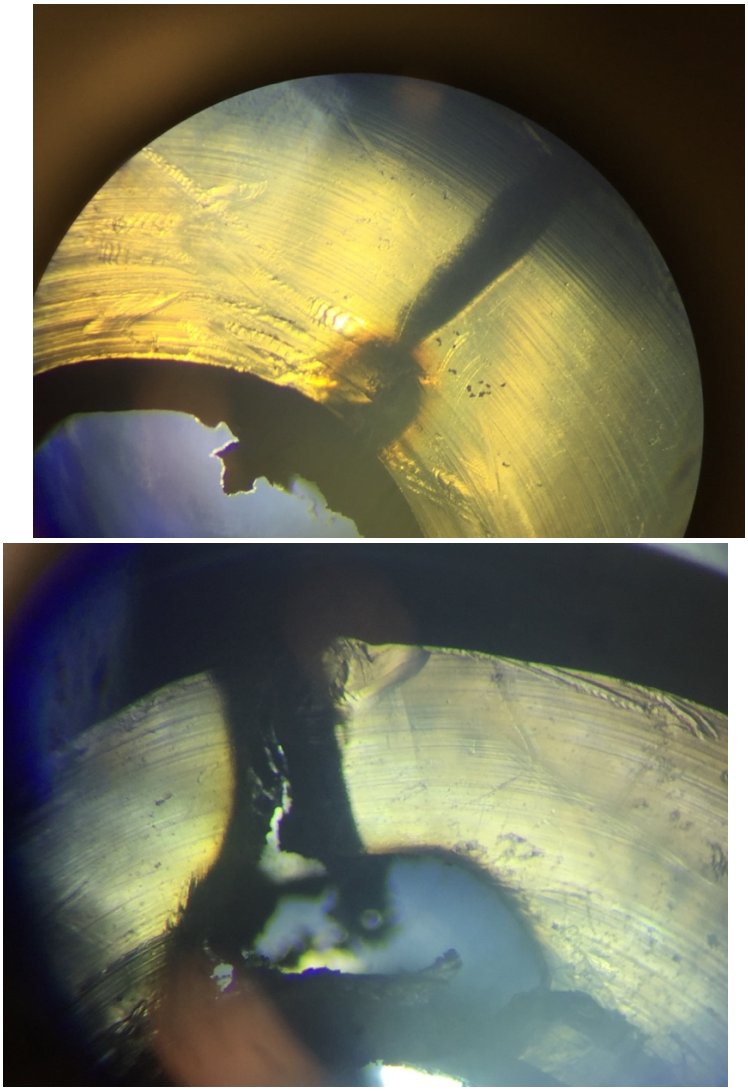

Figure 4-20 Bush type electrical tree morphology

The charge value for the dipole model can be calculated from the equation (1). The dipole moment is calculated by considering the worst case, i.e. for the streamer like discharge mechanism. According to Lemke publication [19], this dipole moment has been approximated by the following equation:

$$P_m = (270\ pC/mm).d_c^2. \tag{13}$$

By calculating the dipole moment from above equation and inserting its value in equation (1) provides the value of charge.

For ABC-model, the charge is calculated by calculating the capacitance and voltage across the cavity. Another approach for calculating the charge value is from the output voltage obtained from the detection circuit. The charge value, in this case, is given by the following equation:

$$Q = \frac{E.2}{V} = \frac{2.V^2 t}{R.V} \tag{14}$$

where R=50Ω and E is the energy across capacitor.

The results obtained after the simulations are given in Figure 4-21.

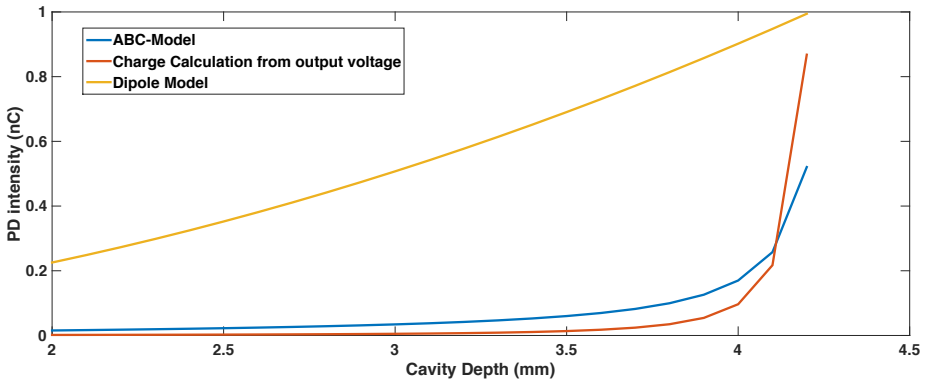

Figure 4-21 Partial discharge simulation results based on abc-model and dipole model

The dipole model presents an almost linear increase in PD value with the increase in depth of the cavity. The laboratory results provided earlier in the PD monitoring section also illustrates the increasing behavior after the initiation of electrical tree, though the behavior is not as linear as presented by the computer simulations. Whereas, the PD activity represented by the abc-model has quite different pattern. From the simulation plot, it can be observed that the intensity of partial discharge is quite low around 50 to 100 pC. It rises sharply if the distance between the conductor and the cavity is very small. The PD intensity observed in the laboratory work given in Figure 4-5 has shown that the maximum PD value after prolong insulation ageing is around 800 pC. The charge value evaluated on the basis of dipole model has been in the same range.

The PD models are helpful in describing the discharge intensity, however, their validity can only be examined by interpreting the results according to the physical phenomenon taking inside the PD source.

Part II

PARTIAL DISCHARGE SIGNALS DE-NOIZING

Chapter 5 INTRODUCTION TO PARTIAL DISCHARGE SIGNALS DE-NOISING

Partial discharge measurements have been widely accepted as an efficient online insulation condition assessment method in high voltage equipment [33]. Recently, the on-site measurements and online condition assessment of the electrical equipment have gained significant importance over the traditional periodic maintenance due to various factors [42]. Detection of the partial discharge (PD) signals in the early stages of their development by continuous monitoring is an effective solution to prevent the complete breakdown failure. Also, the online continuous monitoring requires no interruption in the service supply for diagnostic measurements. However, during the on-site measurements, the measured partial discharge signals encounter the wide range of disturbances in the shape of noise signals. The application of the non-conventional sensors such as HFCT, D-dot etc. in the online condition monitoring has increased the sensitivity of the measurement system which results in coupling of these undesired noise signals with useful partial discharge signals [34]. This may affect the reliability of the PD data and consequently the false assessment of insulation conditions. Therefore, the online PD measurement system requires an efficient signal processing technique in order to reject the disturbing signals from the measured signals. Recent developments in modern Digital Signal Processing (DSP) techniques has provided vast scope in removing these interferences. One of the DSP techniques, Wavelet analysis has come of an age in detecting the real time transients like PD pulses from the noisy environment [33].

The major external interferences encountered during the on-site PD measurements are divided into following categories [36,37]:

- **Discrete Spectral Interference (DSI)** from radio, TV or other mobile communication networks is a narrowband interference. Using band pass filters centered on the communication channel frequencies can easily block such kind of interference.
- **Periodic pulse shaped interferences** from the periodic switching of the power electronic devices i.e. thyristor firing circuit. They can easily be removed by implementing the gating circuit.
- **Stochastic pulse shaped interferences** are random pulses produced due to switching operations, lightning or by the arcing between the contacts.
- **White noise** is the Electromagnetic Interference (EMI) caused by the measuring instrument or other surrounding equipment's.

During the online testing, the test equipment is exposed to pulsive interferences from the grid which have characteristics (both in time and frequency) quite similar to those of the

PD pulses. These pulsive interferences are the main challenge in implementing a successful online PD measurement setup. Therefore, this study includes an in-depth analysis of de-noising techniques which can be applied to recover the measured PD signals from these intermittent kind of noises. In this regard, a novel adaptive de-noising technique has been proposed on the basis of frequency analysis of the noise and PD signals. The efficiency and performance of this technique are evaluated by applying the algorithm on different kind of measured on-site PD signals which are coupled with the different type of noise signals. The PD signal measurements are recorded with the help of non-conventional HFCT sensors in the laboratory. Whereas, the onsite disturbances are observed with the D-Dot sensors at switchgear feeding an industrial load in Helsinki region. De-noising results are compared with several existing de-noising techniques proposed earlier in research on the basis of various performance indices.

A brief introduction to existing de-noising algorithms and their limitations for applicability in online condition monitoring systems is given below:

5.1 Noise Reduction Algorithms

Generally, the de-noising techniques are divided into following two categories [43]:

1. Closed Loop
2. Open Loop

The closed loop techniques are used in order to reduce the DSI and radio communication frequency noise signals which are centered on certain band frequencies and are periodic in nature. Whereas, the open loop techniques imply the comparison between the signal characteristics of the PD signal and noise to eliminate the noise from the measured signals. The open loop techniques are more effective for broadband white noises and stochastic pulsive interferences as compared to closed loop noise reduction techniques [43]. These de-noising techniques are implemented with the help of various DSP methods and circuits depending on the kind of noise to be eliminated.

5.1.1 Fast-Fourier Transform Based De-Noising

This method is generally implemented in recovering the PD signal from sinusoidal noise with peaks occurring at periodic intervals. Discrete Fourier transform (DFT) is used in order to evaluate the Fourier coefficients of the signal under analysis. Threshold is set on the basis of the varying frequency of the signal and is calculated according to the following equation [33]:

$$thr = (j-1)^2 \times 60 + 10 \quad (15)$$

For N points FFT the value of j=1,..,N.

The Fourier coefficients with values larger than the threshold are dropped off. The reconstructed de-noised signal is obtained by applying the inverse discrete Fourier transform. The Fourier transform based de-noising methods have limitations for both intermittent type noises and pulsive interference which requires analysis in both time and frequency domain. This method is also known as FFT thresholding technique [36].

5.1.2 Least Mean Square Method (LMS)

This method assumes the fact that the characteristics of the desired output signal are well known before performing the de-noising analysis. It is an iterative approach which tries to minimize the error vector by calculating the difference between the desired output and the actual output of the filter [45].

Consider a filter with its coefficient vector as 'W' and the noisy input signal as 'X'. The filter's output after applying the least mean square method is given according to the equation [45]:

$$W(n+1) = W(n) + \mu \times E(n) \times X(n) \tag{16}$$

where E(n) is the error vector and μ is filter dependent constant value.

The Infinite Impulse Response (IIR) filter is one of the variants of the least mean square method which is used quite significantly in analyzing the transient type signals. However, for the online monitoring system, the application of this method has limitations because of the fact that the PD signals possess random characteristics which are dependent on various factors and are not predictable.

The LMS method is relatively slow and exhibits a non-uniform convergence. These shortcomings are overcome by using recursive least square method. Weighting factor α is introduced in equation (14) which accounts for recursion procedure. The recursive least square method is governed by following equations:

$$W(n+1) = W(n) + \alpha \times R^{-1}(n) \times E(n) \times X(n) \tag{17}$$

where $R^{-1}(n)$ is given by :

$$R^{-1}(n) = R^{-1}(n-1) - \frac{R^{-1}(n-1)\, X(n)\, X^{T}(n) R^{-1}(n-1)}{1 + X^{T}(n) R^{-1}(n-1)\, X(n)} \tag{18}$$

This method is computationally more complex but it converges quite rapidly and produce more efficient results as compared to LMS.

5.1.3 Frequency Domain Adaptive Filtering

The LMS filtering technique is limited to time domain analysis. Further, the technique is also non-adaptive for the transient's type signals. The LMS technique can be implemented in the frequency domain by using any of the signal processing techniques available such as discrete Fourier transform, discrete cosine transforms or the discrete wavelet transform [45]. The equation (14) in this case modifies to

$$W_i(n+1) = W_i(n) + \mu \times E(n) \times X_i^*(n) \tag{19}$$

where W, E and X can be outputs of any of the above mentioned transforms. Comparing to LMS this method is computationally less complex and more efficient for analysis of transients.

The frequency domain adaptive filtering technique was first used by Su [46]. He implemented this technique by injecting the calibration pulses as a reference signal to the equipment terminals. So in order to apply the frequency domain adaptive filtering technique, prior knowledge of the noise and PD signal frequency characteristics must be known. This limits its applicability in the online condition monitoring system.

Besides these useful DSP techniques, various other application dependent filtering techniques have been introduced in the literature. For instance, the notch filters are specifically used in de-noising the sinusoidal noise present in the signal [33]. Matched filtering technique has been used in order to recover the PD signal by matching the impulse response of the filter to input signal [47]. The application of these methods in the on-line condition monitoring system is restricted mainly because of the following reasons:

1. These techniques require human involvement in order to manually perform the de-noising process on the data which is being transferred to remote end for analysis.
2. These techniques are dependent on the specific type of noise characteristics such as the periodic sinusoidal noises or DSI type communication channels interferences.

Wavelet Analysis has been successful in de-noising techniques in the field of digital imaging and signal processing. Recently, its application in the HV engineering as a powerful tool for recovering the PD signals from the noisy environment has been greatly accepted. Various distinct features of the wavelet transformation namely the time and frequency domain analysis and multi-resolution analysis distinguish it from the other DSP techniques.

Chapter 6 WAVELET TRANSFORMATION

The on-site noises such as white noise and PD signals exhibits different frequency characteristics; thus frequency domain analysis can be fruitful in rejecting the white noise. However, the periodic pulse shape noises require the signal analysis in the time domain. Hence, the extraction of the PD signal from the noisy environment requires knowledge of both time domain and frequency domain. Comparing to the Fourier transform which provides only the frequency domain analysis on the basis of moving sinusoidal coefficients, the wavelet transformation is helpful in providing both time and frequency domain analysis [35]. The wavelet transformation involves the selection of single wavelet function also known as mother wavelet. Wavelet transformation decomposes the original signal into several small signals by scaling and shifting the original wavelet function. This decomposition procedure is known as Multi-resolution Signal Decomposition (MSD). The choice of an optimal wavelet function in the de-noising methods is a topic of significant importance in research nowadays.

6.1 Wavelets

A wave is an oscillating function either of time or space i.e. a sinusoidal wave. Similarly, a wavelet is a small wave of limited duration with zero mean value [32]. In contrast to smooth sinusoids of Fourier transform, the wavelets are asymmetric and irregular in shape and considered more suitable for analyzing the transient type PD signals. Few example of wavelets is shown in Figure 6-1.

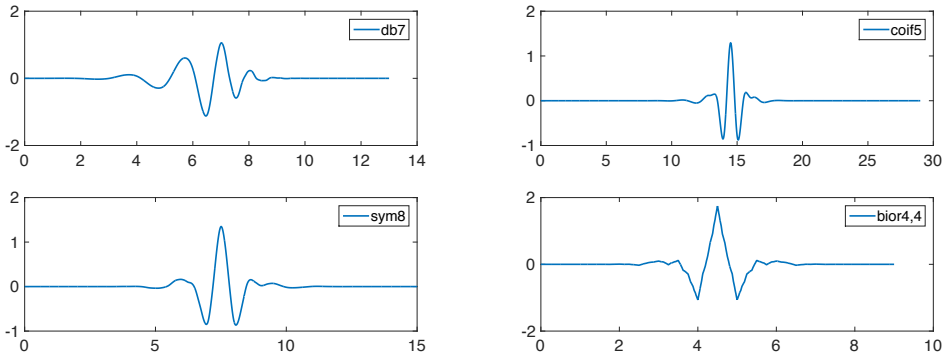

Figure 6-1. Various Wavelet Functions

6.1.1 Mathematical Representation of wavelets

Similar to Fourier transform, which decomposes the signal into sine waves of various frequencies, wavelet transform decomposes the signal into a basic set of wavelet functions which are scaled and shifted version of the single wavelet also known as mother wavelet. These wavelet functions are obtained after scaling and shifting as shown by the following equation:

$$\psi_{a,b}(t) = \frac{1}{\sqrt{a}}\psi\left(\frac{t-b}{a}\right) \tag{20}$$

Where ‘a’ is the scaling factor which determines the amplitude and duration of the wavelet and ‘b’ is shifting factor which determines the delaying or hastening of the wavelet. Therefore, the properties of a signal under analysis can be determined both in the time and frequency domain simultaneously while using these wavelets [38].

6.2 Discrete Wavelet Transformation (DWT)

Discrete Wavelet Transformation calculates the wavelet coefficients on the basis of dyadic scales and positions i.e. based on the power of two. This system can be implemented by using a pair of filters, high pass filter produces the ‘details’ of the signal and the other low pass filter produces ‘approximations’ of the signal. The details are low scale, high frequency components of the signal whereas the approximations are the high scale, low frequency components of the original signal. The high and low pass filters used in the decomposition of the signal are called as quadrature mirror filters (QMF) [32].

6.2.1 DWT Algorithm

Consider a signal ‘X’ of length ‘N’. At level 1, DWT decomposes X into two sets of coefficients by convolving it with low pass filter and high pass filter followed by down sampling by two to obtain approximation coefficients vector CA1 and detail coefficient vector CD1 respectively. The length of each filter is equal to twice the length of original signal i.e. 2N. Down sampling divides the filtered signal of length N into N/2 length signal by keeping the even indexed elements as shown in Figure 6-2 [30]. For multilevel decomposition, the lower frequency approximation coefficient vector CA1 further decomposes into a set of approximation and detail coefficient vectors. This continues for each decomposition stage. This decomposition procedure as explained above is known as the Multi-Resolution Signal Decomposition (MSD).

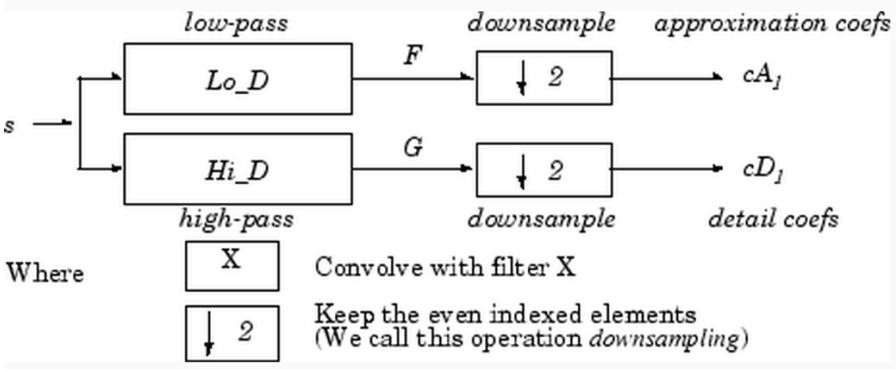

Figure 6-2. Discrete Wavelet Transformation Procedure [30]

The general De-noising methods using the discrete wavelet transformation are based on following steps:

1. Find the number of decomposition levels (N).
2. Choose the optimal wavelet function from the set of wavelets library.

3. Apply the discrete wavelet transformation to obtain the detail and approximation coefficients for levels 1 to N.
4. Apply thresholding on the detail coefficients or on the selected detail coefficients to obtain the modified detail coefficients.
5. Reconstruct the signal by using the modified detail coefficients and the original approximation coefficients.

Reconstruction of the signal involves the inverse discrete wavelet transformation which is explained in next section.

6.2.2 IDWT Algorithm

The reconstruction of the signal is completely inverse of the signal decomposition procedure. Starting from the detail coefficient vector CD and approximation coefficient vector CA at level N as shown in the Figure 6-3 [30], the IDWT reconstructs the approximation vector at level N-1 by up sampling the original vectors and then convolving the resultant vectors with the low pass and high pass filters for approximation and detail coefficient vectors respectively. For next level i.e. N-1, approximation vector obtained by reconstruction at level N is used as signal input. This continues for each level until N =1.

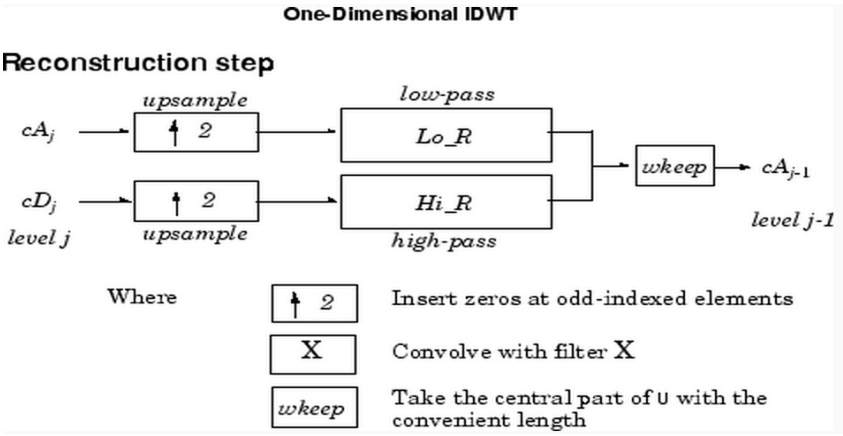

Figure 6-3. Inverse Discrete Wavelet Transformation Procedure [30]

The up sampling of the vectors involves the addition of zeroes in the coefficient vectors to equalize the length of the signal.

6.3 Selection of Optimal Mother Wavelet

Lately, the selection of optimal wavelet for performing the de-noising techniques based on wavelet transformation has been considered of great importance. Techniques based on the maximum correlation coefficient value between the PD signal and wavelets, energy based wavelet selection or lately the SNR based wavelet selection has been introduced. Correlation based wavelet selection methodology best correlates the PD signal with the wavelet functions under study and apply the selected wavelet on all the decomposition

levels. Level dependent wavelet selection methods were introduced on the basis of selecting the wavelet function for each level that maximize the energy of approximation coefficients [32].

The optimal wavelet for analyzing the given signal is the one which is capable of generating as many coefficients with maximum values as possible within the time scale domain [38]. This can be realized by considering PD pulse and perform its wavelet transformation up to five scales by using db2 and db7 wavelets. The wavelet deformation pattern for both wavelets is depicted in Figure 6-4 and 6-5 respectively. As we can see, the PD pattern can be characterized within 5 levels but the wavelet coefficients have slightly different values for both wavelets. Hence, for analyzing this PD pulse, db2 is more appropriate then db7 as it has restored more of the original PD signal energy within a smaller number of decomposition levels. Later, this concept will be used in determining the maximum number of decomposition levels for wavelet transformation.

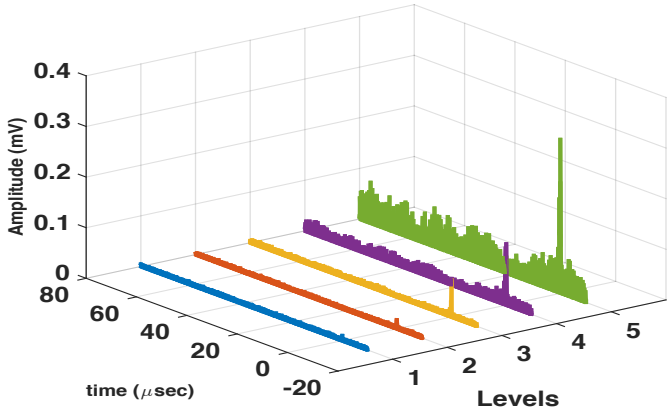

Figure 6-4. Wavelet Deformation pattern for typical PD signal by using db2 wavelet function

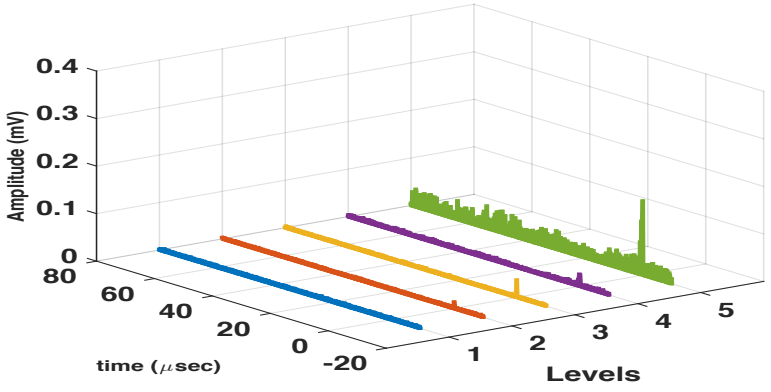

Figure 6-5. Wavelet Deformation pattern for typical PD signal by using db7 wavelet function

The most suitable wavelet families for performing the PD data analysis should have the properties such as compactness, orthogonality and asymmetrical. Among the available wavelet families, Daubechies (dbN), Symlets (symN) and Coiflets (coifN) wavelet families exhibit all the desired properties suitable for analyzing the transient type signals [32]. Therefore, in this study only these mother wavelets have been considered for analysis.

6.3.1 Correlation based Wavelet Selection (CBWS)

In statistical analysis, correlation coefficient (γ) is commonly used for measuring the strength of two signals. Perfectly correlated data will have correlation coefficient value of 1 and uncorrelated data will have correlation coefficient value of 0. Therefore, correlation coefficient γ can be used as efficient criteria for selecting the optimal wavelet [38].

Correlation coefficient value is calculated according to equation (19). The calculations require the two signals to be of equal length with their peaks matching at the same position. The procedure of matching the signals length is known as the normalization of the signal.

$$\gamma = \frac{\sum_{i=0}^{n}(x_i - \overline{x})(y_i - \overline{y})}{\sqrt{\sum_{i=0}^{n}(x_i - \overline{x})^2 \sum_{i=0}^{n}(y_i - \overline{y})^2}} \tag{21}$$

where the variable x_i and y_i are the ith sample values and x and y are their mean values.

A. CBWS Algorithm

The CBWS algorithm works on the principle of maximizing the correlation coefficient value for the PD signal with different wavelet functions from the wavelets library. Later, the selected wavelet function will be applied for each decomposition level of wavelet transformation.

The CBWS algorithm works on the following steps:

1. From the list of pre-selected wavelet families, choose wavelet function.
2. Perform the iterations on the wavelet function until its size becomes equal to the size of PD signal under analysis.
3. Shift either the PD signal or wavelet function so that peak of both will be at the same position.
4. Calculate the correlation coefficient γ between the two signals.
5. Choose the next wavelet function and repeat steps 2-4.
6. Select the wavelet function, which gives the maximum correlation coefficient value.

For performing the iterations in step 2, the Matlab inbuilt function wavefun produces the approximations of the wavelet and scaling functions. The function uses the ITER as an input variable, which provides the extent to which the wavelet function approximations can be refined. Figure 6-6, shows the refinement of db7 wavelet function up to 14 iterations having 106497 data points which are slightly larger than the PD signal 100002 data points under analysis.

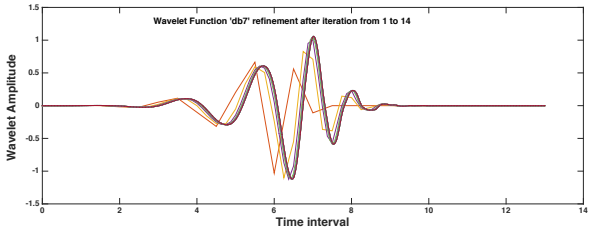

Figure 6-6. Refinement of the wavelet function 'db7 ' for iterations 1 to 14

The wavelet function is shifted according to the PD signal so that the peak of the two will be at the same point. Zero padding technique can be used in order to add zeroes to the front or end of the signal. It is observed that the two signals are not necessarily of equal or normalized magnitude as suggested in [31] however, they must be of equal lengths with the peaks at the same position in order to calculate the correlation coefficient.

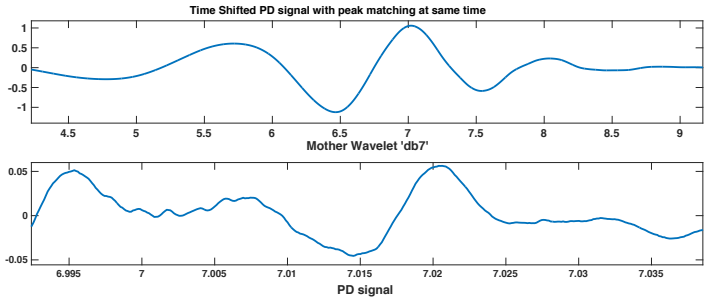

Figure 6-7. Time shifted PD signal and wavelet function 'db7' with peaks occurring at same position

B. Results

The CBWS method was applied to 20 different PD signals measured by HFCT sensor each coupled with 10 different type of noise signals. One of the significant features of CBWS method is its application in finding the optimal wavelet function for a particular type of PD detection circuit i.e. type of sensor being used to detect the PD signal [32]. Therefore, this method was used to evaluate the optimal wavelet function for the HFCT sensor which is being now widely used in the on-site PD measurements.

Figure 6-8 and Table 6-1, illustrates the results of CBWS algorithm for 200 signals under analysis. It can be observed that lower order wavelet functions of each wavelet family i.e. db2, db3 of Daubechies, sym2 and sym3 of Symlets and coif 1 of Coiflets family have a higher number of correlation coefficient γ.

Figure 6-9 and Figure 6-10 represents the maximum correlation coefficients value for each PD signal corresponding to the optimal wavelet function selected. Db2 and db3 clearly have the largest number of matchings with the PD signals under analysis i.e. 77 and 73 respectively. The lower order wavelet functions produce significant results with respect to HFCT detected PD signals.

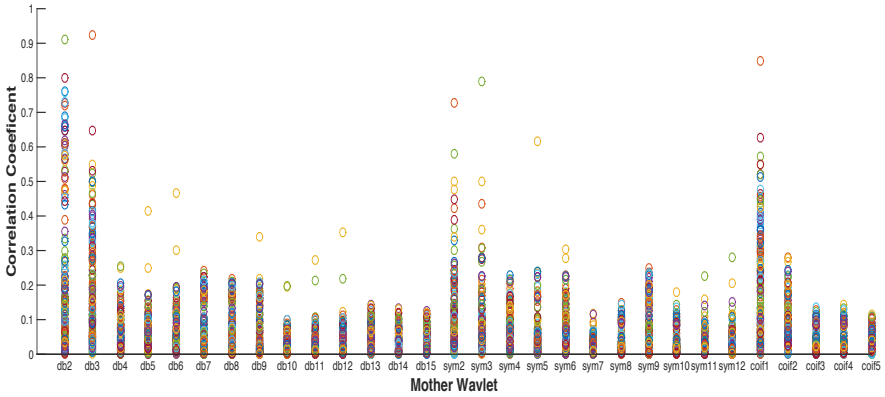

Figure 6-8. Results of Correlation Coefficient values for different wavelet functions

Table 6-1. Optimal Wavelets Selection on the basis of Correlation Based Wavelet Selection

PD Signals	Noise Type									
	N1	**N2**	**N3**	**N4**	**N5**	**N6**	**N7**	**N8**	**N9**	**N10**
S1	db2	db3	db3	db3	sym2	db3	db3	db3	db3	db6
S2	db2	db3	db3	db2	db2	db2	db2	db3	db3	db6
S3	db2	db3	db3	db2	db2	db2	db2	db2	db3	coif2
S4	db2	db3	db3	db2	db2	sym2	sym2	db2	sym4	db6
S5	db2	db3	db3	db3	db2	db2	sym4	db3	db3	db2
S6	db2	db3	db3	db3	db2	db2	db2	db3	db3	db9
S7	db2	db3	db3	db2	db2	db2	db2	db2	sym4	db6
S8	db2	db2	db2	sym9	db2	sym2	sym2	sym2	sym4	sym2
S9	db2	db3	db3	db2	db2	db2	db2	db2	db3	db6
S10	db2	db3	db3	db3	db2	db3	sym4	db3	db3	db6
S11	db2	db3	db3	db2	db2	sym2	sym2	db2	sym4	sym2
S12	db2	db3	db3	db3	db2	db3	db3	db3	db3	db6
S13	db2	db3	db3	db3	db2	db3	coif1	db3	db3	coif1
S14	sym3	db3	db3	db2	db2	sym2	sym4	sym4	sym4	db8
S15	db2	db3	db3	db2	db2	db2	db2	db2	db2	db2
S16	db2	db3	db3	db3	db2	db3	sym4	db3	db3	coif1
S17	db2	db3	coif1	db3	db2	sym7	db4	db3	sym4	db9
S18	sym5	db3	sym3	db2	db2	db2	coif2	db2	db2	db4
S19	db2	db3	coif1	db3	db2	db3	coif1	db3	db3	coif1
S20	db2	db3	db3	db3	db2	db3	db4	db3	db3	sym12

C. Conclusions

The selection of the mother wavelet is dependent on the type of the detection circuit used in the PD measurements [32]. 90% of PD signals detected by the HFCT sensor has damped type exponentially decaying PD pulse waveform. The lower order wavelet functions (db2, db3 sym2 and coif 1) are more suitable for performing de-noising analysis on these type of PD pulses. This can be observed by considering the waveform of PD signal S19 as shown

in Figure 6-11. The PD signal waveform has similar characteristics and properties as compared to wavelet function db3 which is shown in Figure 6-12. On the other hand, the higher order wavelet functions are more suitable for analyzing the PD signals having high frequency oscillations. This can be observed by comparing the high frequency oscillating PD signal of Figure 6-13 with high order optimal wavelet function sym12 shown in Figure 6-14.

Correlation Coefficient algorithm has an average run time of 8 seconds for wavelet selection of one PD signal. The algorithm requires a large number of computations in order to perform the function iterations, normalization of the signals and zero padding technique. These complex computations make the CBWS algorithm inappropriate for real time/adaptive de-noising techniques. On the contrary, the results also concluded that for a particular type of sensor, the CBWS method provides a unique wavelet function i.e. db2 or db3. Later, comparison has been done between the performances of CBWS based wavelet selection and pre-selected wavelet functions (db2 and db3) in multi-level de-noising method. The comparison concludes that there is only a slight difference in the performance parameters by selecting the single wavelet function instead of using CBWS algorithm. Hence, it can be concluded that for HFCT PD measurements, either db2 or db3 as wavelet functions can be used for de-noising algorithms.

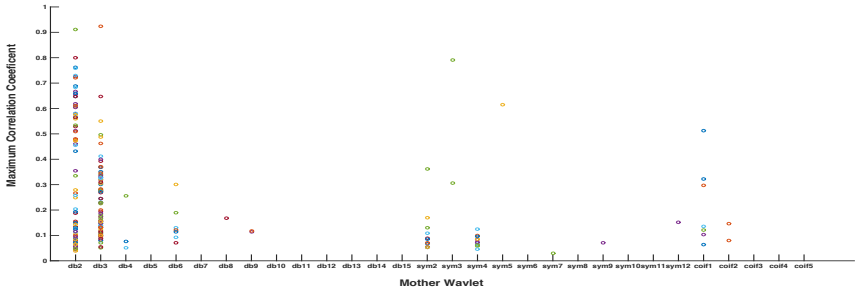

Figure 6-9. Maximum Correlation Coefficients value for each PD signal under analysis

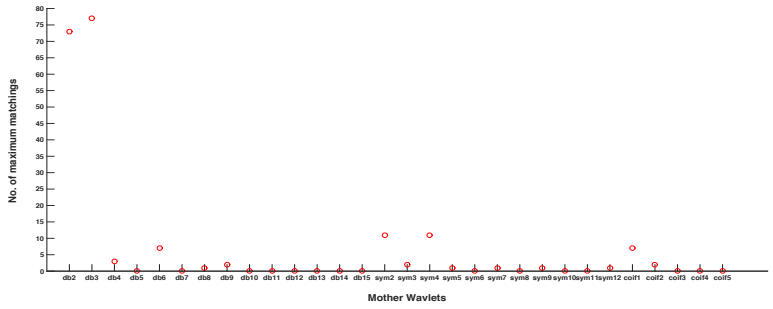

Figure 6-10. Maximum number of Correlation coefficients matching for different Wavelet

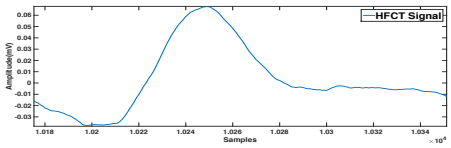

Figure 6-11. Damped Exponential type PD pulse measured with HFCT sensor

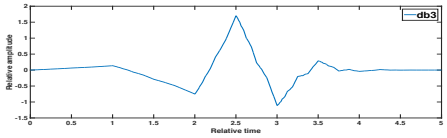

Figure 6-12 Wavelet function 'db3'

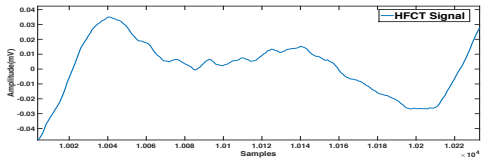

Figure 6-13. Damped Oscillating type PD pulse measured with HFCT sensor

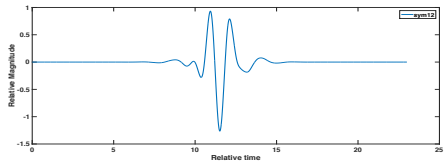

Figure 6-14. Wavelet function 'sym12'

6.3.2 Energy Based Wavelet Selection (EBWS)

The energy based wavelets selection presented in [31] is level dependent wavelet selection method. This means for each decomposition level, the EBWS algorithm computes a new optimal wavelet function suitable for de-noising analysis. The method works on the principle of maximizing the energy percentage in the approximation coefficient considering the fact that the detail coefficient will have lesser energy content if the optimal wavelet function produces the approximation coefficient of maximum energy. This energy percentage is calculated according to the following equation [31]:

$$E_a = \frac{\sum_k {a_{j,k}}^2}{\sum_k {a_{j,k}}^2 + \sum_{i=1}^{j} \sum_k {d_{j,k}}^2} \qquad (22)$$

Where $\boldsymbol{a_j} = [a_{j,1}, a_{j,2}, \ldots\ldots a_{j,k}]$ and $\boldsymbol{d_j} = [d_{j,1}, d_{j,2}, \ldots\ldots d_{j,k}]$ are approximations and details coefficient vectors at level j.

Figure 6-15 & Figure 6-16 illustrates the energy distribution of typical PD waveform when decomposed into detail and approximation coefficients from level 1 to 9 respectively. let's consider the energy distribution at the level 8. Wavelet function Coif5 produces the largest energy concentration in the approximation coefficient of that particular level compare to

other wavelet functions. Correspondingly, the equivalent detail coefficient has the least energy concentration. It is known that the de-noised signal will lose less energy and have smaller waveform distortion if the detail coefficient $\boldsymbol{d_j}$ is set equal to zero or minimum [31]. Using this concept, energy based algorithm selects the optimal wavelet function at each decomposition level which maximizes the energy concentration of the approximation coefficients.

A. EBWS Algorithm

For N level decomposition of the PD signal, the EBWS algorithm works as follows:

1. For level 1, select the wavelet function from the wavelet family library.
2. Perform a single level wavelet decomposition on the signal to obtain the approximation and detail coefficient of level 1.
3. Calculate the energy concentration of the approximation coefficient according to equation (20).
4. Choose the next wavelet function from the wavelet family library and repeat the steps (2&3).
5. After computing the energy percentage of approximation coefficients for all the wavelet functions, determine the optimal wavelet function on the basis of maximum energy concentration value.
6. For the next level decomposition, set the decomposition signal to be the approximation vector from the last level and perform the steps 1-6.
7. Obtain the optimal wavelet functions for each level.

The selection of the optimal wavelets on the basis of EBWS for one typical noisy PD waveform is given in Figure 6-17 and Table 6-2 for 16 levels decomposition. The optimal wavelets chosen on every level is different defining the maximum concentration of the energy in that particular level. EBWS procedure tries to concentrate the maximum energy on the approximation coefficients by considering the fact that the detail coefficients will have minimum energy concentration at that particular level. However, once again consider the Figure 6-15 where at level 7 the energy (60%) is much more concentrated in detail coefficients rather than in approximation coefficients. The EBWS algorithm still tries to maximize the energy of the approximation coefficients which lies around only 20%. Hence, the wavelet function selected for this level is not the optimal wavelet function.

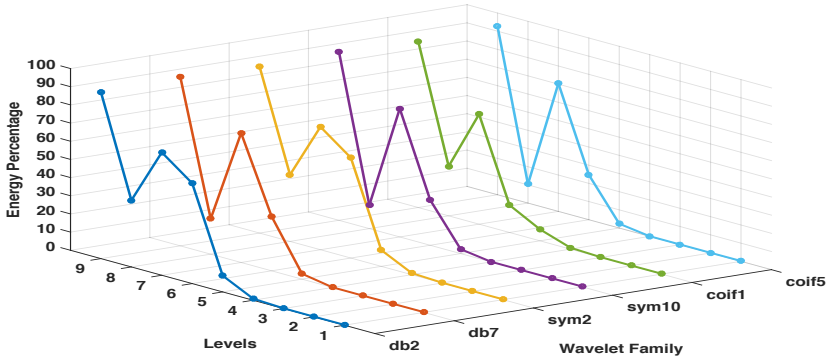

Figure 6-15.Energy concentration of the details coefficients from level 1 to 9 for different wavelet families

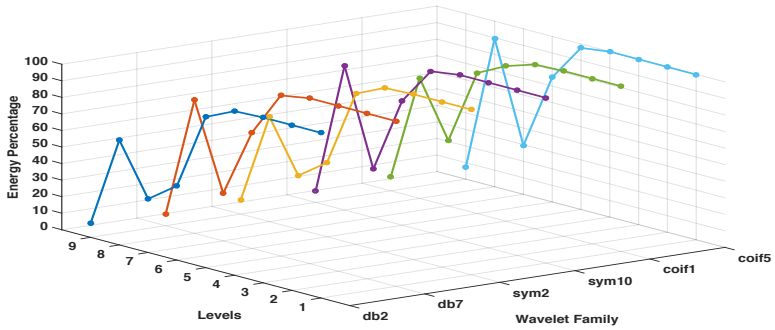

Figure 6-16.Energy concentration of the approximation coefficients from level 1 to 9 for different wavelet families.

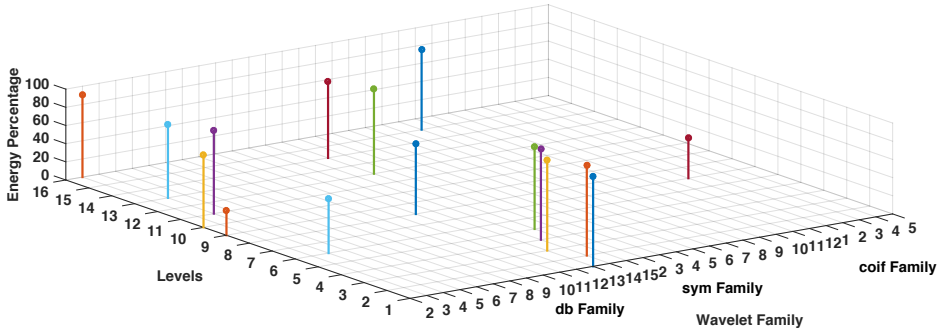

Figure 6-17. Selection of Optimal wavelet functions for 16 levels decomposition on the basis of EBWS and their Energy concentrations

Table 6-2. Selection of Optimal Wavelets for each level by EBWS method

Level	Wavelet Function	Level	Wavelet Function	Level	Wavelet Function
1	db13	7	coif1	13	db4
2	db14	8	db12	14	db15
3	db13	9	db2	15	sym9
4	db14	10	db2	16	db3
5	db15	11	db4		
6	db4	12	db15		

6.3.3 SNR Based Wavelet Selection

An alternative method for selecting the wavelet function on the basis of energy concentration is presented in [34]. This method known as SNR Based Wavelet Selection (SNRBWS) introduces two types of bands; signal band and the noise band. Signal band is defined as the band having the maximum absolute coefficient value of either the detail or approximation coefficients vector. The other vector is assumed to have less information about the original PD signal and is called the noise band. Wavelet function is then chosen among the wavelets family on the basis of having the largest signal to noise ratio between the two selected bands.

The SNRBWS method assumes that the coefficient vector having the highest absolute value corresponds to highest energy concentration. Hence, by finding the maximum valued coefficient vectors among the details and approximations this method concentrates the energy of the PD signal in a smaller number of coefficients with larger amplitudes as compare to EBWS method [34]. The SNR variations for wavelet functions at different levels for one of the noisy PD signals are given in Figure 6-18. At each level, different wavelet function produces the maximum SNR.

Consider now a noisy PD signal as shown in Figure 6-19. The signal and noise bands selected on each level are shown in Figure 6-20 and Figure 6-21 respectively. It can be seen that the signal bands correspond to the original PD signal and noise bands mostly concentrates the white noise in the signal.

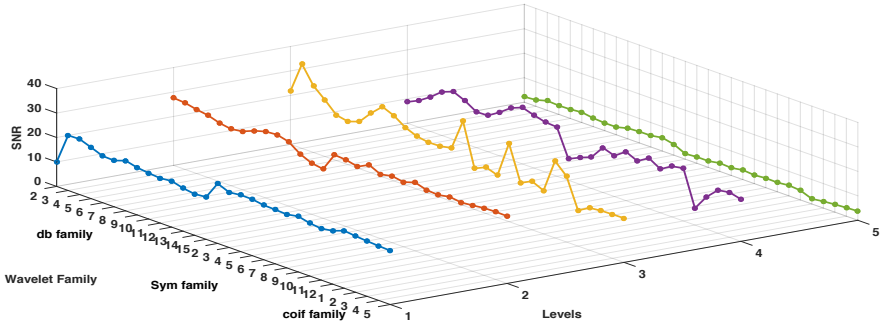

Figure 6-18. SNR variation among wavelet functions at different decomposition levels

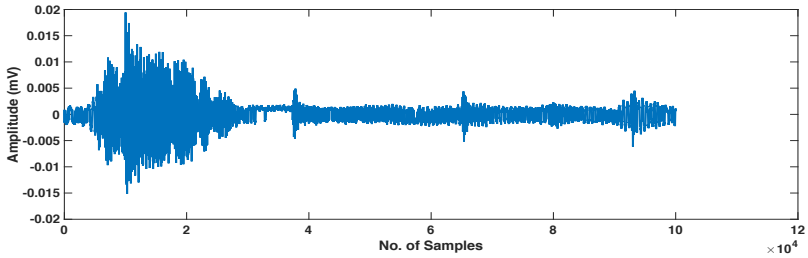

Figure 6-19. Noisy PD signal for SNRBWS analysis

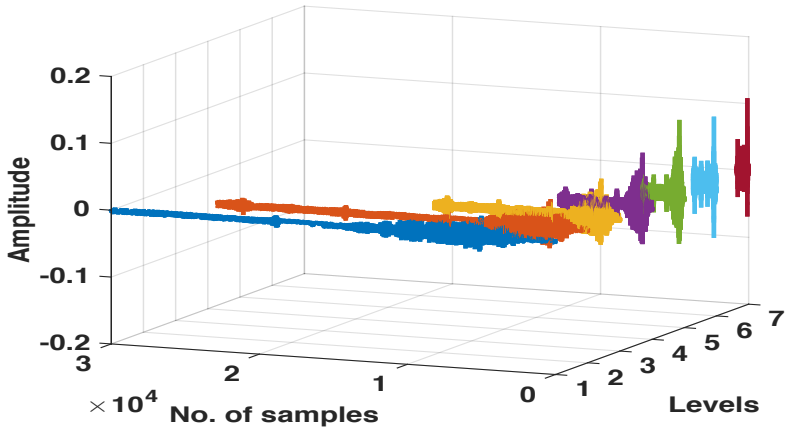

Figure 6-20. Signal Bands at each level by SNRBWS method

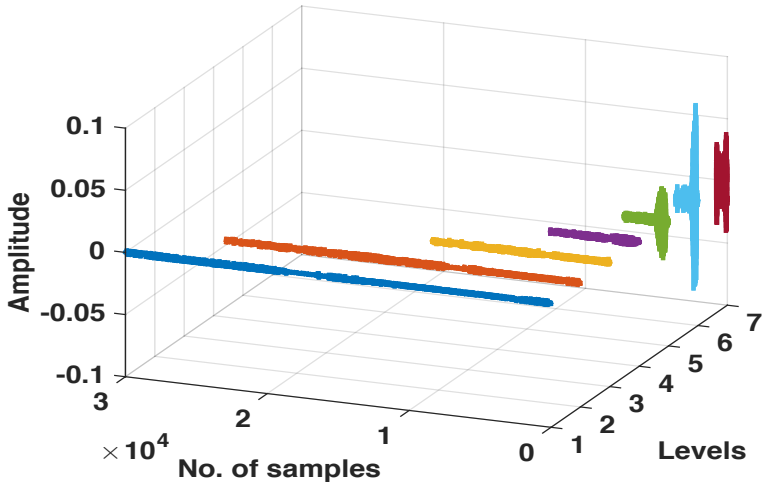

Figure 6-21. Noise Bands at each level by SNRBWS method

A. SNRBWS Algorithm

For N level decomposition of the PD signal, the SNRBWS algorithm works as follows:

1. At level 1, select the wavelet function from the wavelet family library.
2. Perform a single level wavelet decomposition on the signal to obtain the approximation and detail coefficient of level 1.
3. Calculate the maximum absolute value of the detail and approximation coefficients and assign the coefficients with maximum value to signal band and other to noise band.
4. Calculate the signal to noise ratio according to the equation:

$$SNR = \frac{\max(|signal\ band|)}{\max\ (|noise\ band|)} \tag{23}$$

5. Choose the next wavelet function from the wavelet family library and repeat the steps 2-4.

6. After computing the SNR for all the wavelet functions, determine the optimal wavelet function on the basis of maximum SNR value.
7. For the next level decomposition, set the decomposition signal to be the approximation vector from the last level and perform the steps 1-6.
8. Obtain the optimal wavelet function for each level.

6.4 Selection of Number of Decomposition Levels

Generally, the number of decomposition levels are selected on the basis of hit and trial method or by selecting the maximum number of decomposition levels which is suitable to provide better de-noising results. However, the random selection of the decomposition levels may result in wastage of computational time for the de-noising process.

The maximum number of decomposition levels (N) for a signal of length (X) and the wavelet filters length (X_w) is given by equation [30]:

$$N_{max} = fix\left(\log_2\left(\frac{X}{X_w - 1}\right)\right) \tag{24}$$

This method for the maximum number of decomposition levels is suitable for using in the multi-level de-noising schemes. However, as described later the level dependent de-noising schemes requires the wavelet functions to be different at each level. In this case the equation (22) modifies to $N_{max} = fix(\log_2 X)$ [34].

In order to avoid the excessive computation and selection of an appropriate number of decomposition levels, a procedure based on the lowest frequency component of the signal known as the **number of wavelet decomposition levels selection (NWDLS)** was presented in [34]. Figure 6-22 describes the energy spectral density of the polluted PD signal. The vertical dashed line corresponds to the minimum frequency (F_{min}) at which the signal energy is greater than a certain percentage of the total signal energy which is shown as horizontal dashed line. The number of decomposition levels is then given as:

$$N = fix\left(\log_2\left(\frac{F_s}{F_{min}}\right)\right) \tag{25}$$

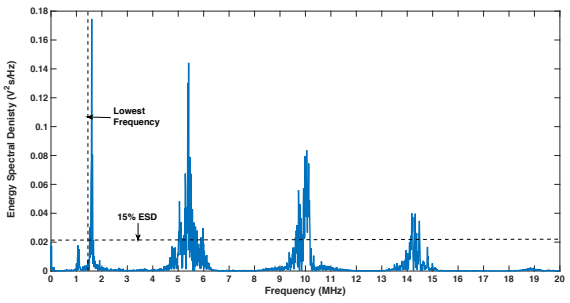

Figure 6-22. Energy Spectral Density of Noisy PD signal

All the lower energy components which are of lesser importance in the de-noising process are discarded by selecting the appropriate number of levels. If the number of decomposition level exceeds the maximum number of decomposition levels, N_{max} given by equation (22) must be assumed.

6.4.1 Results

The performance of NWDLS on the signals under analysis is as follows:

1. 80 out of 200 PD signals (40%) under analysis have a number of decomposition levels higher than the maximum number of decomposition values.
2. The average number of decomposition levels comes out 12, whereas the maximum number of decomposition levels by using equation (22) are 14 for a data size of 100002 and wavelet filters of 'db3'.

6.5 Threshold Determination

Consider the wavelet patterns of the noisy PD signal and the noise as shown in Figure 6-23. It can be observed that they present different wavelet patterns which allow us to extract the PD pattern on the basis of the PD feature extraction. A threshold selection technique must be applied in order to retain the wavelet coefficients which are associated with the PD pulse patterns and discarding the rest of wavelet coefficients which corresponds to noise in the signal [38].

The threshold estimation procedure is considered the most difficult part of the de-noising process. The estimation can be done on the basis of trial and error by manually selecting the coefficients which are similar to PD signature or by prior knowledge of the PD and noise characteristics. Several threshold estimator models have been introduced which are well suited for the purpose of eliminating the white noise. They include the adaptive threshold selection based on the Stein's unbiased risk estimate known as rigrsure threshold selection or on the basis of minimaxi principle which is used in statistics for the purpose of finding the estimators [30]. However, both these functions are ineffective in eliminating the indeterminate noise [40]. Performance evaluation of different thresholding techniques is discussed later in the de-noising algorithm section.

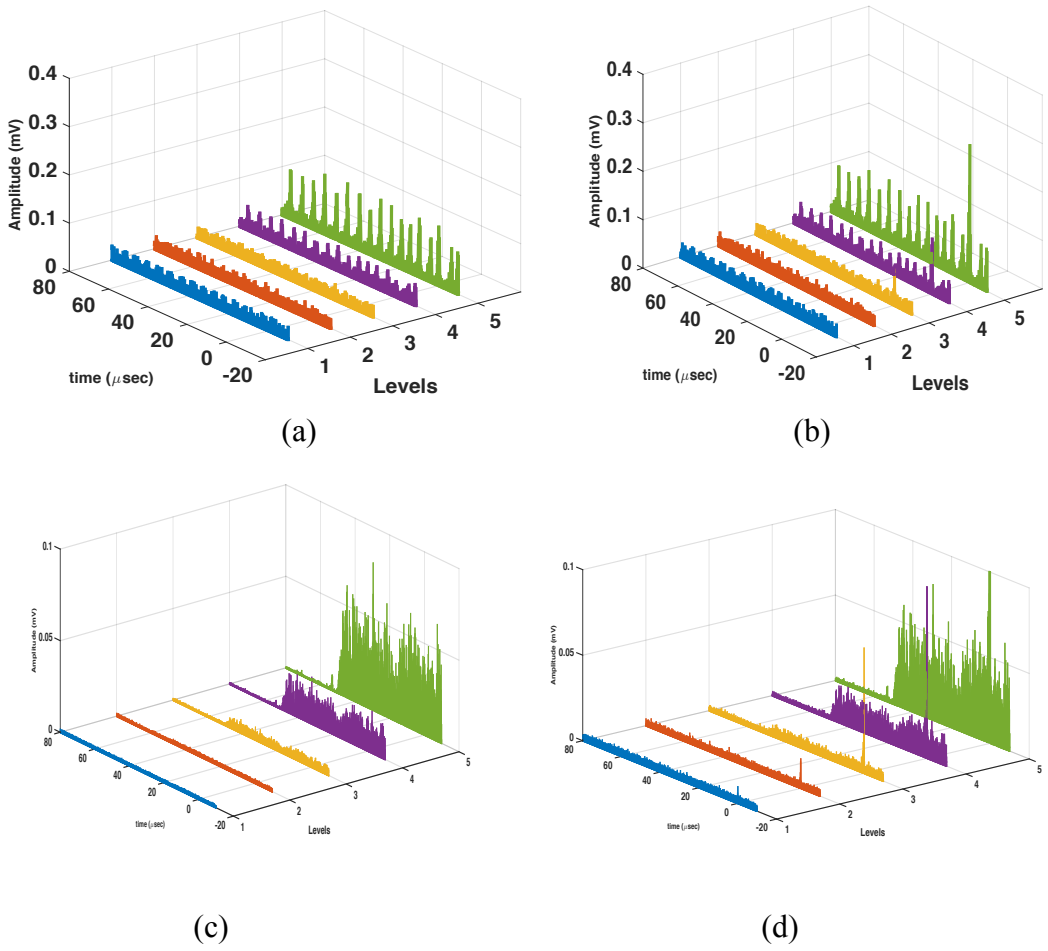

Figure 6-23. Wavelet Patterns for noise and polluted PD signals (a&c) for noise signals , (b&d) for Polluted PD signals

6.5.1 Automated Threshold Determination

For designing an adaptive and fully automated de-noising technique, a universal threshold rule introduced by Donoho and Johnston can be used [39]. Their threshold level is defined by:

$$\lambda = \sigma \,.\sqrt{2\times \log(X)} \qquad (26)$$

where σ is a noise estimating rescaling factor and X is the length of the original signal under analysis.

This universal threshold level given by the equation (24) is recommended to be used on the detail coefficients at each level and on the approximation coefficient of the last level across the decomposition by wavelet transformation [40]. The level dependent threshold estimation can be achieved by replacing X in equation (24) by the length of the detail coefficient associated with the particular level. The multiplicative threshold rescaling factor given in equation (24) estimates the noise level in detail coefficients by calculating

the standard deviation of details from the input signal. The Median Absolute Deviation / 0.6745 estimator is used for this purpose. The equation (24) is modified as:

$$\lambda_i = \sigma_i \cdot \sqrt{2 \times \log(X_i)} \tag{27}$$

where λ_i is the estimated threshold value of the detail coefficient at level i. σ_i is the multiplicative threshold rescaling factor given by $\sigma_i = \frac{m_i}{0{,}6745}$, m_i is the median value of absolute deviation. X_i is the length of detail coefficients at level i.

The de-noising process can be carried out by applying either the soft or hard thresholding techniques. These techniques will determine how the wavelet coefficients are shrinked or zeroed so that the noise can be eliminated most efficiently. Hard thresholding works on the principle of keeping the wavelet coefficients whose absolute values are larger than the threshold value estimated by equation (25) and set the rest to zero. This can be expressed mathematically as:

$$\delta_\lambda^H = \begin{cases} x \ if \ |x| > \lambda \\ 0 \ if \ |x| \leq \lambda \end{cases} \tag{28}$$

The soft thresholding shrinks the coefficients towards zero value as it can be seen from the mathematical expression:

$$\delta_\lambda^H = \begin{cases} x - \lambda & if \ x > \lambda \\ 0 & if \ |x| \leq \lambda \\ x + \lambda & if \ x > -\lambda \end{cases} \tag{29}$$

Later the de-noising results prove that the hard thresholding is much better than soft thresholding in producing a better PD signal to noise ratio.

Chapter 7 DE-NOISING METHODS

7.1 Level Dependent De-Noising

The level dependent wavelet transformation methods use the optimal wavelet function selected on the basis of energy based wavelet selection or SNR based wavelet selection method for each decomposition level. The level dependent Denoising applies all the major steps of DWT mentioned in section 6.2. However, the application of wavelet function for each level requires a single stage decomposition for DWT of the original signal and single level reconstruction for IDWT. This can be explained further in the level dependent algorithm.

7.1.1 Level Dependent De-Noising Algorithm

The algorithm works on following steps:

1. Find the number of suitable decomposition levels (N) on the basis of method described in section 6.4.
2. Apply the energy based wavelet selection or SNR based wavelet selection algorithm for wavelet function selection at level 1.
3. Apply single level discrete wavelet transformation using the selected wavelet function by step 2 to obtain the detail and approximation coefficient vectors.
4. Apply the automated threshold function as defined in section 6.5.1 to the detail coefficient vector to obtain the threshold value.
5. Apply hard thresholding to obtain the modified detail coefficient.
6. Set the approximation coefficient vector as a next level signal for decomposition.
7. Repeat steps 2-6 for each level to obtain the modified detail coefficients until the last level N.
8. Starting from level N, reconstruct the signal by applying the single level inverse discrete wavelet transformation to modified detail coefficient vector and approximation coefficient vector at level N.
9. Obtain the reconstructed approximation vector at level N-1.
10. Apply zero padding technique if required in order to equalize the length of detail coefficient vector at level N-1 and reconstructed approximation vector obtained at step 9.
11. Repeat steps 8-10 until the first level to obtain the reconstructed de-noised signal.

7.2 Multilevel De-Noising

Compare to the level-dependent Denoising, multi-level Denoising is a level independent technique which uses only a single wavelet function for the decomposition of the signal into N levels. Correlation based wavelet selection method can be used in order to select the wavelet function for the de-noising process. As already mentioned the correlation based

wavelet selection method is not suitable for applying in the real time onsite data measurements because of large computational time, however, an optimal wavelet function based on the knowledge of the detection circuit can be used as concluded earlier. Comparison between the performance indices of the multi-level de-noising based on correlation based wavelet selection and single pre-defined wavelet function is provided at the end of this section which proves that using a single wavelet function instead of the correlation based wavelet function results in only a slight variation of the performance indices.

7.2.1 Multi-Level De-Noising Algorithm

As described above, the multi-level de-noising algorithm is level independent and hence less complex as compared to level dependent de-noising. The main steps of de-noising process are more or less similar to the common DWT algorithm.

The algorithm works on following steps:

1. Find the number of suitable decomposition levels (N) depending on the size of the signal.
2. Choose the optimal mother wavelet on the basis of correlation based wavelet selection or pre-defined wavelet function.
3. Apply the 1-D multi-level wavelet decomposition on the signal using the mother wavelet from step 2.
4. Extract the detail coefficients at each level and approximate coefficient of the last level from the decomposition structure.
5. Apply appropriate thresholding technique on the detail coefficients at each level to obtain the modified detail coefficients.
6. Reconstruct the signal by using the modified detail coefficients and the approximate coefficient at level N.

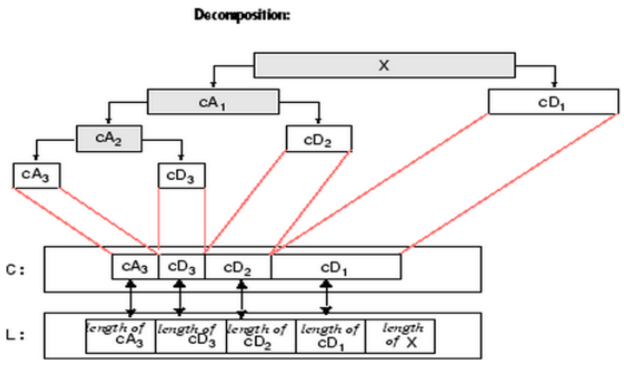

Figure 7-1. Decomposition Structure by using Wavedec Function [30]

Multi-level decomposition of the signal under analysis is performed by using the Matlab function **wavedec** instead of using a single level discrete wavelet transformation**.** The function performs decomposition on the signal on the basis of specific wavelet or filters at

level N. The output of the function is a decomposition structure having approximate coefficient at level N and detail coefficients of each level. Figure 7-1 describes the decomposition principle use by wavedec function [30].

7.3 Analysis of De-noising methods

7.3.1 Performance indices

The de-noising process may result in the attenuation and distortion of the original PD signal which needs to be recovered from the polluted PD signal. In order to evaluate the performance of de-noising techniques various indices are defined which indicates how efficiently the noise is suppressed with minimum attenuation and distortion of the PD pulse [36]. Following indices are used in this study for comparison of different de-noising techniques:

A. Signal to Noise Ratio (SNR)

If the de-noised signal is given by X_{de} and the original PD signal as X and both signals are of length N, then the signal to noise ratio is defined by the equation:

$$SNR = 10\times \log\left(\frac{\sum_{i=1}^{N} X_{de}^2(i)}{\sum_{i=1}^{N}\left(X(i) - X_{de}(i)\right)^2}\right) \tag{30}$$

Positive SNR value indicates that the power of the PD signal is greater than of noise and negative value implies a greater power of the noise as compared to the PD signal [36].

B. Reduction in Noise Level

As in practical situation, there is no reference PD signal which can be used to compare the signal to noise ratio by applying the equation (28). Hence, the extent to which the noise is suppressed can be found by applying the equation (29) which uses the original noisy signal as reference [36]. Reduction in noise level is given in dbs.

$$Reduction\ in\ Noise\ level = 10\times log \sum_{i=1}^{N} \frac{1}{N}\left(Z(i) - X_{de}(i)\right)^2 \tag{31}$$

C. Mean Square Error

The mean square error calculation on the basis of average noise power is another factor for evaluating the de-noising methods. For a noisy PD signal Z and de-noised signal X_{de} the mean square error (MSE) is given by:

$$MSE = \frac{\sum_{i=0}^{N}[X_{de}(i) - Z(i)]^2}{N * Pnoize} \quad (32)$$

where $Pnoize$ is the total average power of the noise signal.
Now, if the de-noising process removes all the noise the value of MSE from equation (30) will be unity. Therefore, an efficient de-noising method will have MSE value near to unity or larger.

D. Reduction in PD pulse Amplitude

The attenuation of the PD signal due to the de-noising process can be calculated on the basis of calculating the peak values of the de-noised and the original PD signal. The percentage reduction in amplitude is given by:

$$\%reduction\ in\ amplitude = \frac{X - X_{de}}{X} \times 100 \quad (33)$$

where X and X_{de} are original PD signal and de-noised signal respectively.

E. Correlation Coefficient

Statically, the correlation coefficient defines a measure of the degree of linear relationship between the two variables. It measures the extent to which the linear model may describe the relationship between the two variables [41]. Hence, the correlation coefficient can be applied to measure the degree of similarity and distortion between the PD signal and the de-noised signal by using the equation:

$$\gamma = \frac{\sum_{i=0}^{n}\left(X_i - \overline{X}\right)(X_{de_i} - \overline{X_{de}})}{\sqrt{\sum_{i=0}^{n}(X_i - \overline{X})^2 \sum_{i=0}^{n}(X_{de_i} - \overline{X_{de}})^2}} \quad (34)$$

where $\overline{X}$ and $\overline{X_{de}}$ are the mean values of the original X and de-noised signal X_{de} respectively.

The correlation coefficient may take a value between -1 to +1. The sign of correlation coefficient indicates the direction of the relationship. A positive correlation means as the value of one variable increases the other variable increases and vice versa. However, taking the absolute value of the correlation coefficient measures the strength of the relationship. Therefore, both +1 and -1 indicates a perfect relationship between two variables [41].

7.3.2 Measurements

A. Partial Discharge Measurements

Partial discharge signals measurements were made in MV switchgear inside the laboratory. The measurement setup with the artificial PD source in the MV switchgear is shown in the Figure 7-2. High frequency current transformer (HFCT) is used in order to detect twenty different PD signals. The capturing time of the PD signal was 100µs at sampling frequency of 2Ghz.

The artificial PD is created with the help of a voltage indicator circuit used inside in the MV switchgear panel which comprises insulation (silver part) and capacitor unit inside the mastic. The capacitor unit in this setup acts as a protective device and is placed between high potential terminal and ground through switchgear.

(a) (b)

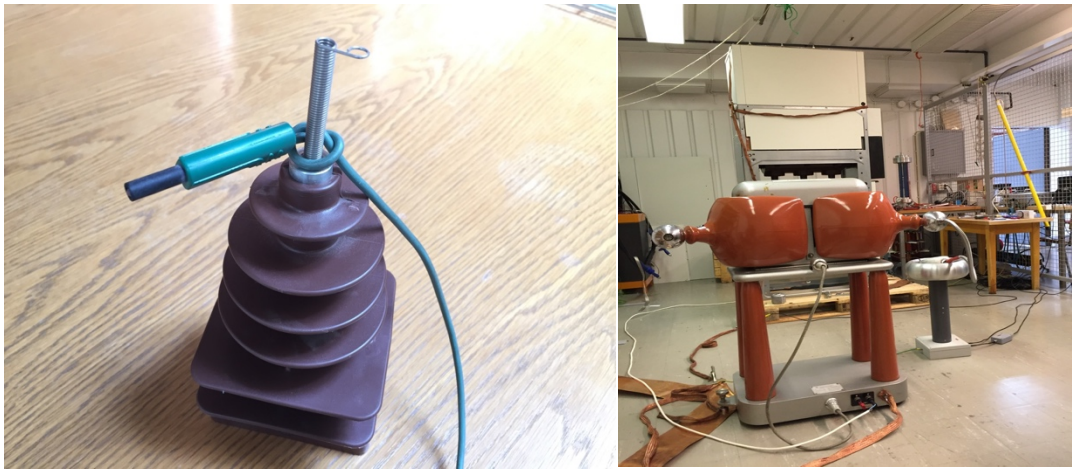

(c) (d)

Figure 7-2 PD Measurement Setup (a &b) MV Switchgear with artificial PD source, (c) Voltage transformer for creating artificial PD, (d) HV transformer and coupling capacitor arrangement for conventional PD measurements

B. On-Site Measured Noise

The noise signals used in the study are measured at HELEN substation with the help of a D-Dot sensor placed inside switchgear feeding an industrial load. Various types of noises were recorded by D-Dot sensor at the on-site conditions. D-Dot sensors are preferred in the measurements because of its high sensitivity. Table 7-1 shows the SNR values of the 10 type of different noises observed. The lower SNR signals N1, N4, N6, N8 and N10 are shown in Figure 7-3. These noise signals when coupled with the PD signals exhibits the pattern quite similar to the original PD signals and are difficult to eliminate by de-noising methods.

Table 7-1. SNR of noise signals

Noise	SNR	Noise	SNR
N1	0,2871	N6	0,2174
N2	3,3281	N7	6,7870
N3	7,4532	N8	0,5632
N4	1,5109	N9	7,0240
N5	8,3451	N10	1,1276

The noise signals set comprises almost all of the noises referred in the introduction section except the DSI type interference. For removal of DSI, wide band filters centered on the communication frequencies can be used in the de-noising algorithms. Further, noise N9 is a periodic repetitive pulse which can be removed by using the gating circuit. The implementation of both these circuitries are beyond the scope of this study and not considered further in the analysis.

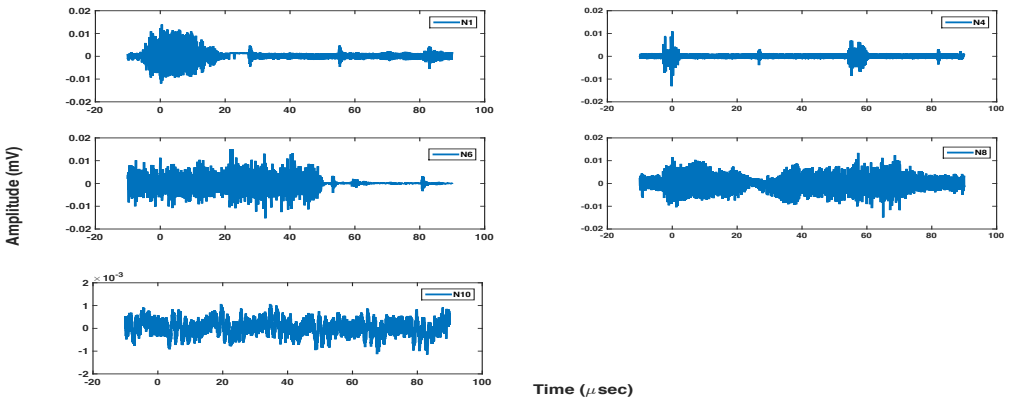

Figure 7-3. Measured Noise signals with lower SNR values

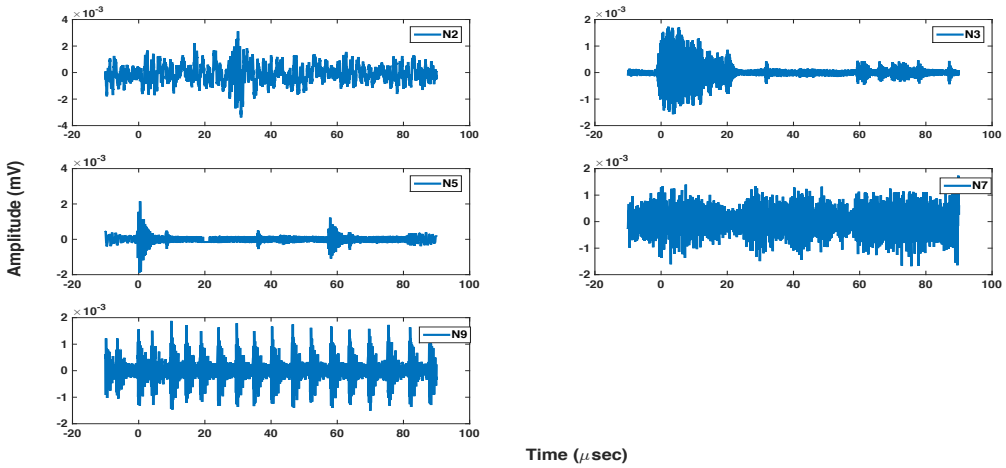

Figure 7-4. Measure noise signal with high SNR values

C. Selection of Wavelet Functions Library

As already discussed in the optimal wavelet selection methods, the wavelet function is chosen on the basis of maximum similarity to the PD signal under analysis. On the basis of literature review and realizing the desired properties of analyzing the transit type PD signals, following wavelet families with their corresponding wavelet functions are selected in this study for analysis.

1. Daubechies wavelets (db2-db15)
2. Symlet Wavelets (sym2-sym12)
3. Coieflet Wavelets (coif1-coif5)

7.4 Analysis and Results

Figure 7-5 shows one of the PD signals under observation coupled with the noise signal for evaluating the performance of the level-dependent and multi-level de-noising algorithms. Let's say this signal be S1. The method is applied considering both the EBWS and SNRBWS algorithms for selecting the wavelet function at each level for level dependent de-noising and correlation based wavelet selection for the multi-level de-noising.

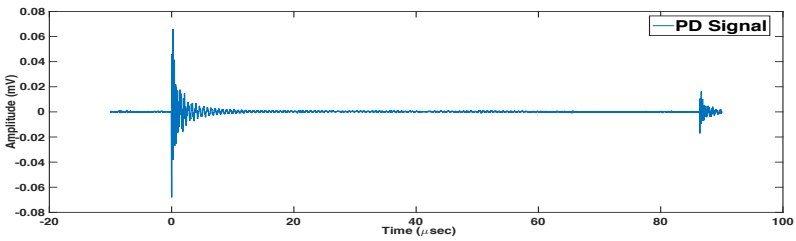

(a)

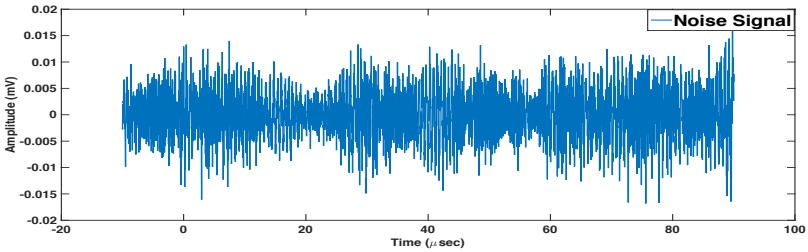

(b)

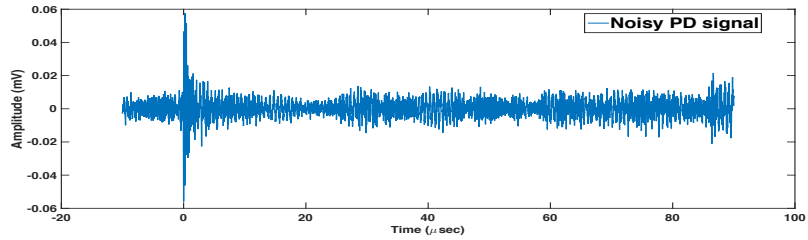

(c)

Figure 7-5. Signal for analysis of level dependent and multi-level de-noising techniques (a) Original measured PD signal, (b) White Noise Signal (c) PD coupled with noise signal

The wavelet functions selected on the basis of EBWS and SNRBWS are shown in Table 7-2. As it can be seen, the wavelet functions selected on the basis of EBWS and SNRBWS are totally different from each other. Figures (7-2 & 7-3) compares the original and modified detail coefficients obtained by the level dependent de-noising algorithm with the multi-level de-noising algorithm.

Table 7-2. Wavelets Selected on the basis of EBWS and SNRBWS methods

Level	EBWS	SNR BWS	Level	EBWS	SNR BWS
1	sym8	db12	6	db3	coif1
2	db11	coif4	7	sym5	db15
3	db9	db10	8	db2	sym11
4	db2	db15	9	sym2	db13
5	db2	db9			

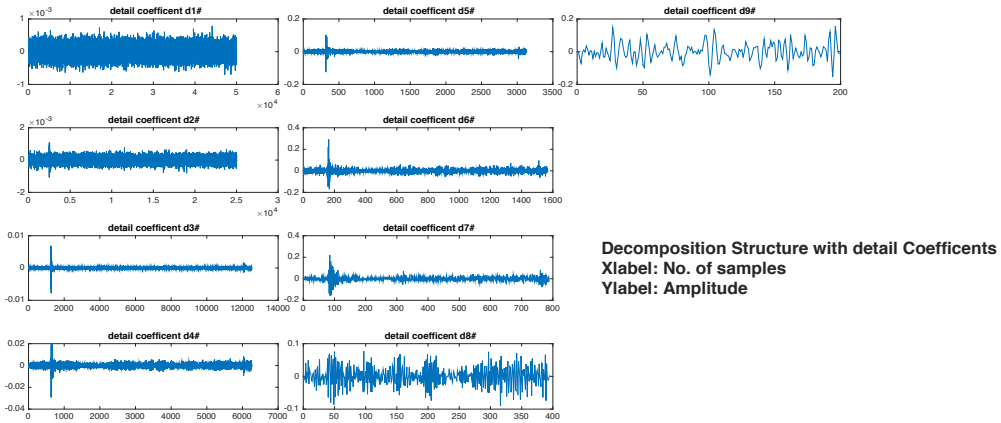

(a)

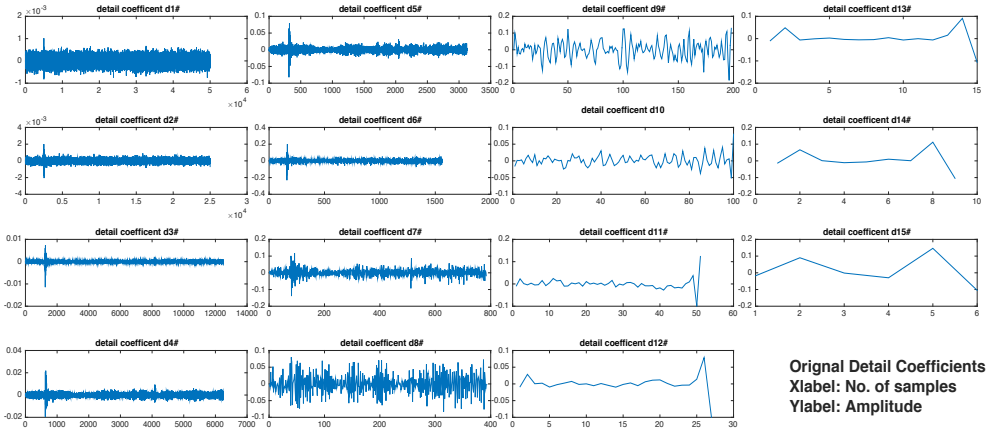

(b)

Figure 7-6 Decomposition structure with detail coefficients for each level (a) Decomposition by using the EBWS method and number of decomposition levels selected on the basis of NWLDS method (b) Decomposition by using the CBWS method on the basis of maximum number of decomposition levels

It is observed that there is no significant difference between the decomposition structure by the EBWS and SNRBWS methods. Hence, for comparisons, only one of the decomposition structures for level dependent de-noising method is shown in Figure 7-6. The level dependent decomposition produces the detail coefficients which have wave pattern much similar to the PD signal as compared to the multi-level Denoising decomposition structure. This can be realized by considering the detail coefficients d5 and d7 of the two methods.

The thresholded detail coefficients referred as the modified detail coefficient vectors have almost similar patterns for both the level dependent and multi-level de-noising methods. However, it can be observed that multi-level den-noising method suppresses the high frequency noises more efficiently as compared to lower frequencies as seen at modified detail coefficients vector d1 in Figure 7-7.

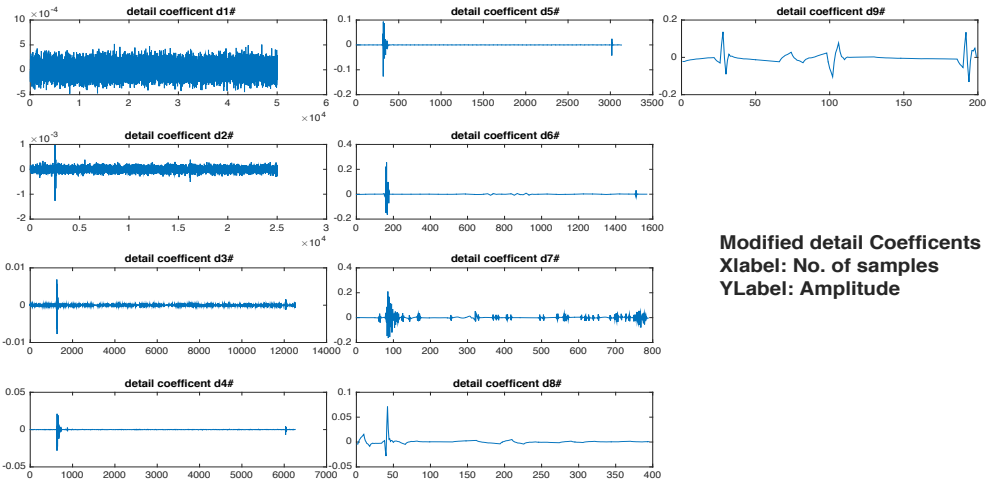

(a)

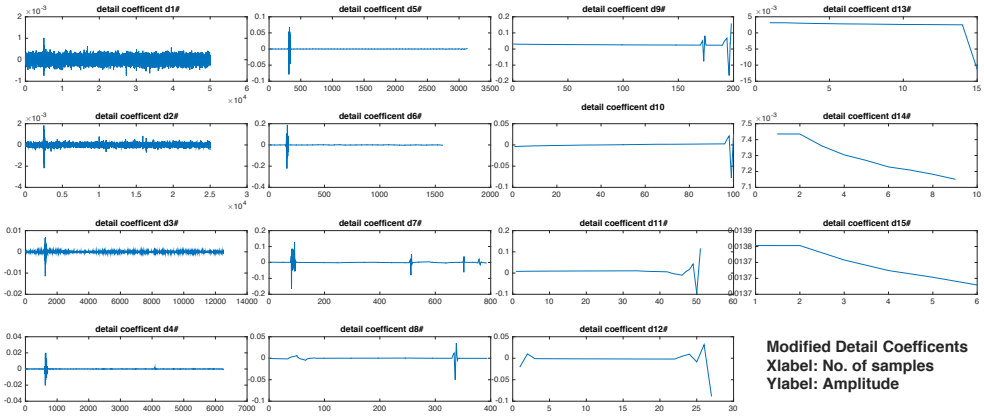

(b)

Figure 7-7. Modified Detail Coefficients after Thresholding (a) level dependent method (b) multi-level Denoising method

Both algorithms successfully de-noises the noisy PD signal as shown in Figure 7-8. Both methods EBWS and SNRBWS for the level dependent de-noising produces almost similar results with no major differences in the performance evaluation indices as well. However, the SNRBWS produces a much more refined de-noised signal as can be seen from the figure as well as the evaluation parameters given in Table 7-3.

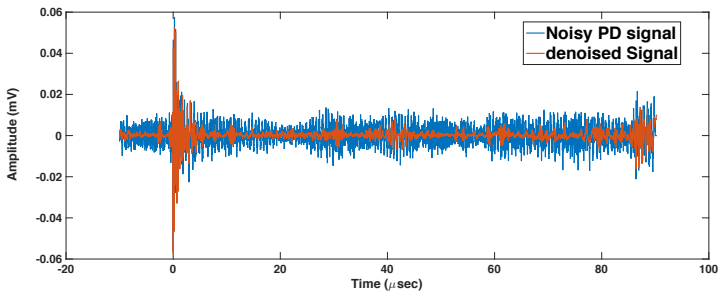

(a)

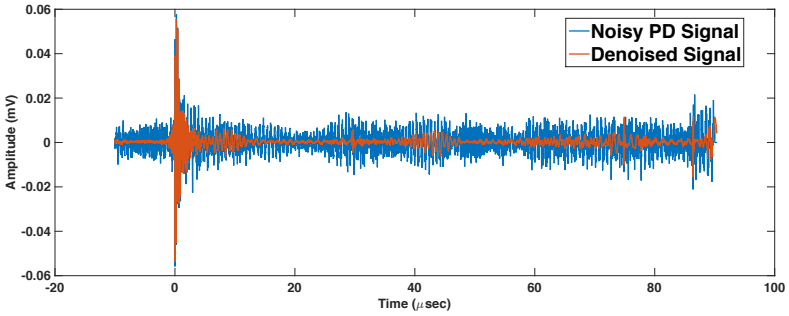

(b)

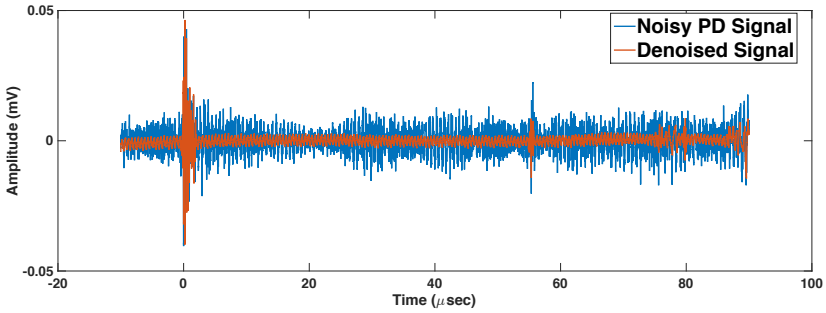
Noisy PD Signal
Denoised Signal
Amplitude (mV)
Time (μsec)

(c)

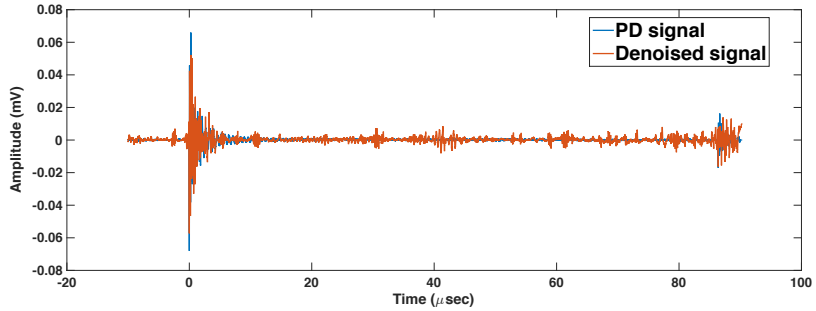
PD signal
Denoised signal
Amplitude (mV)
Time (μsec)

(d)

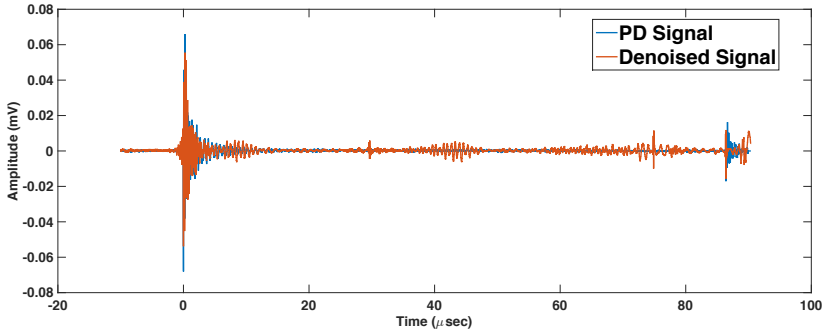
PD Signal
Denoised Signal
Amplitude (mV)
Time (μsec)

(e)

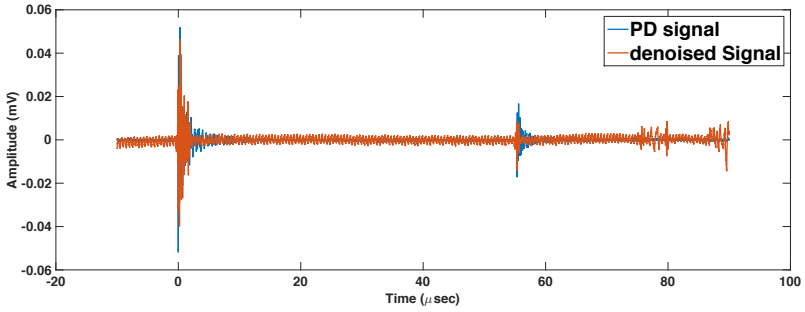
PD signal
denoised Signal
Amplitude (mV)
Time (μsec)

(f)

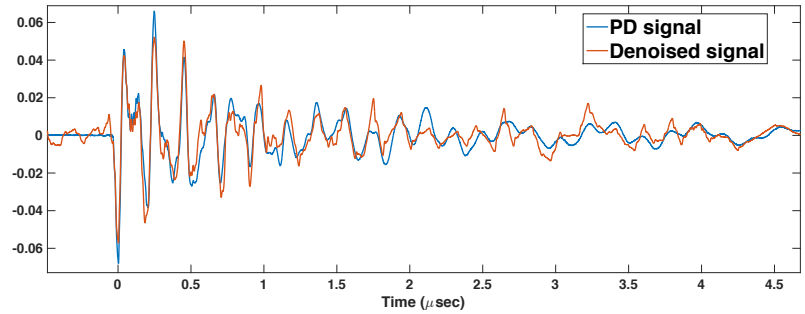
PD signal
Denoised signal
Time (μsec)

(g)

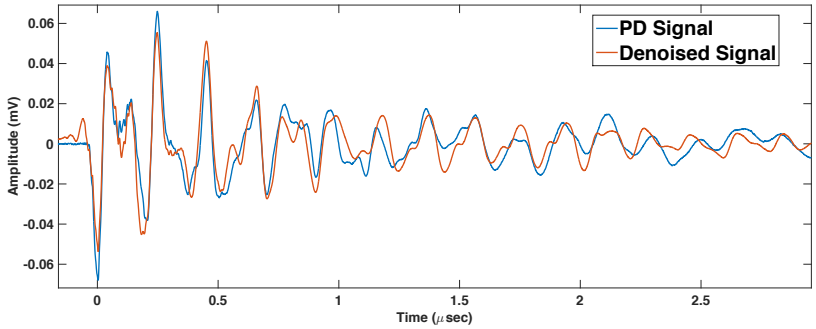

(h)

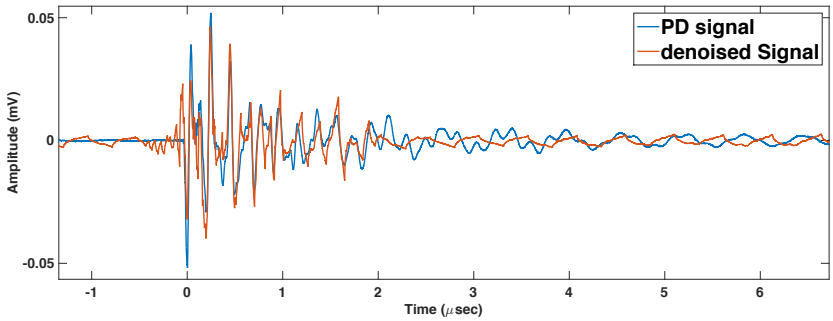

(i)

Figure 7-8. De-noising results (a, b & c) comparison of the de-noised signal with noisy PD signal, (d, e & f) comparison of the de-noised signal with original PD signal, (g, h & i) Zoomed analysis of the de-noised signal for analyzing the wave pattern for level dependent (EBWS, SNRBWS) and multi-level de-noising methods respectively.

As expected, due to selective wavelet function for each level the performance indices for the level-dependent de-noising is slightly better as compared to the multi-level de-noising. Also, for multi-level de-noising the de-noised signal has slightly distorted wave pattern compares to the other which is also indicated by the lower value of correlation coefficient for correlation based method given in Table 7-3.

Table 7-3. Comparison of performance indices for level dependent (EBWS & SNRBWS) and multi-level de-noising techniques

Signal (S1)	Correlation Coefficient	Mean Square Error	Reduction in amplitude (%)	Reduction in noise level (dB)	SNR
EBWS	0.691	0.258	11.225	-52.889	2.636
SNRBWS	0.721	0.266	15.899	-53.460	2.811
Correlation Based	0.677	0.234	13.138	-53.311	2.14

For multi-level de-noising, the comparison between the correlation based wavelet selection and pre-defined wavelet selection for the 200 signals under analysis is performed in order to understand the significance of using the optimal wavelet for wavelet transformation. The average values of the performance indices are provided in Table 7-4.

Table 7-4. Performance indices for evaluation of correlation based wavelet selection method and pre-defined wavelet selection

Multi-Level Denoising	Correlation Coefficient	Mean Square Error	Reduction in amplitude	reduction in noise level (dB)	SNR
db2	0.7284	0.4002	5.8066	-56.2377	5.2113
Correlation	0.7289	0.3989	7.9924	-56.2631	5.2154
db3	0.7256	0.4015	9.4832	-56.2208	5.1824

As it can be seen, there is no significant difference between the performances indices and using the time consuming correlation based wavelet selection method is baseless. Hence, it can be concluded from the observations made in the study that for PD measurements made by the HFCT sensor, the optimal wavelet functions to be used for multi-level de-nosing techniques are db2 and db3.

As previously discussed, the performance of online and on-site PD diagnostics of an electrical equipment is hindered by the presence of the noise in the surrounding environment which may completely swamp the PD signal. The elimination of the noise and recovery of the PD signal of interest is a major challenge in the implication of the online condition assessment system. Further, an efficient de-noising technique may result in reducing the amount of data to be transferred from the site location to the local control center for monitoring and asset management purpose [37]. Another challenging factor is the processing time for analyzing the PD data. The repetition rate of PD pulses is very high and single PD pulse has a pulse duration in nano-seconds. This requires the on-site online system to have de-noising process which computes and sends data as fast as possible. Considering all the above mentioned facts, an improved adaptive de-noising method based on the dominant frequency and amplitude of the signal has been proposed in this research.

According to research publication in the reference [42], the noise can be separated from the PD signal on the basis of various factors. One of the factors includes a comparison of the frequency spectrum of the noise signal with the PD signal which concludes that the central band which is the dominant frequency component of the signal is three to five times larger than the side bands. These side bands are considered to have noise content of the signal whereas the useful PD signal is concentrated much in the dominant frequency bands as depicted in Figure 8-1. The research also concludes that the noise levels measured during the onsite measurements are much smaller as compared to the PD signals. Using these conclusions, self-adaptive de-noising method is implemented by carefully selecting the detail coefficients on the basis of the dominant frequency and amplitude comparisons.

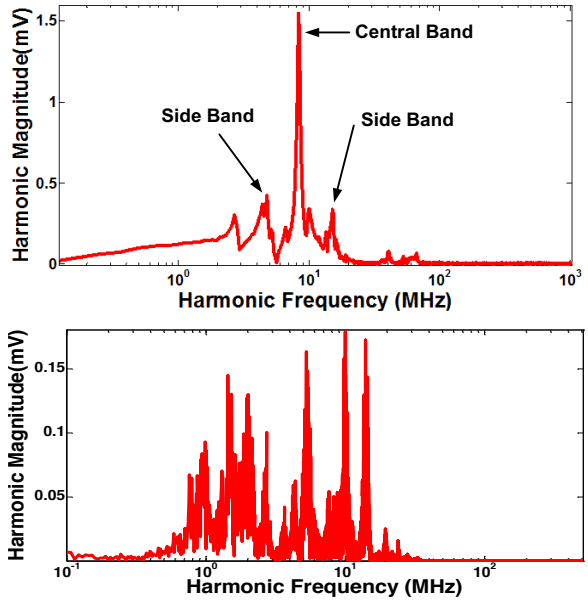

Figure 8-1. FFT of the typical PD and noise signal [42]

Consider a noisy PD signal with the frequency spectrum as shown in Figure 8-2. Dominant frequency is defined as the frequency at which the signal has the highest amplitude in the

whole frequency spectra. As it can be seen, the dominant frequency for this particular signal is 1595 KHz

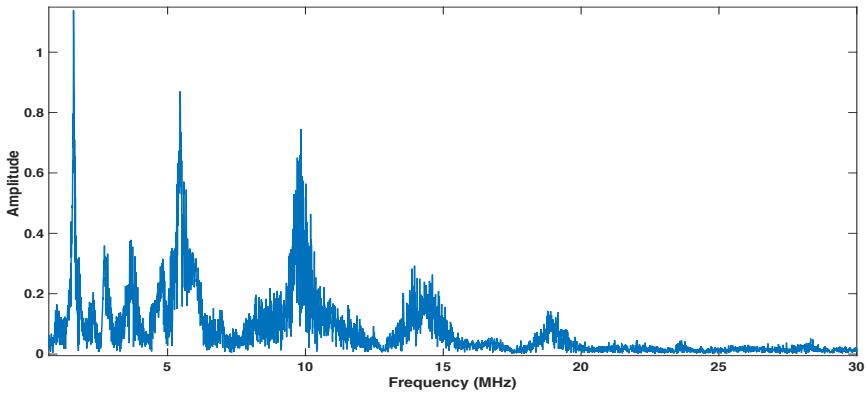

Figure 8-2. Frequency Spectrum of noisy PD signal

Now let's analyze the frequency spectra of the decomposition structure of this signal. Figure 8-3 illustrates the detail coefficients and their frequency spectrum for 12 levels decomposition of polluted PD signal by using 'db2' wavelet filters.

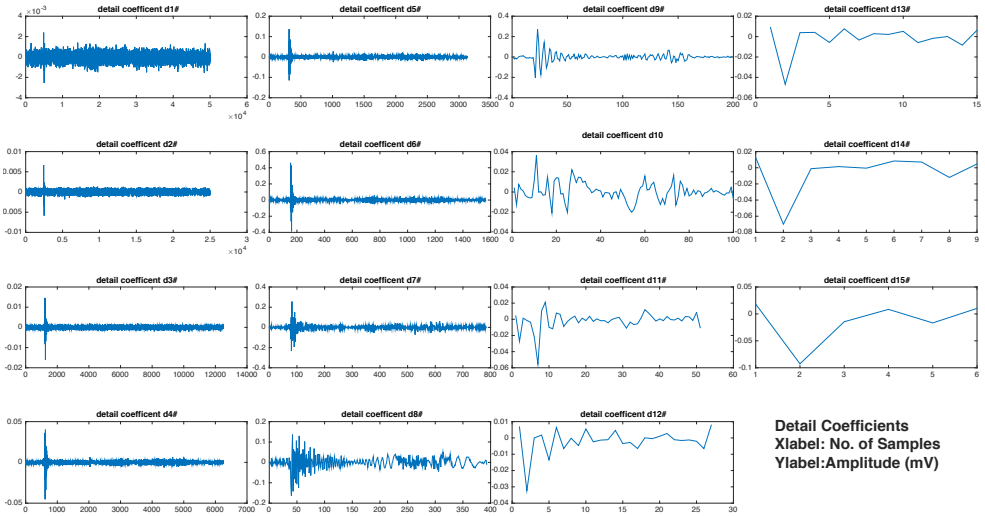

Figure 8-3. Decomposition structure for 12 levels using the 'db2' wavelet filter

The detail coefficients having the dominant frequencies comparable with that of the signal have the PD pattern similar to the original PD signal i.e. detail coefficients 7, 8 and 9. Besides these useful detail coefficients detected on the basis of the dominant frequencies, the detail coefficients 5, 6 and 7 have a pattern similar to the PD signal as well. By analyzing the peak to peak amplitude of the noisy PD signal and compare it with the peak to peak values of the detail coefficients these useful detail coefficients can also be selected. All the useful selected coefficients are then reconstructed by using the thresholding techniques described in section 6.5 to obtain the de-noised signal. This shortlisting of the coefficients based on the amplitude and frequency comparison and discarding the rest of components results in not only improved computational time but the sensitivity of the PD detection measurement system is greatly enhanced. The experimental results presented in section 8.2 confirms the above statement.

8.1 Self-Adaptive De-Noising Algorithm

The basic DWT steps as discussed in section 6.2 are implemented in this adaptive de-noising technique which includes the selection of the decomposition levels, wavelet filters and applying the threshold values on the selected detail coefficients. The de-noised signal is obtained by applying the inverse discrete wavelet transform on the modified detail coefficients and the last level approximation coefficients. The major challenge in implementing the algorithm was setting the limits to compare the dominant frequencies and amplitude of detail coefficients with the noisy PD signal. The results in section 8.2 show that setting the dominant frequency limits to ± 30% and amplitude limits to ± 60% results in optimum de-noising results.

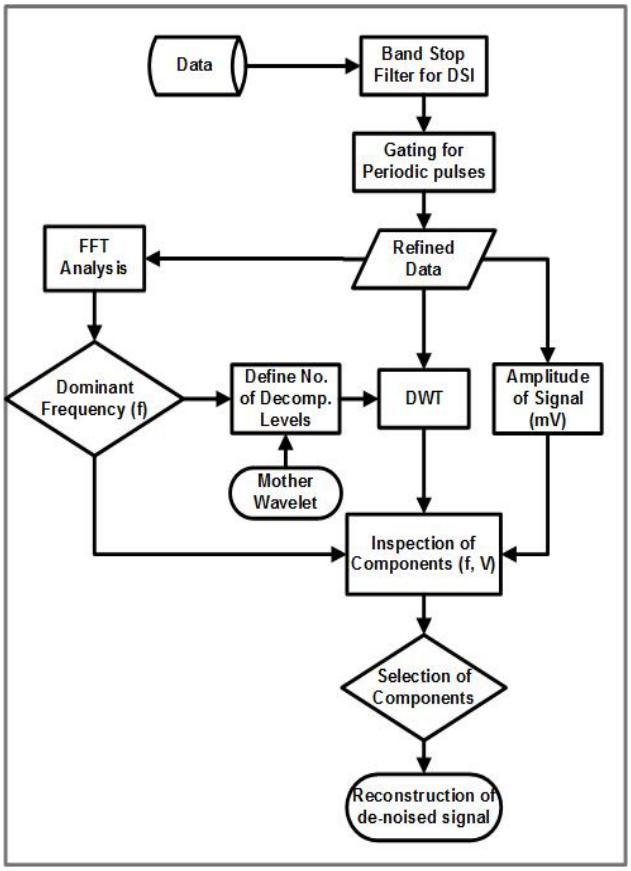

Figure 8-4. Flow chart of Self-Adaptive De-noising technique

The flow chart of the algorithm is given in Figure 8-4. Implementing the band stop filtering and gating circuit will eliminate the DSI and periodic pulses from the polluted PD signal. The refined PD data with most probable white noise and pulsive noise is subject to the de-noising process. The basic steps of the algorithm are as follows:

1. Select the appropriate number of decomposition levels by the method described in section6.4.
2. Choose a mother wavelet on the basis of Correlation based mother wavelet selection as described in section 6.3.1.
3. Apply the FFT to find the dominant frequency of the noisy PD signal under analysis. Set the limits to maximum and minimum percentage of dominant frequency.
4. Calculate the peak to peak amplitude of the noisy PD signal under analysis. Set the limits to maximum and minimum percentage of amplitude.
5. Apply multi-level wavelet decomposition as described in section 7.2 by using the wavelet function selected on the basis of the correlation based wavelet selection method.
6. Obtain the detail coefficient vector for each level and apply the FFT to compare the frequency spectra with the limits set in step 3. Similarly, compare the peak to peak amplitude of each detail coefficient vector with the limits set in step 4. Select the detail coefficients which lies within the limits.

7. Select the threshold values for selected detail coefficients and apply hard thresholding to obtain the modified detail coefficients.
8. Reconstruct the signal with the modified detail coefficients by using the inverse discrete wavelet transformation.

8.2 Performance Evaluation of the Adaptive De-Noising

For setting the frequency and amplitude limits, an analysis was performed on the set of signals in order to observe the variations in the performance parameters for selecting the optimized limits for de-noising algorithm. Figure 8-5 and Table 8-1 indicates that selecting the frequency limits to ±30% and Amplitude to ±60% produces the best de-noising results.

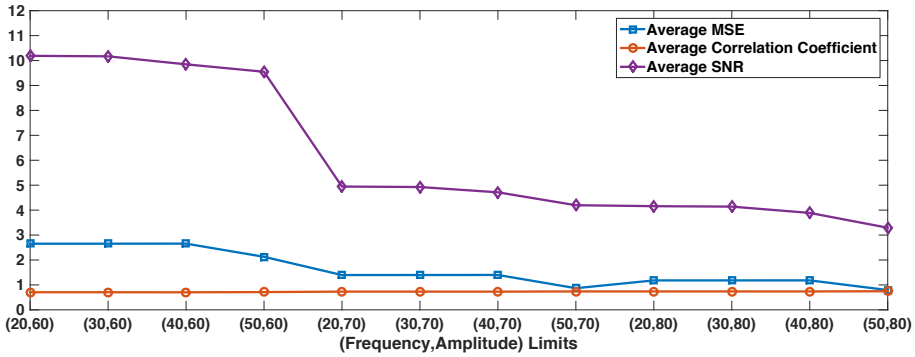

Figure 8-5. Frequency and Amplitude limits setting for self-Adaptive de-noising based on various performance indices

Table 8-1. Performance indices for different frequency and amplitude limits settings

Limits (±) % (Frequency, Amplitude)	**MSE**	**SNR**	**Correlation Coefficient**
(20,60)	2.6530	10.1884	0.7061
(30,60)	**2.6535**	**10.1697**	**0.7059**
(40,60)	2.6563	9.8480	0.7044
(50,60)	2.1271	9.5496	0.7126
(20,70)	1.3964	4.9451	0.7314
(30,70)	1.3970	4.9268	0.7312
(40,70)	1.3997	4.7142	0.7300
(50,70)	0.8687	4.1967	0.7385
(20,80)	1.1806	4.1587	0.7388
(30,80)	1.1812	4.1406	0.7386
(40,80)	1.1825	3.8882	0.7382
(50,80)	0.7935	3.2932	0.7462

For efficiency evaluation of the adaptive de-noising method, consider two partial discharge signals with single and double pulses in one measurement respectively. Figure 8-6 illustrates the original PD signal (S1), applied noise signal and the noise coupled PD signal.

As shown in Figure 8-7, the adaptive de-noising method yields an effective de-noising results as compared to the other techniques. Correlation coefficient γ between the original and de-noised signal has a value of 0.811 and less than 2% reduction in the PD pulse amplitude which shows a greater similarity between the original and de-noised signal. Consider another noisy PD signal (S2) with two recorded PD pulses in one cycle as shown in Figure 8-9. Detail Coefficients 8 and 9 are detected on the basis of frequency and 5,6 and 7 on the basis of amplitude. Reconstructing them gives the de-noised signal as shown in Figure 8-10. The algorithm successfully de-noises the whole signal and recover both the PD pulses buried inside the noise. The performance indices of the adaptive de-noising for the above mentioned two noisy PD signals are shown in the

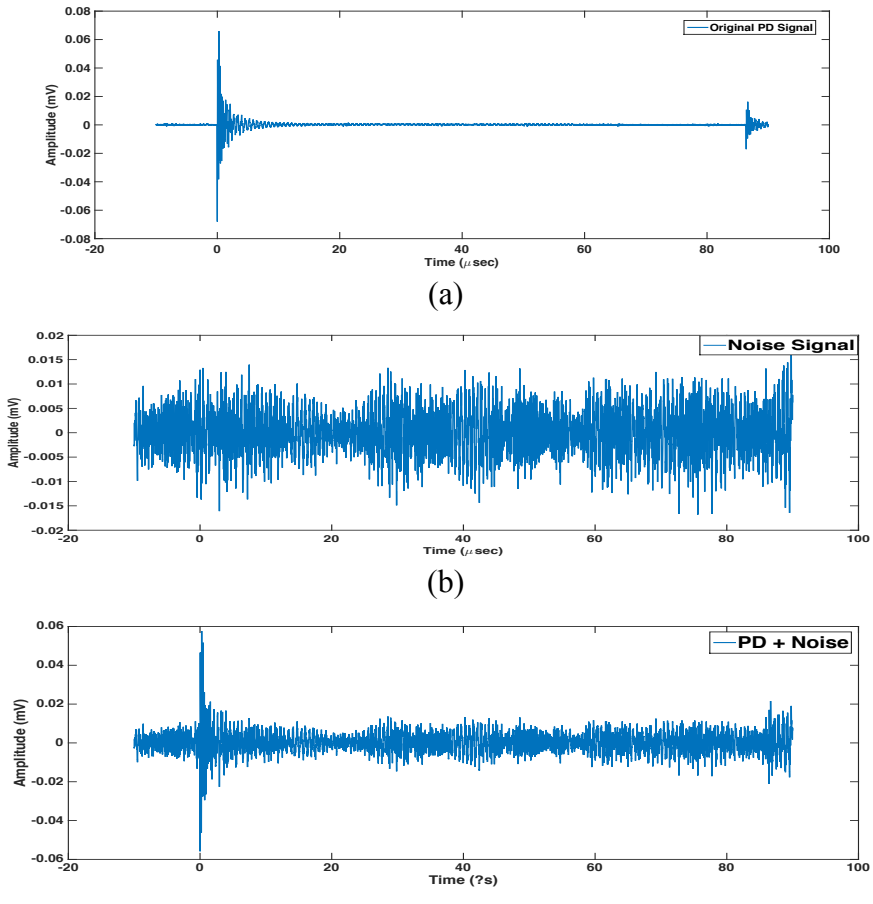

Figure 8-6. Signal (S1) for analysis of Self-Adaptive de-noising technique (a) Original measured PD signal, (b) White Noise Signal (c) PD coupled with noise signal

As concluded in the section 6.3.1, the HFCT sensor produces the damped exponentially decaying pulse (DEP type). Ma et al observe that the wideband white noise when with the DEP type PD signal, the frequency spectrum of the noise overlaps with that of PD signal which results in less efficient de-noising results particularly when the signal noise ratio is very low [38]. Comparison of the average performance indices for the de-noising of the signals with very low SNR and relatively high SNR are tabulated in

Table 8-2. Performance indices for signals S1 and S2 de-noised by adaptive de-noising technique

Adaptive De-Noising results	Correlation Coefficient	Mean Square Error	Reduction in amplitude (%)	Reduction in noise level (db)	SNR
S1	0,813	0,118	1,516	-56,29	3,36
S2	0,788	0,178	0,990	-54,492	2,614

Table 8-3. This method performs quite efficiently for both low and high SNR value signals.

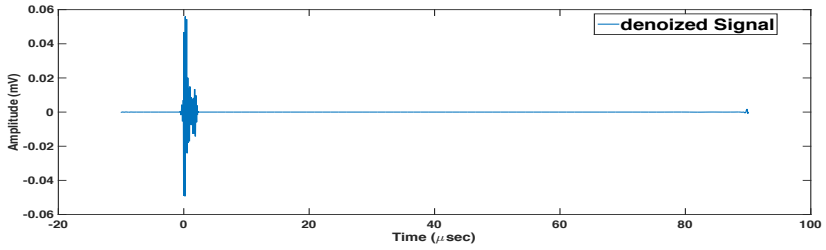

(a)

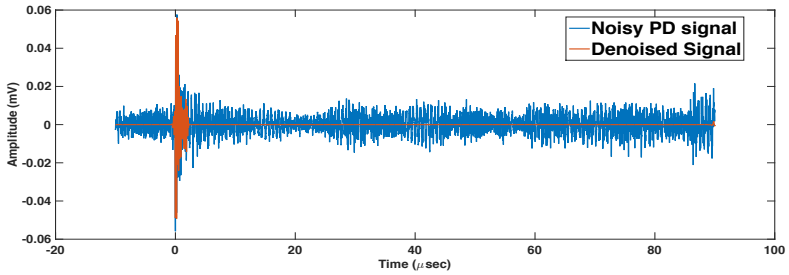

(b)

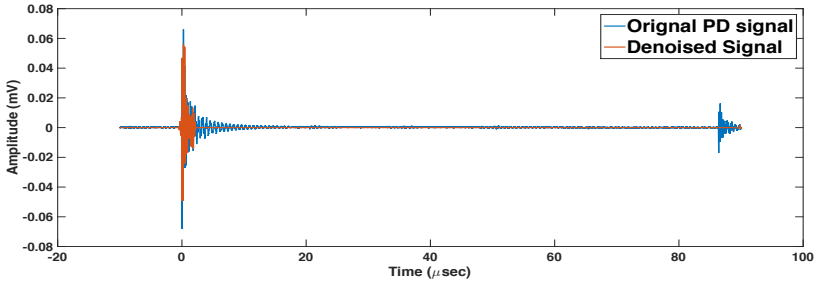

(c)

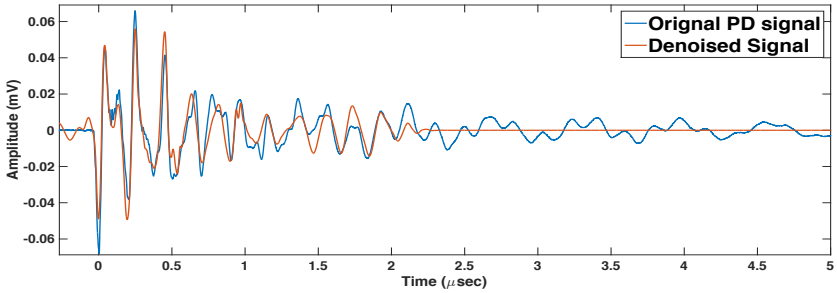

(d)

Figure 8-7. De-noising results for Adaptive de-noising technique (a) De-noised signal (b)De-noised signal with noisy PD signal (c) de-noised signal with original measured PD signal (d)zoomed analysis of the de-noised signal for wave pattern analysis.

Table 8-2. Performance indices for signals S1 and S2 de-noised by adaptive de-noising technique

Adaptive De-Noising results	Correlation Coefficient	Mean Square Error	Reduction in amplitude (%)	Reduction in noise level (db)	SNR
S1	0,813	0,118	1,516	-56,29	3,36
S2	0,788	0,178	0,990	-54,492	2,614

Table 8-3. Comparison of performance for Low SNR noises with high SNR noises

Adaptive De-noising	Average Correlation	Average Mean Square Error	Average Reduction in amplitude	Average reduction in noise level	average SNR
High SNR	0,7787	1,5322	10,9364	-57,6054	4,9977
Low SNR	0,6989	0,8290	5,1234	-55,4136	3,2915

The satisfactory performance of the adaptive de-noising can be observed in the histograms of performance indices as illustrated in Figure 8-8. More than 70% of the de-noised signals have correlation coefficient value larger than 0.6. The reduction in amplitude is also limited within 1 to 20% with relatively moderate SNR value between 2 to 6.

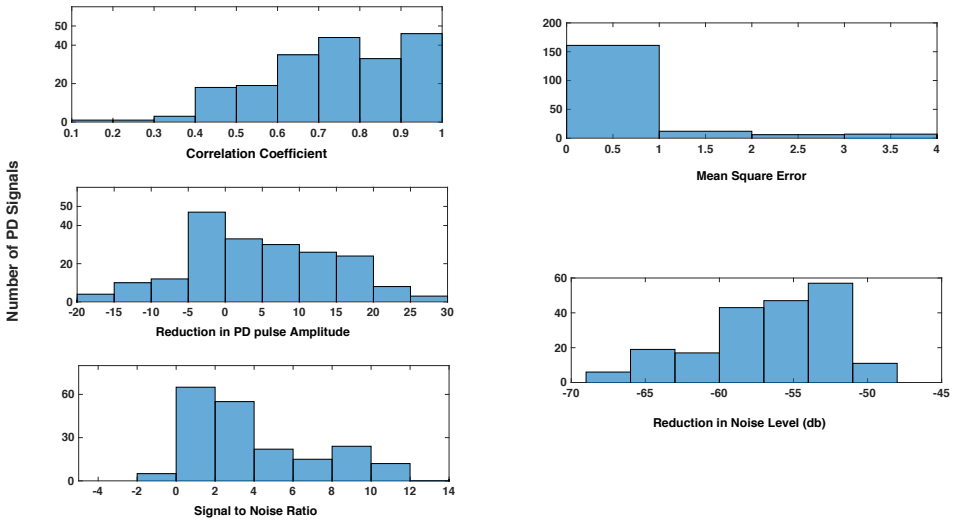

Figure 8-8. Performance indices for the set of signals under study

8.2.1 Performance comparison with other techniques

The three methods discussed in this study namely the level dependent de-noising, multi-level de-noising and adaptive de-noising have impressive de-noising results as illustrated before. However, the simulation results suggest that the adaptive de-noising method has slightly better performance indices as shown in
Table 8-4. Key performance indices correlation coefficient γ, MSE and reduction pulse amplitude for adaptive de-noising method have best values among the three methods discussed. Furthermore, comparisons with respect to set of noises are shown in Figure 8-11 which also verifies the better performance of adaptive de-noising technique.

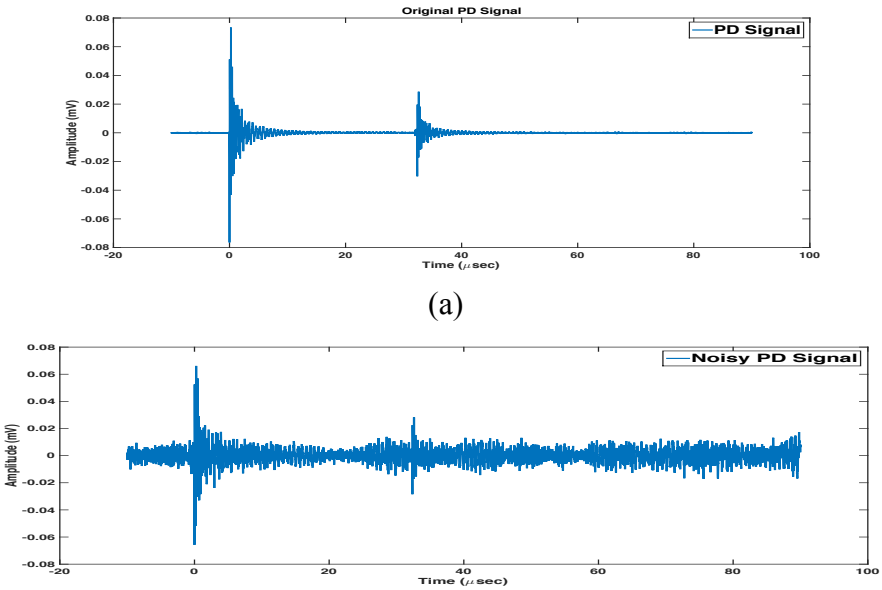

Figure 8-9 Signal (S2) for analysis of Self-Adaptive de-noising technique (a) Original measured PD signal, (b) PD coupled with noise signal

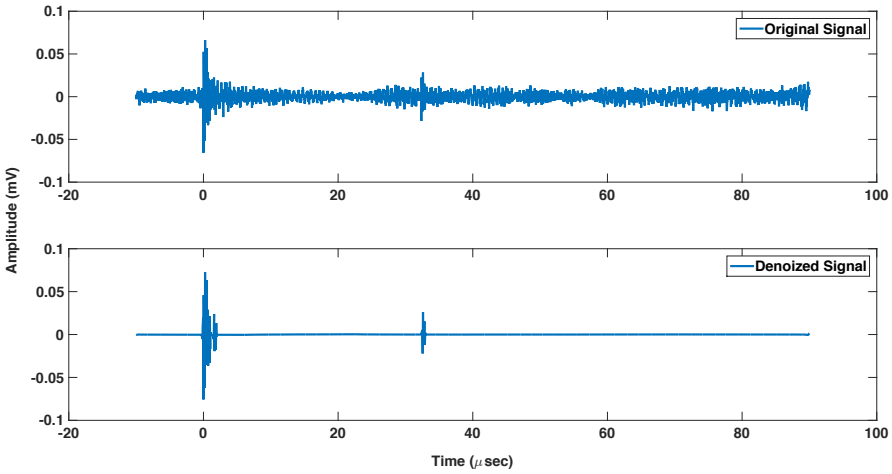

Figure 8-10. De-noised signal with two PD pulses recovered

Table 8-4. Comparison of Performance indices for three methods

Methods	Average Correlation	Average Mean Square Index	Average Reduction in amplitude	Average reduction in noise level	average SNR
Energy Based	0,7292	0,7259	8,0962	-56,6201	5,0653
Multilevel Correlation based	0,7289	0,7597	7,9924	-56,2631	5,2154
SNR based	0,7313	0,7330	6,4269	-56,5510	5,1190
Adaptive De-Noising	**0,7388**	**1,0806**	**4,1587**	**-56,5095**	**4,1446**

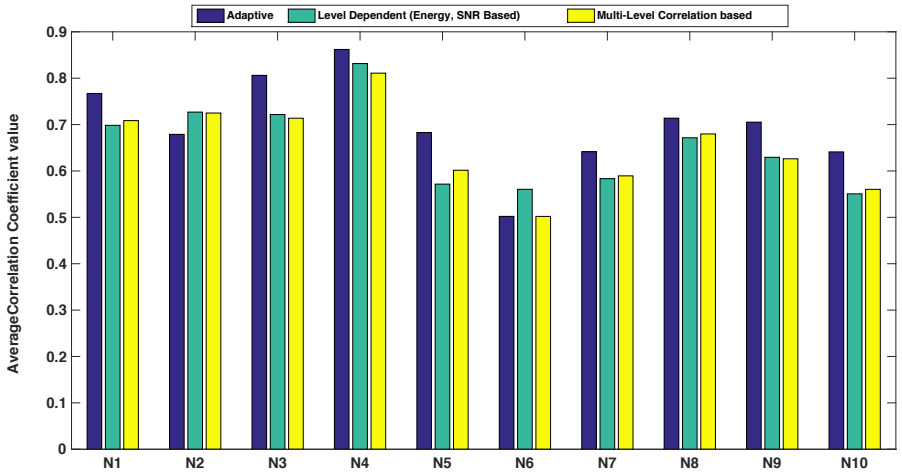

(a)

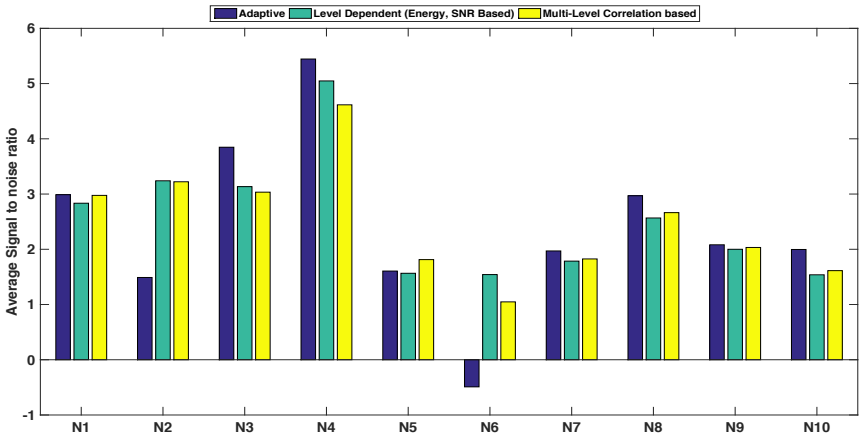

(b)

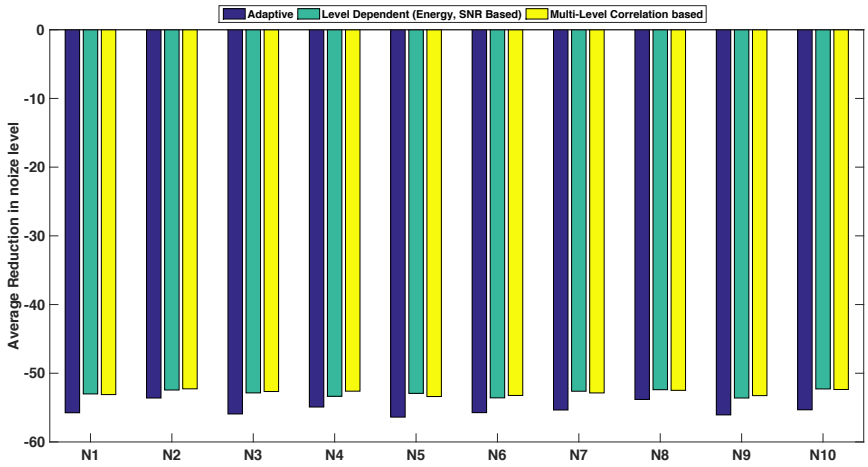

(c)

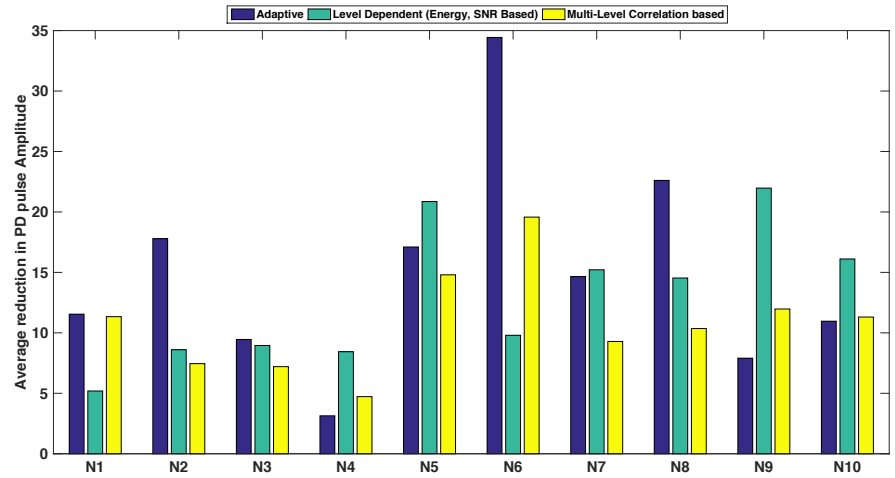

(d)

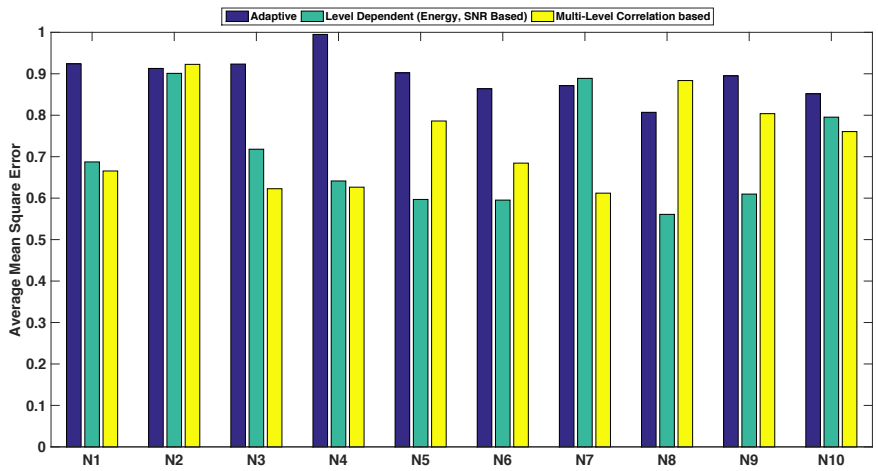

(e)

Figure 8-11. Average values of performance indices for different noises (N1 to N10) coupled with 10 different PD signals de-noised by three methods (a) correlation coefficient (b) SNR (c) reduction in noise level (d) reduction in PD pulse amplitude (e) Mean Square Error

8.2.2 Run Time Comparisons

The significant factor in evaluating the performance of the de-noising technique is the run time of the algorithm. The adaptive de-noising method is computationally less complex as compared to the other methods. Hence, it can produce results swiftly which is the major requirement in implementing the online condition monitoring system. Table 8-5 provides the results of run time analysis of the three methods discussed. The simulations were run on the Matlab 2015 interface on 2.4 GHz i-7 intel processor. The data measurements were made at 100002 samples per signal which makes the computations more time consuming. However, for practical implementation smaller data sets can be used which will shorten the run time of algorithm.

Table 8-5. Run time comparisons

Run time's	**Multi-Level De-noising based on Correlation Coefficient wavelet selection**	**Level dependent de-noising**	**Adaptive De-noising**
200 signals	650 seconds	430 seconds	286 seconds
Per signal	3.25 seconds	2.15 seconds	1.43 seconds

Chapter 9 CONCLUSIONS AND FUTURE WORKS

9.1 Conclusions

Part I

The experimental results and research methodology established by this study has laid the foundation for conducting a broader research in the field of quantification of the partial discharge signals. This study started with the aim to analyze the characteristics of partial discharge pulses which can allow us to predict the behavior of insulation deterioration and degradation. The whole study was part of learning and discovering the issues related to conducting research in such a wide field of random partial discharge phenomenon. The extensive literature review and the successful experimental work lead to many conclusive results. Particularly, a variety of quantities has been studied and examined which can provide useful information about the temporal behavior of partial discharge activity.

The establishment of the discharge (Corona) free testing setup is one of the key success. Thorough understanding of the PRPDA technique has been gained during the experimental work. Post processing Matlab software program has been developed which can provide continuous PD data recorded with the decrypted ICM system data file. The PD measurement setup and computer programs developed can be used further for any kind of long term partial discharge measurements.

Long term PD monitoring has been performed in order to observe the progressive stages of partial discharge. The typical PD pattern observed has four stages. Initially, the discharge sites start to accumulate charge across the cavity surface resulting in the formation of by-products and also surface erosion. Also, during this phase the surface conductivity of the cavity is believed to have increased. Second stage of partial discharge activity is the charge concentration period at the discharge site. This is characterized with stable partial discharge intensity. After prolonged insulation ageing, the electrical treeing phenomenon starts to develop at the tip of the crystal structures. High intensity as well as high frequency of partial discharge signals are observed during this stage. The last stage is the final breakdown of the insulation. Before the insulation breakdowns, it has been observed that the discharge intensity decreases to very low levels which allows time for taking some emergent action. Also, during this stage, the insulation resistance reduces. Apart from monitoring analysis, the partial discharge activity can also be observed with the help of different statistical operators as well as by the study of the individual discharge pulses in time and frequency domain. The variations in these quantities can be used to distinguish between the ageing mechanisms and also predict the partial discharge activity behavior. However, only the experts with experience can analyze the patterns and requires

continuous monitoring. Therefore, the development of automated pattern recognition methods based on machine learning has gained significance in research nowadays. In addition, the time & frequency domain analysis of the individual discharge pulses provides useful information regarding the physics of discharge mechanisms involved during the partial discharge activity.

Part II

The onsite PD measurements are badly affected by the presence of several interferences present around the equipment surroundings. These interferences have characteristics which are quite similar in nature to typical PD signals. This work has studied the various possible methods to eradicate the noise and recover the PD signal efficiently with as little loss of information as possible. In order to design an efficient de-noising filter for onsite and online PD monitoring system, various factors such as optimal wavelet selection, number of decomposition levels and threshold setting has been studied. The characteristics of PD signal measured with the HFCT sensor were explored which concludes that the wavelet functions 'db2' and 'db3' are optimal wavelet functions which can be used in the wavelet transformations. An efficient way to select the number of decomposition levels based on energy concentration of the signal is presented. This method reduces the computational time of algorithm. An automated thresholding technique based on the analyses of the noise content in the signal has been used. Hard thresholding is preferred over the soft thresholding.

In this work, a novel technique for de-noising of measured PD signals has been presented. This technique has been analyzed over a wide range of disturbances measured at the on-site conditions. It performed satisfactorily for all the available data sets used in this study and can be used as an effective solution for the online condition monitoring system.

The PD signals measured in the laboratory are relatively larger in magnitude as compared to the noise signal measured at the onsite conditions. The proposed algorithm will work efficiently for de-noising of laboratory measured PD signals, however, in practical applications where the charge magnitude in the initial stages of partial discharge development has very low value and the PD signal may gets completely buried inside the noise signal, the performance of this algorithm may not be accurate. Nevertheless, these low magnitude developing PD signals are comparatively less important in insulation condition assessment and diagnostic systems.

9.2 Future Works

Part I

1. The continuation of work related to estimating the propagation rate of electrical tree phenomenon. As mentioned earlier, the efficient method is the use of latest technology i.e. CCD camera. The continuous monitoring can provide very useful information regarding the onset of tree and the propagating properties.
2. Similar kind of study can be performed for the different type of partial discharge sources. This may include the study about surface discharges and also the long term study without the use of electrode configurations.
3. The next stage of partial discharge quantification is automated pattern recognition. This includes formation of large number of discharge parameters libraries. These pattern libraries for different type of discharge sources can then be used for mapping and clustering analysis. The efficient learning algorithm can be developed for creating an intelligent insulation diagnostic system.
4. Life prediction model described in this study can be strengthened by including several other parameters in addition to the stress indictor. For example, the variation in the partial discharge activity with respect to depth, diameter and location of the cavity
5. The evolution of PWM inverters and other power electronic devices has significantly effected the power quality by introducing voltage harmonics in the power network. These harmonics has been reported to have an accelerating effect on the electrical treeing process. A study can be conducted in order to understand the effect of voltage harmonics on electrical treeing on XLPE [26].

Part II

1. Practical implementation of the algorithm at on-site conditions to explore its applicability and observe the issues related to on-site de-noising.
2. Detailed analysis for understanding the nature and characteristics of the challenging pulsive type interferences.
3. The implication of the Wigner-Ville Distribution based de-noising method. This method is similar to wavelet transformation based de-noising on the account that both methods provide the frequency and time domain analysis. The significance of this new method involves the masking of the noise components in the noisy signal which sets the threshold values accordingly as compare to the fixed sqtwolog method used by wavelet transformation analysis [44].
4. Study of the bi-orthogonal wavelet function such as bior family which has been used recently by researchers in de-noising methods [35].

REFERENCES

[1] P. Hyvönen, "Prediction of insulation degradation of distribution power cables based on chemical analysis and electrical measurements", *Doctoral Dissertation*, Helsinki University of Technology (TKK), Espoo, Finland, 2008

[2] G.C.Stone, "Partial discharge diagnostics and electrical equipment insulation condition assessment," in *Dielectrics and Electrical Insulation, IEEE Transactions on* , vol.12, no.5, pp.891-904, Oct. 2005

[3] I.Ticar, J.Pihler, O.Bíró, K. Preis, "Partial discharges in insulation of Medium Voltage Systems", The international journal for Computation and Mathematics in electrical and Electronics Engineering, Vol.20, no.2,pp.473-481, 2001

[4] T. Okamoto, T. Tanaka, "Novel Partial Discharge Measurement Computer-Aided Measurement Systems," in *Electrical Insulation, IEEE Transactions on* , vol.EI-21, no.6, pp.1015-1019, Dec. 1986

[5] P.H.F. Morshuis, "Time-resolved discharge measurements" in *Partial Discharge, 1993., International Conference on* , vol., no., pp.43-46, 28-30 Sep 1993

[6] A. Harlin, M.G.Danikas, P.Hyvönen, "Polyolefin insulation degradation in electrical field below critical inception voltages", Journal of Electrical Engineering. Vol.56, no. 5-6.pp 135-140, 2005

[7] N. Amyot, E. David, S.Y. Lee, I.H. Lee, "Influence of post-manufacturing residual mechanical stress and crosslinking by-products on dielectric strength of HV extruded cables," in *Dielectrics and Electrical Insulation, IEEE Transactions on* , vol.9, no.3, pp.458-466, Jun 2002

[8] Densley, J.; Bartnikas, R.; Bernstein, B.S., "Multi-stress ageing of extruded insulation systems for transmission cables," in *Electrical Insulation Magazine, IEEE* , vol.9, no.1, pp.15-17, Jan.-Feb. 1993

[9] J.Densley, "Ageing mechanisms and diagnostics for power cables - an overview," in *Electrical Insulation Magazine, IEEE* , vol.17, no.1, pp.14-22, Jan.-Feb. 2001

[10] W. Hauschild and E. Lemke, “High-Voltage Test and Measuring Techniques”, Springer-Verlag, Berlin Heidelberg, 2014

[11] S.S. Bamji, A.T. Bulinski, R.J. Densley, "Degradation of polymeric insulation due to photoemission caused by high electric fields," in *Electrical Insulation, IEEE Transactions on* , vol.24, no.1, pp.91-98, Feb 1989

[12] C.Forssén, "Modelling of cavity partial discharges at variable applied frequency", *Doctoral Dissertation*, Kungl Tekniska Hogskolan (KTH), Stockholm, Sweden, 2008

[13] Jouni Kluss, Lecture material for course on Insulation Condition Monitoring

[14] Z. Nawawi, Y. Murakami, N. Hozumi, M. Nagao, "Effect of Humidity on Time Lag of Partial Discharge in Insulation-Gap-Insulation System," in *Properties and applications of Dielectric Materials, 2006. 8th International Conference*, pp.199-203, June 2006

[15] L. Niemeyer, "A generalized approach to partial discharge modeling," in *Dielectrics and Electrical Insulation, IEEE Transactions*, vol.2, no.4, pp.510-528, Aug 1995

[16] P.H.F. Morshuis, "Degradation of solid dielectrics due to internal partial discharge: some thoughts on progress made and where to go now," in *Dielectrics and Electrical Insulation, IEEE Transactions*, vol.12, no.6, pp.1275-1275, Dec. 2005

[17] C. Hudon,R. Bartnikas, M.R. Wertheimer, "Surface conductivity of epoxy specimens subjected to partial discharges," in *Electrical Insulation, 1990., Conference Record of the 1990 IEEE International Symposium* , pp.153-155, 3-6 Jun 1990

[18] G.C. Crichton, A. Karlsson, A. Pedersen, "Partial discharges in ellipsoidal and spheroidal voids," in *Electrical Insulation, IEEE Transactions*, vol.24, no.2, pp.335-342, Apr 1989

[19] E. Lemke, "Analysis of the partial discharge charge transfer in extruded power cables," in *Electrical Insulation Magazine, IEEE* , vol.29, no.1, pp.24-28, January-February 2013

[20] C. Forssen, Hans Edin, "Partial discharges in a cavity at variable applied frequency part 2: measurements and modeling," in *Dielectrics and Electrical Insulation, IEEE Transactions on* , vol.15, no.6, pp.1610-1616, December 2008

[21] M. Hikita, K. Yamada, A. Nakamura, T. Mizutani, A. Oohasi, M. Ieda, "Measurements of partial discharges by computer and analysis of partial discharge distribution by the Monte Carlo method," in *Electrical Insulation, IEEE Transactions,* vol.25, no.3, pp.453-468, Jun 1990

[22] E. Gulski, F.H. Kreuger, "Computer-aided recognition of discharge sources," in *Electrical Insulation, IEEE Transactions,* vol.27, no.1, pp.82-92, Feb 1992

[23] M.Shafiq, "Design and Implementation of Partial Discharge Measurement Sensors for On line Condition Assessment of Power Distribution System Components ", *Doctoral Dissertation*, Aalto University, Espoo, Finland, 2014

[24] M.M.A. Salama, R. Bartnikas, "Fuzzy logic applied to PD pattern classification," in *Dielectrics and Electrical Insulation, IEEE Transactions* , vol.7, no.1, pp.118-123, Feb 2000

[25] L. Satish, W.S. Zaengl, "Can fractal features be used for recognizing 3-d partial discharge patterns," in *Dielectrics and Electrical Insulation, IEEE Transactions* , vol.2, no.3, pp.352-359, Jun 1995

[26] F. Guastavino, G. Coletti, A. Dardano, A. Ratto, E. Torello, "Life prediction of XLPE subjected to distorted voltages in presence of bush-like electrical treeing," in *Electrical Insulation and Dielectric Phenomena, 2006 IEEE Conference*, pp.724-727, 15-18 Oct. 2006

[27] C. Hudon, R. Bartnikas, M.R. Wertheimer, "Analysis of degradation products on epoxy surfaces subjected to pulse and glow type discharges," in *Electrical Insulation and Dielectric Phenomena, 1991. CEIDP. 1991 Annual Report. Conference*, pp.237-243, 1991

[28] G. Paoletti, A. Golubev, "Partial discharge theory and applications to electrical systems," in *Pulp and Paper, 1999. Industry Technical Conference Record of 1999 Annual* , pp.124-138, 21-25 June 1999

[29] T.R. Blackburn, Z. ; R. Morrow, B.T. Phung, "Partial discharges development in a void and its effect on the material surface," in *Properties and Applications of Dielectric Materials, 2000. Proceedings of the 6th International Conference* , vol.1, pp.280-285 vol.1, 2000

[30] M. Misiti, Y. Misitti, G. Oppeneheim, J-M. Poggi, "Wavelet Toolbox Manual-User's Guide' the Math Works, 2015

[31] Jian Li; Tianyan Jiang; Grzybowski, S.; Changkui Cheng, "Scale dependent wavelet selection for de-noising of partial discharge detection," *Dielectrics and Electrical Insulation, IEEE Transactions on* , vol.17, no.6, pp.1705,1714, Dec. 2010

[32] Liu Xin; 'Partial Discharge Detection and Analysis in Low pressure environments' Doctoral Dissertation.

[33] Sriram, S.; Nitin, S.; Prabhu, K.M.M.; Bastiaans, M.J., "Signal denoising techniques for partial discharge measurements," *Dielectrics and Electrical Insulation, IEEE Transactions on* , vol.12, no.6, pp.1182,1191, Dec. 2005

[34] Caio F.F.C. Cunha, André T. Carvalho, Mariane R. Petraglia, Antonio C.S. Lima, A new wavelet selection method for partial discharge denoising, Electric Power Systems Research, Volume 125, August 2015, Pages 184-195, ISSN 0378-7796,

[35] Hao Zhang; Blackburn, T.R.; Phung, B.T.; Sen, D., "A novel wavelet transform technique for on-line partial discharge measurements. 1. WT de-noising algorithm," *Dielectrics and Electrical Insulation, IEEE Transactions on* , vol.14, no.1, pp.3,14, Feb. 2007

[36] Satish, L.; Nazneen, B., "Wavelet-based denoising of partial discharge signals buried in excessive noise and interference," *Dielectrics and Electrical Insulation, IEEE Transactions on* , vol.10, no.2, pp.354,367, April 2003

[37] Hussain, G.A.; Shafiq, M.; Kay, J.A.; Lehtonen, M., "Performance evaluation of noise reduction method during on-line monitoring of MV switchgear for PD measurements by non-intrusive sensors", International Journal of Electrical Power & Energy Systems, Volume 64, January 2015, Pages 596-607

[38] Ma, X.; Zhou, C.; Kemp, I.J., "Interpretation of wavelet analysis and its application in partial discharge detection," *Dielectrics and Electrical Insulation, IEEE Transactions on* , vol.9, no.3, pp.446,457, Jun 2002

[39] Donoho, D.L., "De-noising by soft-thresholding," *Information Theory, IEEE Transactions on* , vol.41, no.3, pp.613,627, May 1995

[40] Ma, X.; Zhou, C.; Kemp, I.J., "Automated wavelet selection and thresholding for PD detection," *Electrical Insulation Magazine, IEEE*, vol.18, no.2, pp.37,45, March-April 2002

[41] online material http://www2.webster.edu/~woolflm/correlation/correlation.html

[42] Hussain, G.A.; Shafiq, M.; Kay, J.A.; Lehtonen, M., "Preemptive Arc Fault Detection Techniques in Switchgear—Part III: From the Laboratory to Practical Installation," *Industry Applications, IEEE Transactions on* , vol.51, no.3, pp.2615,2623, May-June 2015

[43] Hao Zhang; Blackburn, T.R.; Phung, B.T.; Liu, Z., "Application of signal processing techniques to on-line partial discharge detection in cables," *Power System Technology, 2004. PowerCon 2004. 2004 International Conference on* , vol.2, no., pp.1780,1785 Vol.2, 21-24 Nov. 2004

[44] Detection and localization of narrow-band transient signals using the Wigner distribution Rao, Preeti and Taylor, Fred J., The Journal of the Acoustical Society of America, 90, 1423-1434 (1991)

[45] Clarkson,P.M., " Optimal and Adaptive Signal Processing", CRC Press Inc., ch.6, 1993

[46] Larimore,M,; Richard,C.; "Theory and Design of Adaptive Filters", John Wiley and Sons, ch 2-4, 1987.

[47] Hest,M.W; ”Multi-Resolution Analaysis of Partial Discharge Signals” M.S. thesis, Technische Universtat Eindhoven, 1999.